

**Microfluidic platforms for high-throughput  
mammalian cell printing,  
transfection, and dosage-dependent studies**

THÈSE N° 7889 (2017)

PRÉSENTÉE LE 24 OCTOBRE 2017  
À LA FACULTÉ DES SCIENCES ET TECHNIQUES DE L'INGÉNIEUR  
LABORATOIRE DE CARACTÉRISATION DU RÉSEAU BIOLOGIQUE  
PROGRAMME DOCTORAL EN BIOTECHNOLOGIE ET GÉNIE BIOLOGIQUE

ÉCOLE POLYTECHNIQUE FÉDÉRALE DE LAUSANNE

POUR L'OBTENTION DU GRADE DE DOCTEUR ÈS SCIENCES

PAR

**Kristina Pan WOODRUFF**

acceptée sur proposition du jury:

Prof. M. Dal Peraro, président du jury  
Prof. S. Maerkl, directeur de thèse  
Dr G. Kaigala, rapporteur  
Dr M. Meier, rapporteur  
Prof. M. Lutolf, rapporteur



ÉCOLE POLYTECHNIQUE  
FÉDÉRALE DE LAUSANNE

Suisse  
2017





# Acknowledgments

I would first like to thank Prof. Sebastian Maerkl for being an excellent advisor and for his patience and insights.

I am also grateful to Prof. Aleksandra Radenovic, my mentor, and to the PhD committee members who took the time to evaluate my work: Prof. Matteo Dal Peraro, Prof. Matthias Lutolf, Dr. Govind Kaigala, and Dr. Matthias Meier.

I would like to acknowledge Prof. Joerg Huelsken and Zuzana Tatarova for helpful discussions in the early days of my project. I thank Samy Gobaa for his stem cell expertise and Lely Feletti for her help with cell culture supplies. I would like to express my gratitude towards the CMI staff, in particular Georges-André Racine, Kaspar Suter, Cyrille Hibert, Joffrey Pernollet, and Laszlo Petho, for answering my questions about microfabrication. Thanks also to Valérie Glutz and Loïc Tauzin at the FCCF for assisting me with flow cytometry experiments.

My time working in LBNC was truly enjoyable, and I would like to thank José, Henrike, and Nicolas for training me in microfluidics when I first arrived in the lab. Thank you to all of the other LBNC members (Matt, JB, Arun, Sylvie, Amanda, Francesco, Nadanai, Francesca, Ekaterina, Zoe, Ivan, Barbora, Greg, Fabien) for your advice, support, and fun times spent outside of the lab.

I would also like to acknowledge the BioScience Network Lausanne, where I met many great people and explored possible career paths. Many thanks to my Pole Emotion family for making me feel welcome in Switzerland and for giving me opportunities to dance and teach.

Lastly, I thank my family for the love and encouragement they have provided over the years, and Flo for his support and always inspiring me to dream big.

*Lausanne, June 2017*

Kristina Woodruff.



# Abstract

With the advent of high-throughput and genome-wide screening initiatives, there is a need for improved methods for cell-based assays. Current approaches require expensive equipment, rely on large-scale culturing formats not suited for small or rare sample types, or involve tedious manual handling. Microfluidic systems could provide a solution to these limitations, since these assays are accessible, miniaturized, and automated. When coupled with high-content analysis, microfluidics has the potential to drastically increase throughput in cell biology and drug discovery. In light of these benefits, we developed 3 microfluidic approaches for mammalian cell-based assays: (1) printing of live mammalian cells into nanowell arrays, (2) a high-throughput transfection device, and (3) a module that generates complex, continuous concentration profiles.

Our first technique generates high-density nanowell arrays of live mammalian cells (LMCAs) using a standard contact microarray. Both commonly used cell lines and primary cells cultured on the arrays are highly viable and maintain their signature phenotype, making the platform suitable for long-term stem cell differentiation studies. Our 675-well array is ~2.6x more dense than a 1,536-well microtiter plate and can be frozen and thawed, facilitating the handling, storage, and screening of large libraries of cells.

LMCAs are also compatible with transfection, a technique that could enable analysis of the entire proteome in the natural cellular context. Transfection is routinely conducted on high-throughput arrays, but this setup requires manual cell culturing and precludes precise control over the cell environment. To this end, we created a microfluidic chip that streamlines cell loading and culturing and implements 280 independent transfections at up to 99% efficiency. The chip can perform co-transfections, in which the number of cells expressing each protein and the average protein expression level can be precisely tuned as a function of input DNA concentration. This platform is well-suited for optimizing synthetic gene circuits; we co-transfected four plasmids to test a histidine kinase signaling pathway and mapped the dose dependence of this network on the level of one of its constituents. The chip is readily integrated with high-content imaging, enabling the evaluation of cellular behavior and protein expression dynamics over time.

To complement the biological assays that could be performed on our transfection chip, we lastly generated an accurate and automated method to manipulate molecular concentrations on chip. Our pulse-width modulation (PWM)-based microfluidic module combines up to 6 different inputs and produces arbitrary concentrations with a dynamic range of 3-5 decades.

## **Abstract**

---

We created complex concentration profiles of 2 molecules, with each concentration independently controllable. The PWM module can execute rapid concentration changes as well as long-timescale pharmacokinetic profiles under a variety of operating conditions, making it ideal for integration with existing devices for advanced cell and pharmacokinetic studies.

Taken together, the 3 microtechnologies developed in this work integrate and automate mammalian cell handling, culturing, transfection, imaging, and solution preparation. These features have far-reaching implications in fields such as synthetic biology, stem cell research, and drug development.

Key words: microfluidics, microarrays, live cell printing, high-throughput screening, high-content imaging, automated microscopy, transfection, mammalian synthetic biology, stem cells, concentration-time profiles, pulse-width modulation

## Résumé

Avec l'avènement des initiatives de criblage à haut débit et du génome entier, il devient nécessaire de développer des nouvelles méthodes pour les essais cellulaires. Les approches actuelles exigent des équipements coûteux, comptent sur des plate-formes de culture cellulaire à grande échelle qui ne sont pas compatibles avec des échantillons rares ou petits, ou nécessitant une manipulation manuelle. Les systèmes microfluidiques pourraient fournir une solution à ces limitations, puisque ces essais sont accessibles, miniaturisés, et automatiques. Une fois couplé avec le criblage à haut contenu, la microfluidique a le potentiel d'augmenter drastiquement les capacités de la biologie cellulaire et la découverte des médicaments. En considérant ces avantages, nous avons développé 3 approches microfluidiques pour les essais des cellules mammifères : (1) l'impression des cellules mammifères vivantes dans une puce à nano-puits, (2) un dispositif pour la transfection à haut débit, et (3) un module qui génère des profils de concentration complexes et continus.

La première technique utilise un robot spotteur standard pour générer des puces denses en cellules mammifères vivantes (LMCAs). Les espèces de cellules couramment utilisées et aussi les cellules primaires cultivées sur les puces sont très viables et maintiennent leurs signatures phénotypiques. Notre puce à 675 nano-puits est ~2.6 fois plus dense qu'une plaque à 1,536 micropuits et puisse être congelée et décongelée, ce qui facilite la manipulation, le stockage, et le criblage des grandes bibliothèques des cellules.

Les LMCAs sont également compatibles avec la transfection, une technique qui permet l'analyse du protéome entier dans le contexte naturel de la cellule. La transfection est typiquement effectuée sur des puces à haut débit, mais ce système nécessite la culture manuelle des cellules et empêche la gestion précise de l'environnement cellulaire. Par conséquent, nous avons créé une puce microfluidique qui simplifie les processus de chargement, de culture des cellules, et réalise 280 transfusions indépendantes, jusqu'à une efficacité de 99%. La puce est capable d'accomplir des co-transfections, où le nombre de cellules qui exprime une protéine et le niveau d'expression de chaque protéine puissent être réglés en changeant les concentrations initiales de l'ADN. Cette puce est bien adaptée pour optimiser les circuits génétiques synthétiques; nous avons co-transfecté 4 plasmides pour examiner un système de transduction histidine-kinase et ensuite étudié la dépendance de ce réseau sur la quantité d'un de ses constituants. La puce est facilement intégrée avec l'imagerie haut contenu, permettant l'évaluation temporelle du comportement des cellules et de la dynamique de l'expression des protéines.

## Résumé

---

Pour compléter les essais biologiques qui pourraient être effectués sur notre puce de transfection, nous avons généré une méthode précise et automatique pour manipuler les concentrations moléculaires. Notre module microfluidique est basé sur le concept de la modulation de largeur d'impulsion (MLI) et combine jusqu'à 6 solutions pour produire des concentrations arbitraires avec une plage dynamique de 3 à 5 ordres de grandeur. Nous avons réalisé des profils de concentration complexes de 2 molécules en parallèle, avec la capacité de contrôler chaque molécule indépendamment. Le module MLI peut exécuter des changements de concentration rapides et aussi des profils pharmacocinétiques à long terme sous des conditions diverses. Il est donc idéal pour l'intégration avec des dispositifs existants pour des essais cellulaires avancés et des études pharmacocinétiques.

Prises ensemble, les trois micro-technologies présentées dans cette thèse intègrent et automatisent la manipulation et la culture des cellules mammifères, la transfection, l'imagerie, et la préparation des solutions. Ceci ouvre donc de vastes opportunités dans les domaines de la biologie synthétique, la recherche sur les cellules souches, et le développement des médicaments.

Mots-clés : Microfluidique, puces à cellules et ADN, impression des cellules vivantes, criblage à haut débit, imagerie à haut contenu, microscopie automatisée, transfection, biologie synthétique mammifère, cellules souches, profils temporels de concentration, modulation de largeur d'impulsion



# Contents

<b>Acknowledgments</b>	<b>i</b>
<b>Abstract (English/Français)</b>	<b>iii</b>
<b>List of figures</b>	<b>xi</b>
<b>List of tables</b>	<b>xiii</b>
<b>1 Introduction</b>	<b>1</b>
1.1 High-content analysis of large cell libraries . . . . .	1
1.2 Transfection . . . . .	2
1.3 Reverse transfection . . . . .	3
1.4 Mammalian synthetic biology . . . . .	4
1.5 Microfluidic devices for mammalian cells . . . . .	5
1.6 Complex, continuous concentration profiles on microfluidic devices . . . . .	6
1.7 Pharmacokinetic/pharmacodynamic studies on microfluidic devices . . . . .	8
1.8 Objectives and overview of this work . . . . .	9
<b>2 Live mammalian cell arrays</b>	<b>11</b>
2.1 Abstract . . . . .	12
2.2 Introduction . . . . .	12
2.3 Results . . . . .	12
2.3.1 A robust method to array live cells . . . . .	12
2.3.2 Cross-contamination on the arrays . . . . .	14
2.3.3 Viability of multiple cell types after arraying . . . . .	15
2.3.4 High-density LMCAs . . . . .	18
2.3.5 Transfection on the LMCAs . . . . .	19
2.3.6 Primary cells on the LMCAs . . . . .	21
2.4 Conclusion . . . . .	22
2.4.1 Acknowledgments . . . . .	22
2.4.2 Author contributions . . . . .	22
2.4.3 Competing financial interests . . . . .	23
2.5 Methods . . . . .	24
2.5.1 Substrate fabrication . . . . .	24

## Contents

---

2.5.2	Cell culture . . . . .	24
2.5.3	Cell spotting . . . . .	25
2.5.4	Array culture . . . . .	25
2.5.5	Transfection . . . . .	26
2.5.6	Array imaging . . . . .	26
<b>3</b>	<b>A high-throughput microfluidic platform for mammalian cell transfection and culturing</b>	<b>27</b>
3.1	Abstract . . . . .	28
3.2	Introduction . . . . .	28
3.3	Results . . . . .	29
3.3.1	Device design and cell loading/culturing . . . . .	29
3.3.2	Device assembly . . . . .	33
3.3.3	Generating a microfluidic-compatible reverse transfection array . . . . .	34
3.3.4	Microarraying and composition of transfection complexes . . . . .	37
3.3.5	Quantification of cross-contamination . . . . .	40
3.3.6	Simultaneous delivery of multiple plasmids . . . . .	44
3.3.7	Transfection of synthetic genetic circuits . . . . .	47
3.3.8	Supplementary Movies . . . . .	51
3.4	Discussion . . . . .	51
3.4.1	Acknowledgments . . . . .	52
3.4.2	Author contributions . . . . .	52
3.4.3	Competing financial interests . . . . .	52
3.5	Methods . . . . .	52
3.5.1	Microarray printing and slide treatment . . . . .	52
3.5.2	Microarraying mixture preparation . . . . .	53
3.5.3	Standard transfections . . . . .	54
3.5.4	DNA staining . . . . .	54
3.5.5	Cell culture . . . . .	54
3.5.6	Flow cytometry . . . . .	54
3.5.7	Imaging . . . . .	54
3.5.8	COMSOL modeling . . . . .	55
3.5.9	Microfluidic device fabrication . . . . .	55
3.5.10	Microfluidic device operation . . . . .	56
<b>4</b>	<b>A microfluidic module for real-time generation of complex multi-molecule temporal concentration profiles</b>	<b>57</b>
4.1	Abstract . . . . .	58
4.2	Introduction . . . . .	58
4.3	Results . . . . .	61
4.3.1	PWM chip design and technique . . . . .	61
4.3.2	Optimizing PWM total cycle length . . . . .	63
4.3.3	Characterizing response time . . . . .	65

4.3.4	Testing different flow rates on the PWM module . . . . .	66
4.3.5	Characterizing the dynamic range . . . . .	68
4.3.6	Connecting the PWM module to a second chip . . . . .	69
4.3.7	Complex, long-term and PK/PD concentration profiles . . . . .	71
4.4	Discussion . . . . .	73
4.4.1	Acknowledgments . . . . .	74
4.4.2	Competing financial interests . . . . .	74
4.5	Experimental . . . . .	74
4.5.1	Chemicals . . . . .	74
4.5.2	Automated pneumatic setup . . . . .	75
4.5.3	Imaging . . . . .	75
4.5.4	Microfluidic device fabrication . . . . .	75
4.5.5	Microfluidic chip operation . . . . .	76
<b>5</b>	<b>Conclusions and Outlook</b>	<b>77</b>
5.1	Summary of Results . . . . .	77
5.2	Limitations . . . . .	78
5.3	Outlook . . . . .	80
<b>6</b>	<b>Appendix</b>	<b>83</b>
6.1	Co-spotting method for co-transfection . . . . .	83
6.2	Lentivirus transduction on chip . . . . .	83
6.3	Co-culture on the transfection chip . . . . .	85
6.4	Co-transfection of a complex synthetic system . . . . .	88
6.5	Producing protein arrays using the transfection chip . . . . .	88
6.6	MATLAB codes . . . . .	92
6.7	LabVIEW VIs . . . . .	99
<b>Bibliography</b>		<b>105</b>
<b>Curriculum Vitae</b>		<b>119</b>



# List of Figures

1.1	High-content cell assays . . . . .	2
1.2	Reverse transfection technique . . . . .	4
1.3	Cell culturing microfluidic device . . . . .	6
1.4	Diffusion gradient-based concentration profiles . . . . .	7
1.5	Pulse-width modulation . . . . .	8
1.6	Pharmacokinetic profile of an orally administered drug . . . . .	9
2.1	Nanowell array preparation and cell attachment . . . . .	13
2.2	A method to array live mammalian cells . . . . .	14
2.3	Cell depletion from spotting well plate . . . . .	15
2.4	Quantification of cross-contamination . . . . .	16
2.5	Nanowell cell viability . . . . .	16
2.6	Freezing of LMCAs. . . . .	17
2.7	Compatibility of LMCAs with different cell types . . . . .	17
2.8	Applications of the arraying method . . . . .	18
2.9	High-throughput LMCA . . . . .	19
2.10	Transfection techniques on the nanowell array . . . . .	20
2.11	Human mesenchymal stem cell array and differentiation . . . . .	21
2.12	Quantitation of hMSC array . . . . .	23
3.1	High-throughput microfluidic cell culturing and transfection chip design . . . . .	30
3.2	Sieve chip design . . . . .	31
3.3	Schematic of cell loading and culturing on the low-throughput chip . . . . .	32
3.4	Serum quality and transfection efficiency on the sieve device . . . . .	33
3.5	Plasma treatment of lipid-DNA microarrays . . . . .	34
3.6	Generation of a microfluidic-compatible reverse transfection array . . . . .	35
3.7	Optimization of PLL spotting . . . . .	36
3.8	Optimization of the lipid-DNA composition . . . . .	37
3.9	Adapting the microchip to different cell types and transfection methods . . . . .	38
3.10	Investigating DNA cross-contamination on the transfection arrays . . . . .	39
3.11	Evaluating cell cross-contamination on the transfection arrays . . . . .	40
3.12	Cell loading speed and cross-contamination . . . . .	41
3.13	Transfection on the high-throughput chip . . . . .	42

## List of Figures

---

3.14	Transfection efficiencies on the high-throughput chip . . . . .	43
3.15	Quantification of eGFP contamination on the high-throughput transfection chip . . . . .	44
3.16	Co-transfection on the high-throughput chip . . . . .	45
3.17	Ratios of protein expression and transfection efficiency for microfluidic co-transfection . . . . .	46
3.18	Ratios of protein expression and transfection efficiency for 96-well plate co-transfection . . . . .	47
3.19	Flow cytometry analysis for 6-well plate co-transfection . . . . .	48
3.20	Ratios of protein expression and transfection efficiency for various co-transfection and analysis methods . . . . .	49
3.21	Synthetic gene circuits on the high-throughput chip . . . . .	50
3.22	Synthetic gene circuits in 96-well plate transfections . . . . .	51
4.1	Schematic of microfluidic PWM . . . . .	59
4.2	The PWM platform . . . . .	60
4.3	Timing of valve switching . . . . .	61
4.4	PWM chip cycle times . . . . .	62
4.5	0.5 s cycle time performance . . . . .	63
4.6	Duty cycle plots for PWM cycle times . . . . .	64
4.7	PWM chip response times . . . . .	65
4.8	Different flow rates on the PWM chip . . . . .	66
4.9	Duty cycle plots for different flow rates . . . . .	67
4.10	PWM chip dynamic range . . . . .	68
4.11	PWM chip used upstream of a second device . . . . .	70
4.12	Complex experiments on the PWM chip . . . . .	72
4.13	Guide to selecting optimal PWM chip operating conditions . . . . .	73
6.1	Co-spotted vs. pre-mixed transfection mixtures . . . . .	84
6.2	Stable protein expression 14 days after transfection on chip . . . . .	84
6.3	Chip design for a sender-receiver cell system . . . . .	85
6.4	COMSOL modeling of lentivirus diffusion . . . . .	86
6.5	Co-culture on the transfection chip . . . . .	86
6.6	Transfection of a CRISPR repression device . . . . .	87
6.7	Microfluidic chip for protein pull-down from transfected cells . . . . .	89
6.8	Microfluidic chip to study protein-protein interactions from cell samples . . . . .	90
6.9	On-chip mechanical cell lysis and GFP capture . . . . .	91



## List of Tables

1.1	Comparison of transfection methods . . . . .	3
3.1	Detailed composition of transfection mixtures used for optimization experiments	38
3.2	Comparison of reagent requirements for various transfection methods . . . . .	39
4.1	Comparison of our PWM module to previous devices . . . . .	74





# 1 Introduction

## 1.1 High-content analysis of large cell libraries

Molecular cloning technologies for mammalian cells are well-established and constantly improving, resulting in large collections of cell lines. These libraries are perfectly suited for high-content screening (HCS), in which the detailed spatiotemporal information obtained from cellular imaging is combined with the high throughput of automated cell handling techniques<sup>1</sup>. For example, existing stably transfected cell lines and GFP-fusion libraries<sup>2</sup> can be cultured in the presence of therapeutic molecules of interest, yielding insights to drug mechanisms and cell escape from drug action. Monitoring the quantity and localization of fluorescently tagged proteins at high temporal resolution can determine the individual contribution of thousands of proteins to the overall cell response. HCS can also be applied to large compilations of cancer cell lines and samples<sup>3</sup>. Screens performed with a large diversity of cells better reflect the heterogeneity of patient samples and primary tumors. Elucidating the relationship between specific characteristics (e.g. genomic aberrations and transcriptional signatures) of a sample and its response to a drug could help advance early-phase clinical trials and personalized medicine.

Despite the abundance of information that could potentially be gathered (Fig. 1.1), we still lack efficient tools to interrogate these cell libraries. An ideal HCS method should be capable of manipulating small amounts of sample. Most primary cells are available in limited quantities, and cancer and stem cells are susceptible to undesirable changes in phenotype or genotype when expanded<sup>4,5</sup>. Second, cell culturing arrays should be dense, miniaturized, and modular to ensure compatibility with high-throughput screening. Third, analysis platforms should enable long-term and continuous monitoring at the single cell level in order to supply information on molecular mechanisms. Finally, an ideal technique for HCS should offer advanced control over the cell microenvironment for eventual integration with studies such as extracellular matrix niche testing<sup>6</sup>.

One method that can be used for high-content analysis is flow cytometry<sup>8,9</sup>. Flow cytometry provides end-point measurements, preventing a detailed understanding of drug mechanisms

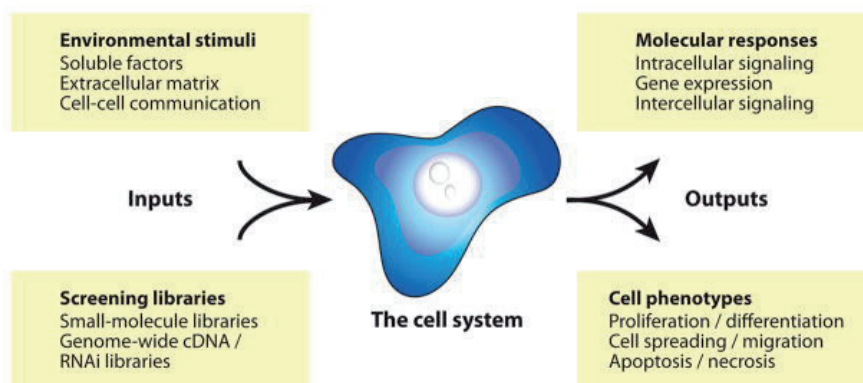


**Figure 1.1.** Examples of cell assays that can be performed using high-content platforms, reprinted with permission<sup>7</sup>. Copyright 2009, Annual Reviews.

and temporal responses. Moreover, cell culturing prior to flow cytometry analysis is typically performed manually and requires large sample sizes. To address this need, several automated approaches for managing large collections of mammalian cells have been developed. One strategy is to couple microtiter plate cell culture with robotic fluidic operation. For the time being this practice remains inaccessible to most researchers because it relies on expensive liquid handling equipment<sup>10,11</sup>. Alternatively, inkjet printers can be used to dispense live cells into dense arrays<sup>12-14</sup>. This technique requires each sample to be individually loaded into the printer and cannot manage multiple samples. Contact spotting, a method widely employed to produce DNA and protein microarrays<sup>15,16</sup>, has also been explored for the micropatterning of cells. Previous studies have succeeded in arraying fixed cells<sup>17</sup> and gelatinous preparations containing a single cell type<sup>18</sup>. Contact spotting is a versatile and standard technique, and cell arrays generated in this manner could be combined with arrays of small molecules, drugs, and proteins to execute more sophisticated experiments. Live cell arrays could be maintained in culture and monitored over time, providing a wealth of information. Nevertheless, to date it remains a challenge to array many types of live cells at once with contact spotting.

## 1.2 Transfection

Cell-based research often entails expressing and studying specific proteins. Transfection is the process of introducing foreign genetic material into mammalian cells<sup>19</sup>. In contrast to those produced in prokaryotic systems, the expressed proteins undergo proper folding and post-translational modifications. This technology is thus pertinent to protein production, functional assays, and therapeutic gene delivery. Transfection can be achieved by many biological, chemical, and physical means (summarized in Table 1.1). Chemical transfection generally involves cationic reagents that neutralize the negative charge of DNA. For instance, cationic lipids are commercially available and widely used, and their structure facilitates entry into the cell by endocytosis or phagocytosis. Other reagent-based approaches include calcium

phosphate precipitation<sup>20</sup> and nanoparticles<sup>21</sup>. A variety of physical strategies including magnetic delivery<sup>22</sup>, optical transfection<sup>23</sup>, sonoporation<sup>24</sup>, electroporation<sup>25</sup>, microinjection<sup>26</sup>, and cell squeezing<sup>27</sup> have also been developed. One shortcoming of the techniques mentioned above is that genetic material is delivered to the cytoplasm and must translocate into the nucleus to permit transcription into mRNA. These approaches work best for dividing cells; the nuclear envelope breaks down during mitosis, allowing foreign genetic material to enter<sup>28</sup>. Viral-mediated methods (called transduction), in contrast, can introduce large quantities of genetic material into a wide range of non-dividing cells<sup>29,30</sup>. This strategy takes advantage of the infection and gene delivery capabilities of retroviruses, lentiviruses, adenoviruses, and adeno-associated viruses. The viral vectors are modified to be replication-deficient for safety reasons<sup>31</sup>. Retroviruses and lentiviruses are able to integrate into the genome, providing stable protein production. Despite their high efficiency of transduction, viral vector production requires several days to weeks, concentration by ultracentrifugation, and a BSL2 laboratory<sup>32</sup>.

### 1.3 Reverse transfection

Integration with contact spotting has adapted transfection for high-throughput screening. In this technique, called reverse transfection, purified cDNA samples are mixed with chemical transfection reagent and spotted onto glass slides<sup>33</sup> (Fig. 1.2). siRNA can also be arrayed for loss-of-function studies. The arrays are next seeded with cells, which undergo transfection *in situ* and convert the cDNA into protein. Unlike protein microarrays<sup>16,34,35</sup>, this method does not require individual purification of each protein and proteins can be analyzed in the natural cellular context. More than 5,000 samples can be printed on a single glass microscope slide

Category	Examples	Advantages	Disadvantages
Chemical	Cationic polymers	High efficiency	Possible toxicity
	Cationic liposomes	High commercial availability	Transient expression
	Calcium phosphate	Easy to use	Efficient only for dividing cells
	Nanoparticles		
Physical	Magnetic particles	Compatible with many cell types	Possible toxicity
	Laser-irradiation	Possible single-cell manipulation	Transient expression
	Sonoporation	No need for vector	Requires special instrumentation
	Electroporation		Tedious optimization
	Microinjection		
	Cell squeezing		
Biological	Retrovirus	High efficiency	Tedious production protocol
	Lentivirus	Genomic integration (stable expression)	Possible mutagenic and immunogenic effects
	Adenovirus	Efficient for primary and non-dividing cells	BSL2 requirement
	Adeno-associated virus	<i>In vivo</i> applications	

**Table 1.1.** Comparison of transfection methods, adapted from Kim et al.<sup>19</sup>

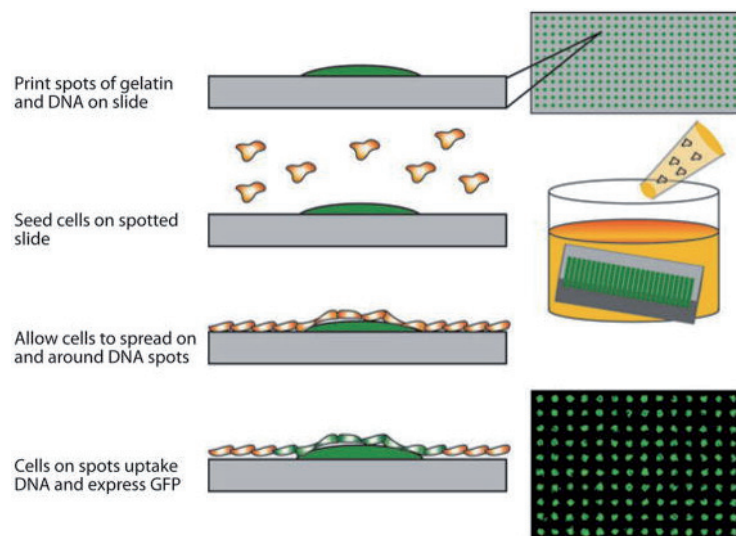


**Figure 1.2.** The reverse transfection technique, reprinted with permission<sup>7</sup>. Copyright 2009, Annual Reviews.

using standard techniques<sup>33,36</sup>, and a recent study was able to further increase this density<sup>37</sup>. This throughput would allow for the screening of genome-wide RNAi and cDNA libraries<sup>38,39</sup>. With the accumulation of data from cDNA microarrays and whole genome sequencing, there is a need to validate protein function and characterize therapeutic targets.

### 1.4 Mammalian synthetic biology

Aside from its utility in proteomic studies, reverse transfection could serve as a valuable tool for mammalian synthetic biology. Synthetic biology is a “bottom-up” approach to engineering synthetic gene networks and is relevant to applications such as biosensors, sustainable energy sources, and biomedical therapies<sup>40</sup>. Prokaryotes are often used for synthetic biology because they are receptive to genetic modifications, but the clinical applications of these models are limited. Engineering mammalian systems remains more difficult due to their advanced mechanisms to evade foreign genetic material, extensive compartmentalization, and tight gene regulation<sup>41</sup>. Nevertheless, mammalian synthetic biology could significantly benefit biotechnology, for instance in protein production and providing novel therapies through stem cell engineering<sup>40,42</sup>.

These potential benefits emphasize the need to develop new approaches for studying mammalian synthetic systems. Successful implementation of these systems requires multiple genetic constructs to be simultaneously delivered to cells at precise ratios, necessitating painstaking optimization of the transfection conditions<sup>43,44</sup>. Typical experiments involve multiwell plates, meaning that cell culturing and transfection mixtures must be prepared by hand. Reverse transfection could accelerate the testing of synthetic networks because

transfection mixture arraying and cell seeding is highly automated and streamlined. Additionally, the high-content imaging that accompanies reverse transfection presents an attractive alternative to the flow cytometry analysis that conventionally follows multiwell plate culture. Continuous imaging of an array of circuit-expressing cells would supply temporal data, which is especially important for oscillating systems<sup>45</sup>. However, to date, reverse transfection has not been applied in the context of synthetic biology.

### 1.5 Microfluidic devices for mammalian cells

Although reverse transfection has been optimized for a variety of genetic materials<sup>46,47</sup> and cell types<sup>48</sup>, methods for cell manipulation on the arrays still stand to be improved. Cell seeding and culturing is performed manually, and spots on the live cell array are not physically separated from one another. This setup offers poor control over the cell microenvironment, preventing more sophisticated downstream experiments from being executed on the array. Cross-contamination on the array is a prominent concern, and efforts have been made to separate DNA spots with silicon gaskets<sup>49</sup> and cell-repellent coatings<sup>50</sup>.

Microfluidic devices present a possible solution to the shortcomings of reverse transfection arrays described above. By enclosing each position on the array in a cell culturing chamber, one could implement long-term experiments and studies with poorly adherent or highly migrant cell types. Despite these advantages, progress in combining transfected cell arrays with microfluidics has been slow. Biochip platforms have obtained between 13 and 80% transfection efficiency<sup>51-53</sup>, with throughputs ranging from 1 to 96 reactions per device<sup>54-57</sup>. These systems do not incorporate mechanisms for medium replenishment in the cell chambers, prohibiting long-term experiments or flow manipulation. In contrast, standard cell culturing chips are capable of variety of functions, including long-term perfusion culture and the ability to individually address cell chambers<sup>58</sup> (Fig. 1.3). This discrepancy highlights the need for an improved microfluidic transfection platform.

Modern microfluidic devices like the one presented in Figure 1.3 contain micromechanical components such as valves, mixers, and pumps that allow them to carry out complex chemical and *in vitro* biological assays<sup>59</sup>. Microfluidic large-scale integration has facilitated massively parallel experiments, in which reactions can be addressed individually on the chip<sup>60</sup>. In addition to high throughput, microfluidic devices are characterized by automation, small sample requirements, and compatibility with other analytical techniques. The micrometer dimensions of these chips equate to a laminar flow regime. The absence of turbulence permits flowing several fluids in parallel, and this feature enables novel diffusion-based experiments. Moreover, the dimensions of average microfluidic elements (10-100  $\mu\text{m}$ ) are perfectly compatible with the diameter of eukaryotic cells, making it possible to achieve complex manipulations on the single cell level. The cell environment on chip can be customized by incorporating microfabricated structures<sup>61</sup> or using contact spotting, a microfluidic-compatible technique, to deposit ECM molecules and growth factors<sup>6,62</sup>. For the reasons mentioned above, mi-

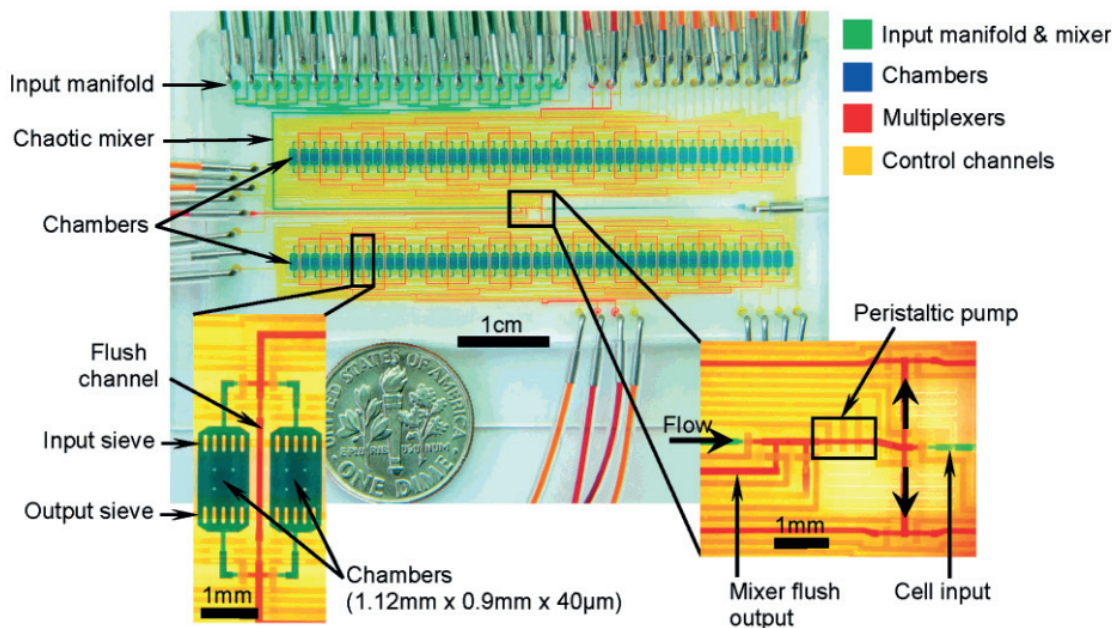


**Figure 1.3.** A microfluidic cell culture system, reprinted with permission<sup>58</sup>. Copyright 2007, American Chemical Society.

crofluidics is positioned to revolutionize the way mammalian cell studies are performed. Mammalian microfluidic chips have already been designed for a large variety of purposes, including drug screening<sup>63,64</sup>, genome analysis<sup>65</sup>, single-cell analysis<sup>66</sup>, and stem cell studies<sup>67,68</sup>. Chips with new applications are constantly being developed, imparting us with a better understanding of cellular processes and guiding the development of new therapies.

### 1.6 Complex, continuous concentration profiles on microfluidic devices

In the wake of the aforementioned developments in microfluidic technology, an increasing number of laboratories is turning to on-chip platforms to implement cell-based assays. Microfluidic devices used for these purposes are connected to a small number of input solutions, and a typical experiment flows one solution through the chip at a time. To introduce a different concentration or a new molecule on the chip a new input solution is used, incurring frequent step function changes. This setup poorly reflects the concentration changes that occur *in vivo*. For example, the quantity of a drug in blood plasma fluctuates over many hours, following a complex, continuous rise and fall pattern. The ability to create complex temporal concentration profiles of one or more substances would enable the accurate study of changing antibiotic concentrations on bacteria, the effect of drugs on mammalian cells, and stem cell differentiation.

Simple concentration profiles have been previously created on chip by means of lateral

## 1.6. Complex, continuous concentration profiles on microfluidic devices

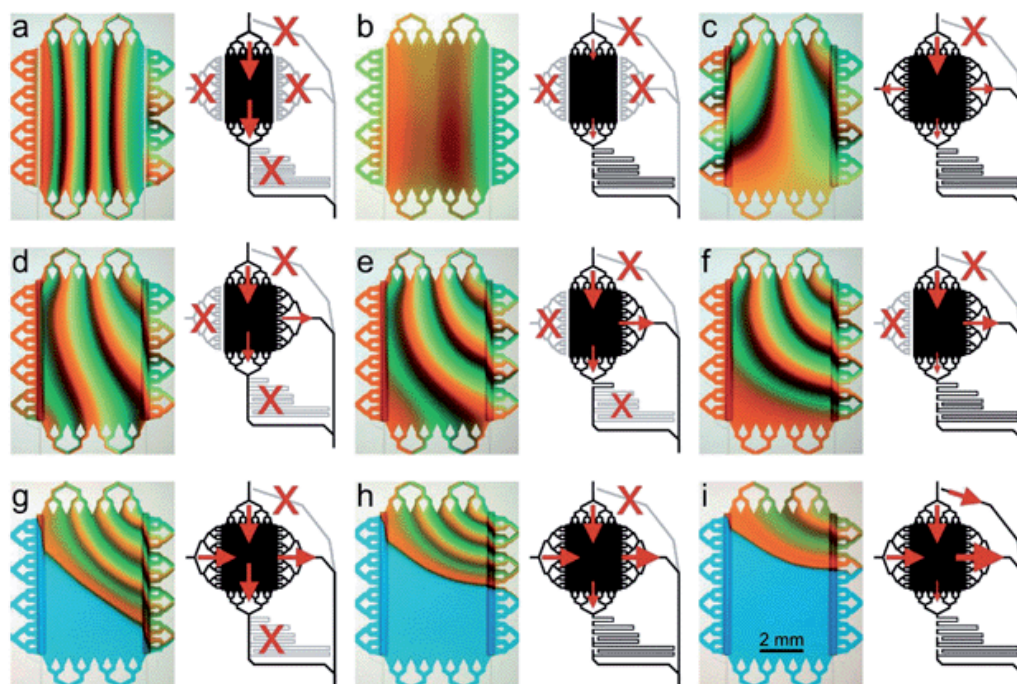


**Figure 1.4.** Examples of diffusion gradient-based concentration profiles on microfluidic chips. Reprinted with permission<sup>69</sup>. Copyright 2009, Royal Society of Chemistry.

diffusion-based gradients<sup>70,71</sup>. Two fluids are simultaneously flowed parallel to one another along the length of a channel or chamber, establishing a gradient that is perpendicular to the direction of the flow (Fig. 1.4). This principle has been used to design microfluidic devices capable of preparing up to 81 chemical combinations<sup>69</sup>. The total possible outputs depend on the number of inputs (16 stock solutions are needed to produce 81 different solutions) and because this approach is diffusion-based, it offers poor spatio-temporal resolution. Several active mixing techniques<sup>72</sup> including mechanical micromixers<sup>73</sup>, microstructures<sup>74</sup>, integrated peristaltic pumps<sup>75</sup>, and serial dilution schemes<sup>76</sup> have been developed to provide fast concentration changes. Nevertheless, on these devices the number of possible concentrations produced is also limited and defined by the number of solution inputs.

To generate small changes in concentration over a large range, dynamic strategies such as pulse-width modulation (PWM) are necessary. PWM (Fig. 1.5) is an electrical engineering concept that encodes an analog signal in a series of repeating on and off pulses of supplied current or voltage<sup>77</sup>. The microfluidic equivalent switches between flowing buffer and substrate reservoirs. Alternating pulses of buffer and substrate are directed through a long mixing channel, where they diffuse to homogeneity. Total cycle time (time to execute one pulse of buffer and one pulse of substrate) is kept constant. Different concentrations are created by varying the duty cycle, which refers to the fraction of time occupied by the substrate pulse in comparison to the total cycle time.

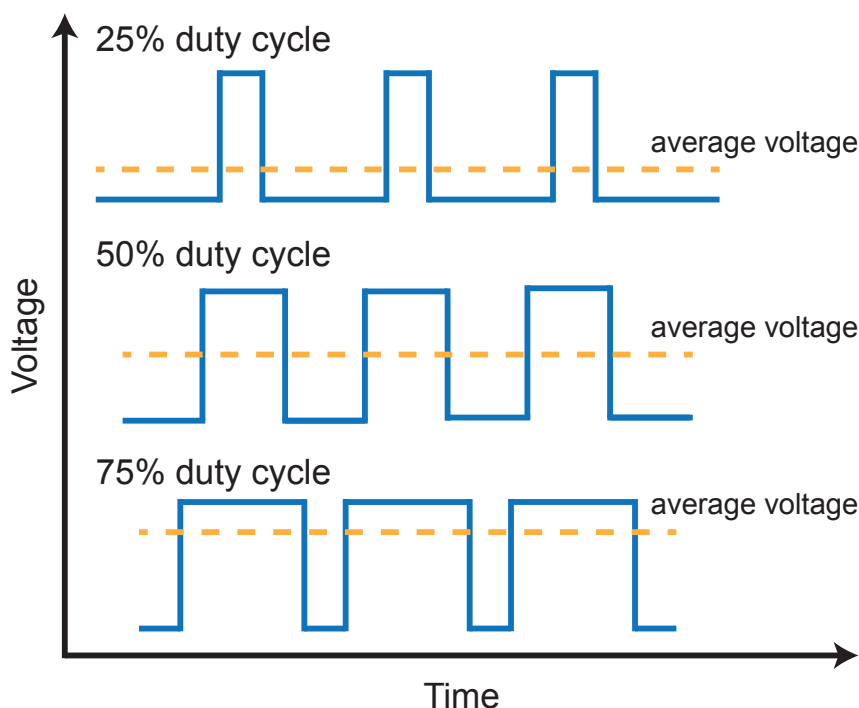


**Figure 1.5.** Using pulse-width modulation with different duty cycles to vary output. On = high level, off = low level.

## 1.7 Pharmacokinetic/pharmacodynamic studies on microfluidic devices

Long-term concentration manipulation orchestrated by PWM on microfluidic devices would be interesting for pharmacokinetic and pharmacodynamic (PK/PD) studies. These assays are central to drug discovery and development<sup>80,81</sup>. For example, monitoring the concentration of a drug in plasma over time reveals information on the efficacy of a drug's delivery method, release from pharmaceutical formulation, adsorption into circulation, distribution into fluids and tissues, and metabolism and excretion (Fig. 1.6). Measuring bacterial load along the course of a well-characterized PK profile could yield information on the mechanism of an antibacterial drug and determine whether adjustments in factors such as drug dosage, administration, or formulation are needed. Performing these assays *in vitro* would provide predictions that could reduce both the cost and duration of clinical trials. Existing *in vitro* PK/PD models generally consist of a central bacteria-containing component connected to drug and medium reservoirs controlled by syringe pumps<sup>82</sup>. While able to properly reproduce the pharmacokinetics of drugs *in vivo*, these models supply only bulk measurements. The simplified, large setup poorly represents the complex *in vivo* environment and is not compatible with techniques that probe single cell phenotypes. Although microfluidic chips have been designed to address this need<sup>83,84</sup>, these devices lack the ability to simulate the gradually rising and falling concentrations of drugs in plasma. Ideally, a device should be able to create



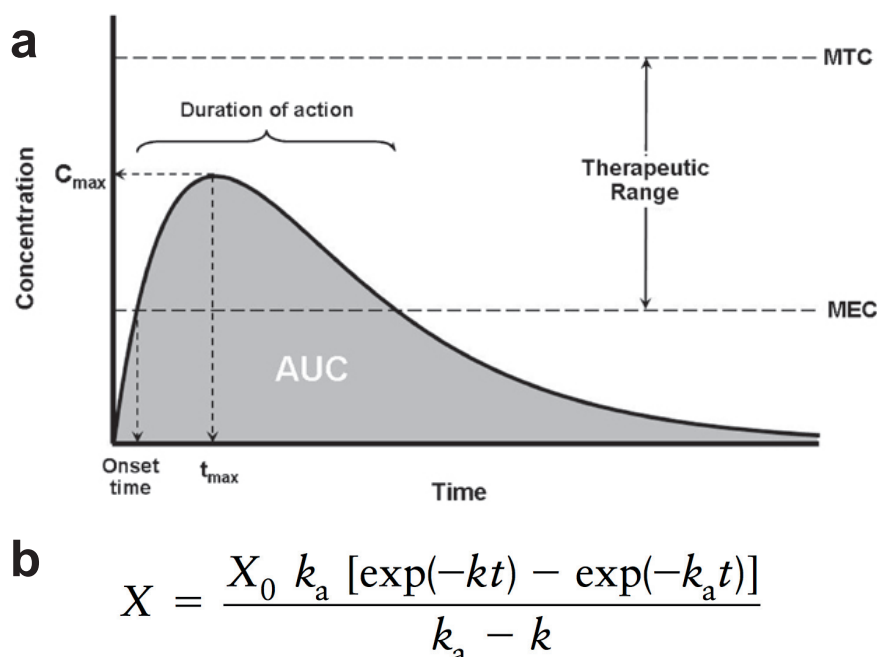


**Figure 1.6.** (a) Pharmacokinetic parameters describing a typical plasma concentration time profile after an oral administration of a drug.  $C_{\max}$ , maximum concentration;  $t_{\max}$ , time to  $C_{\max}$ ; AUC, area under the curve; MEC, minimum effective concentration; MTC, maximum tolerated concentration. Reprinted with permission<sup>78</sup>. Copyright 2006, Nature Publishing Group. (b) The equation<sup>79</sup> characterizing the time-concentration profile for a single oral dose of a drug, such as the one shown in (a).  $k_a$  = absorption rate constant,  $k$  = elimination rate constant,  $X$  = amount of drug in the body,  $X_0$  = amount of drug at the absorption site,  $t$  = time.

realistic PK/PD profiles for multiple substances at once. PWM-based microfluidic devices could facilitate *in vitro* PK/PD studies, but existing PWM chips<sup>85–87</sup> are restricted in versatility (limited suitability for different flow rates, molecule sizes, multiple molecules in parallel, etc.) and have not been used for experiments longer than 1.5 h, limiting their utility for biological assays.

## 1.8 Objectives and overview of this work

As previously described, new and improved high-content screening methods would be beneficial for studying large libraries of cells and rare cell types. In Chapter 2 of this work, we present a contact spotting method to create nanowell arrays of live mammalian cells (LMCAs). The technique uses standard laboratory equipment and is compatible with both primary cells and commonly used cell lines. Following deposition of cells into the wells, the arrays can be cultured for extended periods of time and monitored by microscopy. Our technique is a simple yet powerful alternative to robotic fluid manipulation and inkjet printing and can be used for high-content analysis.

## Chapter 1. Introduction

---

Dense cell culturing setups can also be achieved using microfluidic devices, which are likewise easily adapted to high-content imaging<sup>88–90</sup>. Chapter 3 describes the integration of reverse transfection with microfluidics. We addressed the limitations of current platforms by engineering a novel microfluidic device that performs high-throughput transfection, culturing, and manipulation of cells. The microfluidic environment permits time-lapse studies and can introduce fluidic stimuli, for instance changes in the culturing medium or perfusion with a drug<sup>58</sup>. We demonstrated the utility of this device by using it to characterize synthetic gene circuits. Mammalian synthetic biology could have far-reaching clinical implications, but the lack of suitable methods for large-scale transfection optimization and screening represents a significant bottleneck. Our device streamlines the processes of transfection optimization, cell culturing, and circuit testing, increasing the throughput and accessibility of mammalian synthetic biology.

In addition to the high-throughput protein expression platform detailed in Chapter 3, another useful feature for microfluidic chips would be an accurate and automated method to manipulate molecular concentrations on chip. The ability to generate arbitrary and complex temporal concentration profiles would enable biologically relevant experiments. In Chapter 4, we describe the development of a PWM-based microfluidic device that implements concentration changes over both short and long time scales, making it capable of producing complex PK/PD profiles. The module is easily integrated into existing chip designs or connected upstream of a second chip. Our chip can function with a variety of molecule sizes and flow rates, and two substances can be manipulated in parallel. The chip supports a dynamic range of nearly 3 orders of magnitude in output concentrations. The device presented in Chapter 4, taken together with the developments discussed in Chapters 2 and 3, highlights novel applications of microtechnologies while maintaining the original advantages of automation, small sample size, and high-throughput.

## 2 Live mammalian cell arrays

Article published in Nature Methods, 2013

**Authors:**

Kristina Woodruff, Luis M Fidalgo, Samy Gobaa, Matthias P Lutolf & Sebastian J Maerkl

**Contribution:**

KW designed and performed experiments and wrote the paper. LMF and KW contributed equally to this work.

**Bibliographic reference:**

Woodruff, K., Fidalgo, L. M., Gobaa, S., Lutolf, M. P. & Maerkl, S. J. Live mammalian cell arrays. Nature Methods 10, 550–552 (2013). DOI: 10.1038/nmeth.2473

Permission to reproduce the article is granted by Nature Publishing Group.

### 2.1 Abstract

High-content assays have the potential to drastically increase throughput in cell biology and drug discovery, but handling and culturing large libraries of cells such as primary tumor or cancer cell lines requires expensive, dedicated robotic equipment. We developed a simple yet powerful method that uses contact spotting to generate high-density nanowell arrays of live mammalian cells for the culture and interrogation of cell libraries.

### 2.2 Introduction

Cell-based assays and the tools used to perform them are constantly undergoing improvements toward higher experimental throughput, reduced reagent consumption and advanced control of the cell microenvironment<sup>7,91</sup>. There are currently two main approaches for conducting high-content cell culture experiments. In the first, cells are cultured in microtiter plates, and robotic equipment is used to perform all necessary fluidic operations<sup>92</sup>. Although effective, this method remains unavailable to researchers in many laboratories because of the requirement for expensive robotics. A second approach is reverse transfection<sup>33,93,94</sup>, but complex cell libraries cannot be investigated by this method.

As an alternative, contact spotting offers an affordable yet high-throughput platform. This technique is extensively used to generate high-density DNA and protein arrays and has been adapted to other purposes<sup>17</sup>. To date, contact spotting has not been used to array live mammalian cells because of rapid spot evaporation and consequent cell death. Therefore, arraying of live mammalian cells has been limited to inkjet printing, which lacks the ability to handle a large number of different samples<sup>14,18</sup>.

Large collections of mammalian cell lines have recently become available, including primary tumor and cancer cell lines<sup>3</sup>, stably transfected expression cell lines, and GFP-fusion libraries<sup>2</sup>. Novel approaches are required to efficiently assemble complex arrays of hundreds to thousands of genetically diverse cells. We developed a simple, fast, and scalable method that uses standard microarray printing tools to generate high-density nanowell arrays. A minimal sample requirement of 500 cells enables the interrogation of cells that are available in limited quantities or cells that cannot be expanded because of undesirable changes in phenotype or genotype, as in the case of stem cells and cancer cell lines<sup>5</sup>.

### 2.3 Results

#### 2.3.1 A robust method to array live cells

We generated live mammalian cell arrays (LMCAs) of both primary cells and commonly used cell lines. We collected cells from standard culture formats and resuspended them in Percoll, a high-density, cell-compatible colloidal suspension routinely used for the isolation of primary

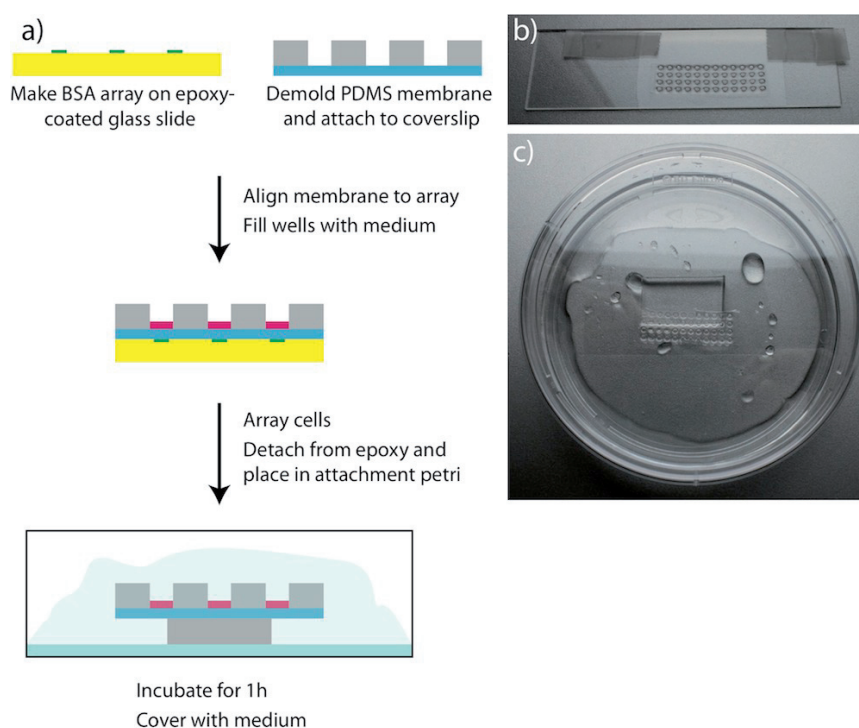


**Figure 2.1.** Substrate preparation and cell attachment. (a) Schematic: a perforated PDMS membrane of approximately  $400\ \mu\text{m}$  thickness was cut and adhered to a microscope coverslip. Separately, an array of 1% BSA matching the pitch of the membrane was spotted onto a microscope slide. The membrane wells on the coverslip were manually aligned to the BSA spots on the slide. The nanowells were filled with medium before cell spotting. Spotted arrays were incubated for one hour in a humidified petri dish to allow for cell attachment. After incubation, the array was covered with medium for culture. (b) Photograph of the PDMS membrane, the coverslip, and the epoxy slide. (c) Photograph of an array inside a petri dish during the cell attachment stage. The water in the dish quickly evaporates, saturating the atmosphere in the petri dish and preventing evaporation from the nanowells while cells attach.

cells. Cells plated in conical 384-well plates were taken up by a microarray spotting pin and delivered to a 48-well poly(dimethylsiloxane) (PDMS) array ( $\sim 20$  wells/ $\text{cm}^2$ ) or a 675-well acrylic array ( $\sim 36$  wells/ $\text{cm}^2$ ) adhered to a coverslip or glass slide, respectively (Fig. 2.1). For comparison, the density of a 1,536-well plate is 14 wells/ $\text{cm}^2$ . Each nanowell has a 500-nl capacity and was filled with medium before array spotting to ensure viability of the added cells and to enable the automated handling of nanoliter volumes of live cells. Once arrayed, cells were incubated in a high-humidity environment for 60 min to allow them to attach to the glass surface (Fig. 2.1). After attachment, the array was submerged in medium for culturing and imaging (Fig. 2.2a).

Arraying cells suspended in standard medium resulted in poor performance in terms of cell transfer, requiring hundreds of thousands of cells per sample (Fig. 2.2b). Resuspending cells

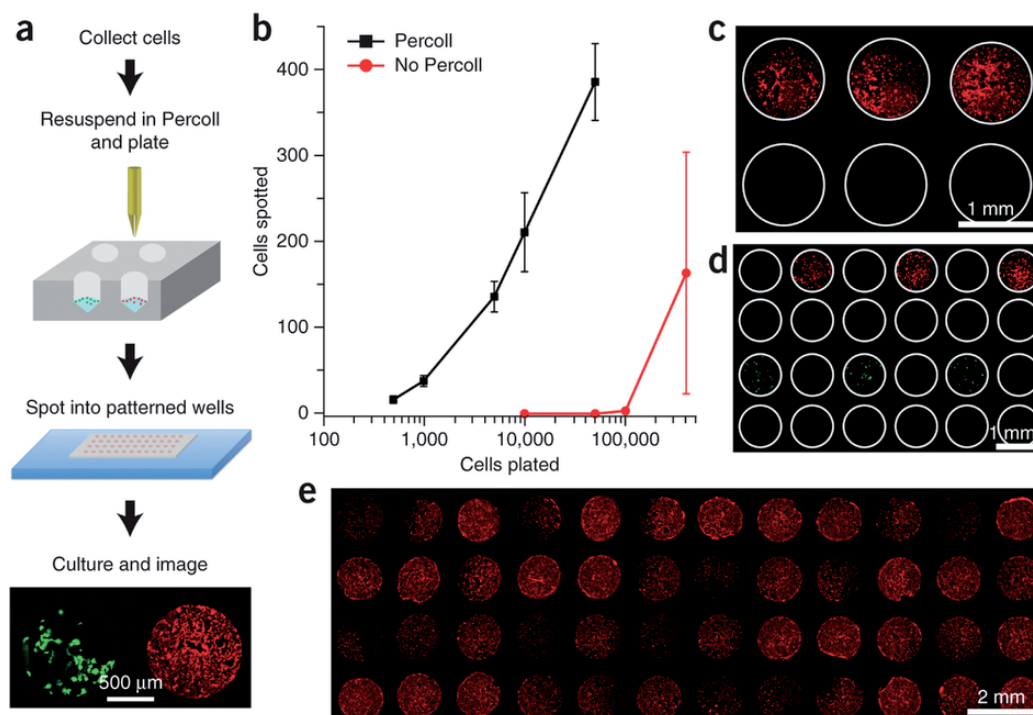


**Figure 2.2.** A method to array live mammalian cells. (a) Schematic of the method. (b) Quantification of cell transfer. The number of cells transferred to a nanowell (cells spotted) from source wells containing the indicated number of cells (cells plated) with and without Percoll. Error bars, s.d. ( $n = 3$ ). (c) Micrograph of NIH-3T3 fibroblasts expressing tdTomato spotted in the top row, to assess cell carryover by the spotting pin. (d) Micrograph of an array in which three wells were spotted with 3T3 fibroblasts expressing tdTomato (first row) and three wells were spotted with HEK293 cells expressing GFP (third row) to assess direct cell transfer across wells. (e) Micrograph of a 48-well array seeded in all wells with NIH-3T3 fibroblasts expressing tdTomato and imaged 2 d after spotting.

in Percoll improved the efficiency of transfer by several orders of magnitude. This approach allowed spots containing  $\sim 40$  cells to be reproducibly arrayed from samples of 1,000 cells (Fig. 2.2b). The number of cells delivered to each nanowell can be tuned by the initial sample cell density, so that  $\sim 10$ -400 cells can be delivered from input samples of 500-50,000 cells (Fig. 2.2b). The number of cells transferred decreased with successive printings, but it was nonetheless possible to print repeatedly from the same sample (Fig. 2.3).

### 2.3.2 Cross-contamination on the arrays

Cross-contamination between nanowells can, in principle, occur by two mechanisms: (i) carryover of cells between spots by the pin and (ii) direct transfer of cells between nanowells when medium is added to the nanowell array. To investigate contamination via carryover, we alternated spotting samples of cells and, as negative controls, samples of medium, with a

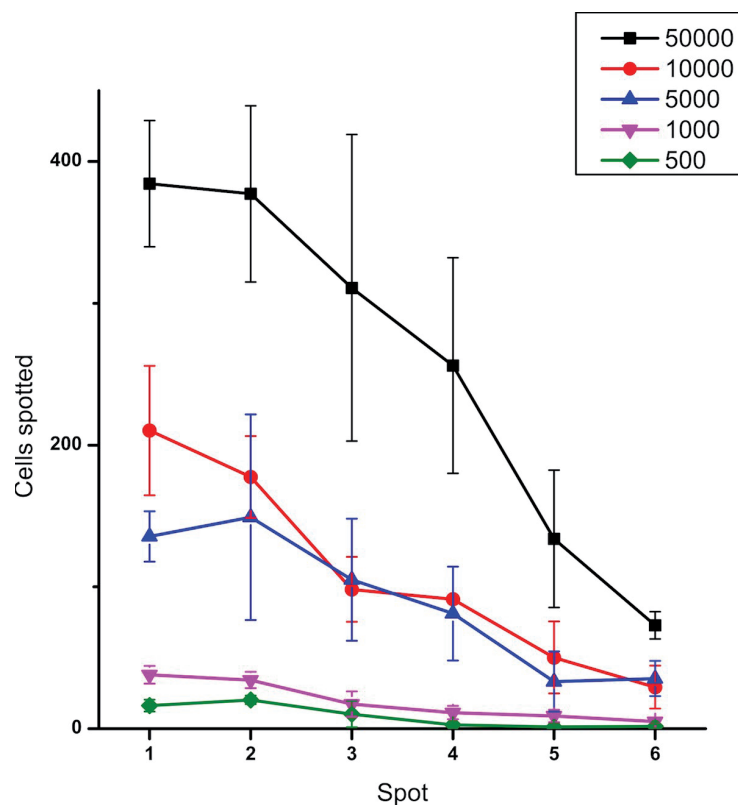


**Figure 2.3.** Quantification of cell transfer vs. number of spots printed from the same well for five different cell densities. The number of cells transferred decreases as multiple spots are printed from the same well, but it is nevertheless possible to reliably print several samples using as few as 1,000 cells. Data points are the mean s.d. (n=3).

pin-wash cycle between each sample (see methods). We found no cells in the negative control nanowells (Fig. 2.2c). To investigate contamination during addition of medium, we spotted an array of cells in which most wells were left empty. These originally empty wells remained uncontaminated after the exchange of medium (Fig. 2.2d). When printing larger arrays in which all nanowells were programmed with cells, we identified a low degree of contamination, amounting to 2 of 48 nanowells (4%; Fig. 2.4).

### 2.3.3 Viability of multiple cell types after arraying

To assess the viability of cells after the arraying process, we prepared 48 separate aliquots of NIH-3T3 fibroblasts on a source plate and transferred each aliquot to a separate nanowell. We washed the pin after spotting each sample, thus simulating the arraying of 48 different cell samples (Fig. 2.2e). The fibroblasts stably expressed a red fluorescent protein that rapidly disperses upon cell lysis, allowing fluorescence to serve as a direct measure of cell viability. After the cells were arrayed, they remained viable and quickly became confluent in the nanowell

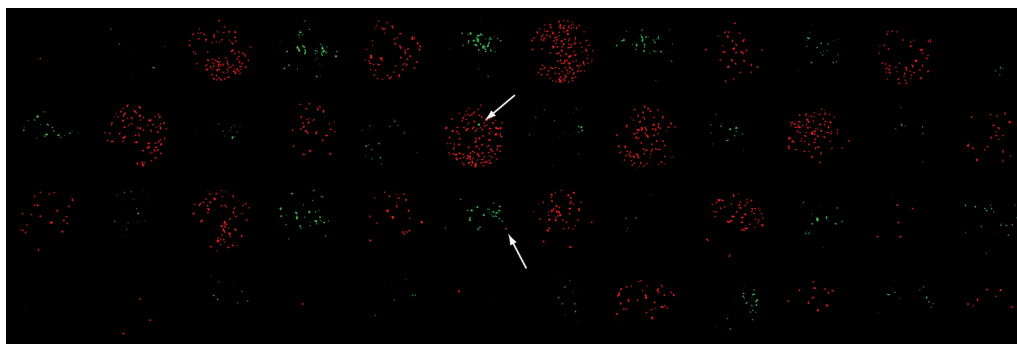


**Figure 2.4.** Quantification of contamination due to direct transfer of cells across wells. Collage of micrographs of an array prepared with a checkerboard pattern of red and green fluorescent cells after one day of culture. The cells used were tomato NIH-3T3 and GFP HEK293. The array was prepared by plating 48 wells with samples containing 5,000 cells each and spotting a single time from each of them. We observed cells that do not correspond to the printed type in two separate nanowells, one cell in each case (arrows).

(Fig. 2.5). We also tested the viability of cells in LMCAs after freezing them. We could freeze and thaw both the 48-well PDMS and the 675-well acrylic LMCAs without substantial effects on cell viability (Fig. 2.6).

The LMCA method can be applied to a variety of mammalian cell types, including NIH-3T3 fibroblasts, human liver carcinoma (Hep G2), human embryonic kidney (HEK) and Chinese hamster ovary (CHO) cells (Fig. 2.7, 2.8a). We also applied this method to primary cells. We spotted human bone marrow-derived mesenchymal stem cells (hMSCs) and maintained them in culture for over 2 weeks with no contamination or detectable decrease in cell viability (Fig. 2.8a).

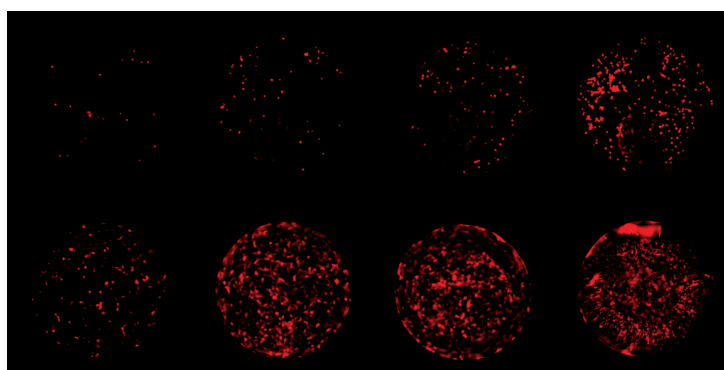


**Figure 2.5.** Micrographs of four nanowells where an increasing number of cells was printed. The upper and bottom rows show cells after one and three days of culture, respectively. Cells grew rapidly, indicating that they sustained no damage during the spotting process.



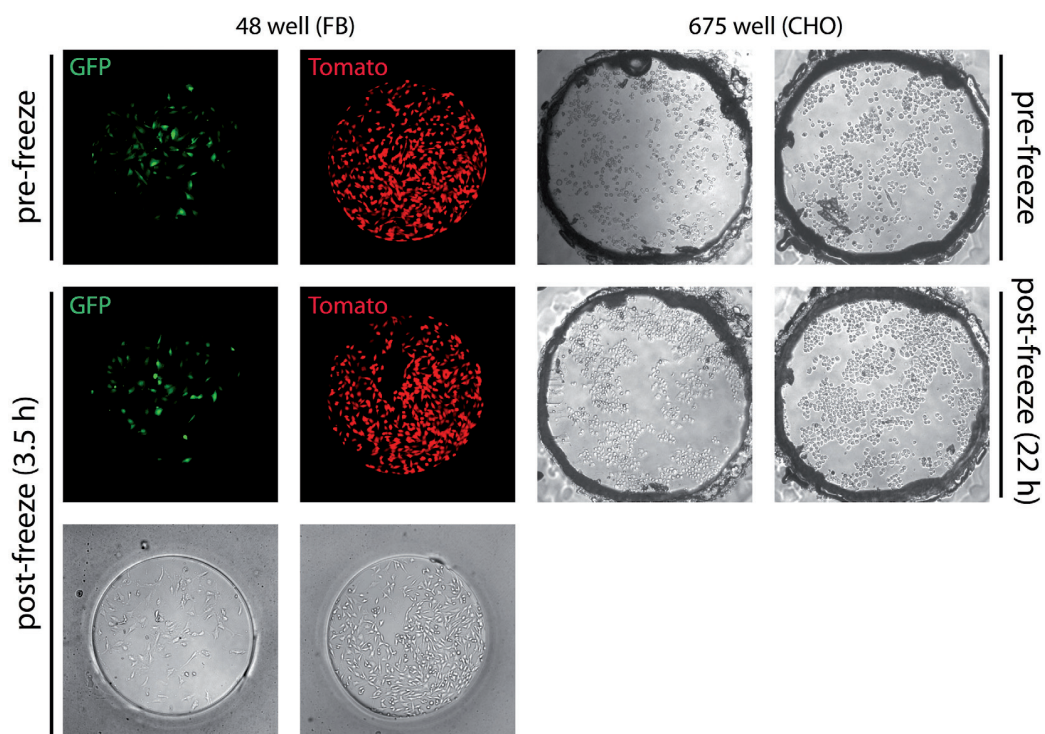


**Figure 2.6.** Freezing of LMCAs. The cells used for the 48 well PDMS array were tomato and GFP NIH-3T3 fibroblasts (left two panels). Micrographs of the 48 well array were taken immediately before freezing and 3.5 h after thawing the array. CHO cells were used for the 675 well array (right two panels). Micrographs of the 675 well array were taken immediately before freezing and 22 h after thawing the array. Cells did not significantly detach from the array during the freeze/thaw procedure and remained viable.

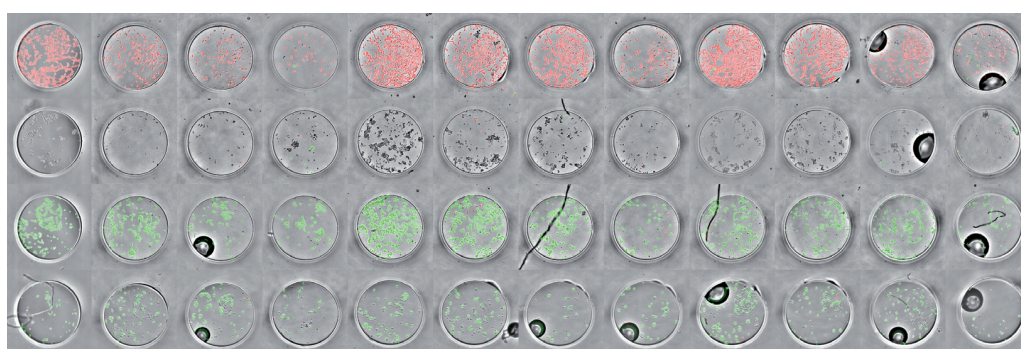


**Figure 2.7.** Collage of micrographs of an array featuring four different cell types separated by rows: NIH-3T3, HepG2, CHO and HEK2993. All cells are viable after one day of culture, and those expressing a fluorescent marker continue to do so. For each row in the array, three separate input wells containing 10,000 cells each were used. Cells were printed sequentially from left to right.

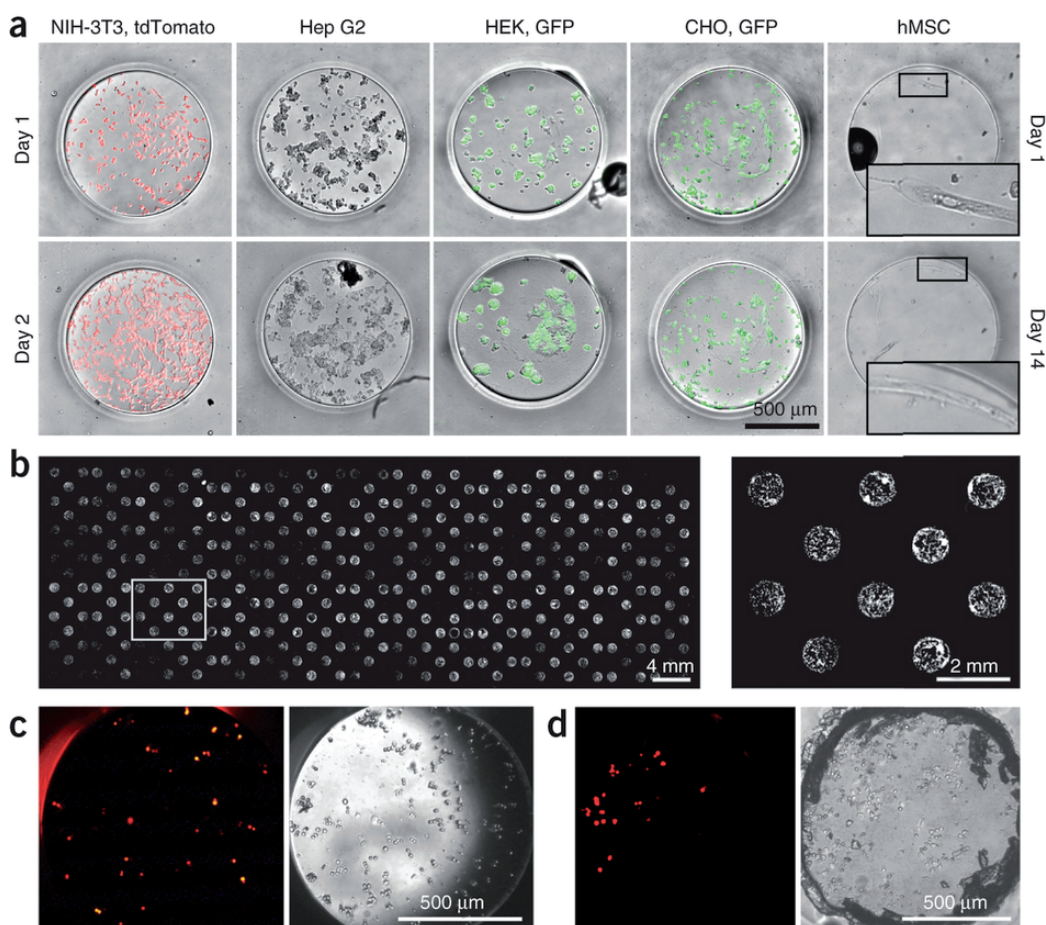


**Figure 2.8.** Applications of the arraying method. (a) Brightfield and fluorescence images of five cell types spotted and cultured in PDMS nanowell arrays. hMSCs were cultured for up to 14 d (insets show magnification of boxed regions); all other cell types were cultured for up to 2 d. (b) Fluorescence micrograph of an entire 675-well acrylic array in which 339 of the wells were spotted with 3T3 fibroblasts by simultaneously using three spotting pins. Boxed region of the array is magnified on the right. (c) Fluorescence (left) and brightfield (right) images, 20 h after reverse transfection of CHO cells with plasmid encoding tdTomato (spotting of a lipid-DNA mixture) in 48 nanowells of a PDMS array followed by manual addition of cells. (d) Regular transfection of CHO cells spotted into the 675-well array, followed by spotting of tdTomato plasmid transfection mixture into the wells. Images were acquired 45 h after transfection.

### 2.3.4 High-density LMCAs

To test the scalability of this technique, we also used acrylic arrays with 675 nanowells (Fig. 2.8b, 2.9). The 675-nanowell arrays are commercially available (ALine, Inc.), and dimensions such as well size and pitch can be customized. Our array had wells of 1 mm diameter and 1.5 mm pitch, enabling the entire substrate to fit on a microscope slide. A single 4-well



**Figure 2.9.** Fluorescence micrograph of an entire 675-well acrylic array in which some of the wells were spotted with tdTomato-expressing 3T3 fibroblasts by simultaneously using three spotting pins. Boxed region of the array is magnified on the right.

microtiter plate could thus be used to culture up to 2,700 cell types. We programmed 339 of the 675 wells with cells (Fig. 2.8b). Twenty-four hours after spotting, 331 of the wells contained viable cells, indicating a 2% failure rate in cell transfer. Forty wells that were not originally spotted contained cells (32 contained a single cell and the rest contained two or three cells). Therefore, 7% (48 of 675) of the nanowells were either contaminated or contained no cells when they should have had cells.

### 2.3.5 Transfection on the LMCAs

LMCAs are compatible with transfection. The standard reverse transfection protocol uses microarraying pins that generate small diameter spots (120-150  $\mu\text{m}$ ) that dry rapidly and uniformly<sup>33</sup>. However, for our LMCA nanowells, spots of 1 mm diameter were required. Larger spots tend to dry slowly and unevenly, causing the majority of the transfection reagent to concentrate at the edges of the nanowell. Reverse transfection has been achieved using the large wells of 24-well microtiter plates<sup>95</sup>, but the microliter volumes of reagents administered to each well preclude the use of a microarrayer. We developed a method that uses the microarraying pin for automated deposition of homogeneous lipid-DNA spots into the nanowells of our PDMS arrays. Upon introducing cells into the wells with a micropipette, we achieved 32% transfection efficiency, with transfected cells uniformly distributed throughout the nanowell (Fig. 2.8c). Manually depositing larger volumes of reagent did not improve efficiency (Fig. 2.10), suggesting that our spotting protocol was sufficient to increase the local concentration of the transfection reagent at the site of cell attachment. Our method addresses two limitations of standard reverse transfection: the physical separation of cells on our array prevents cross-contamination and also allows for the inclusion of additional soluble factors.

We also tested a regular transfection approach, spotting cells before adding lipid-DNA complexes. Using the acrylic 675-well array, transfection efficiency was 20% for the wells with manually added transfection reagent (Fig. 2.8d). Efficiency was lower for wells in which the lipid-DNA was introduced by a microarraying pin (13%), most likely due to the limited  $\sim 20$  nl transfer volume of the pin (Fig. 2.10). We achieved considerably lower efficiency with the PDMS 48-well array (Fig. 2.10).

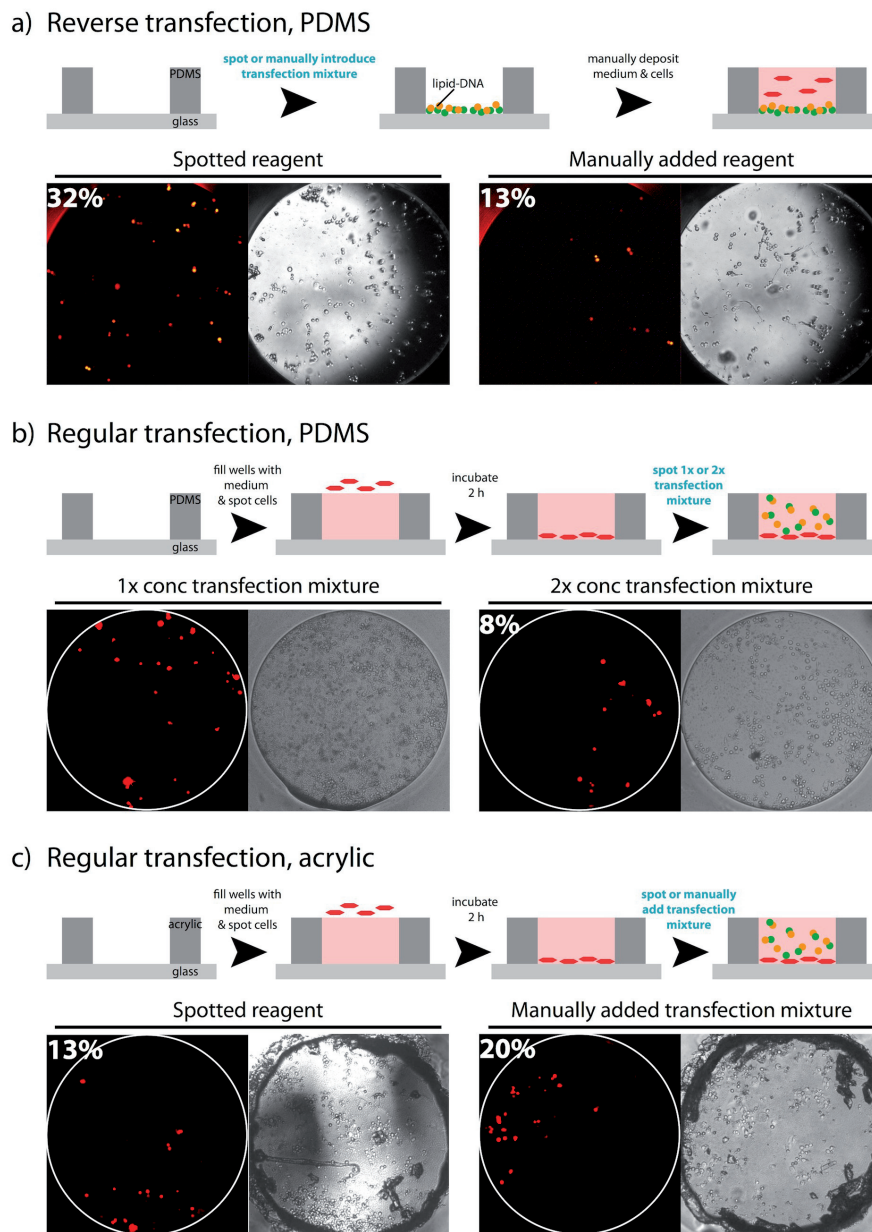


**Figure 2.10.** (a) Reverse transfection, 48 well PDMS array. Lipid-DNA mixture was spotted or manually deposited into the nanowells and dried, then CHO cells were manually added. (Images: 20 h). Left panels: tdTomato fluorescence (transfected cells), right: brightfield. When available, transfection efficiencies are indicated. (b) Regular transfection, 48 well PDMS array. CHO cells were spotted into the array, followed by spotting of a 1x or 2x concentrated transfection mixture into the wells. (Images: 42 h). Transfection efficiency was lower on the PDMS array when compared to the acrylic array and was not improved by using higher concentrations of transfection reagent. The hydrophobic PDMS may sequester the lipid transfection reagent; in regular transfection the lipid-DNA mixture is exposed to the PDMS when it is added to medium-filled nanowells. (c) Regular transfection, 675 well acrylic array. CHO cells were spotted into the array and transfection mixture was spotted or manually deposited into the wells. (Images: 45 h.)

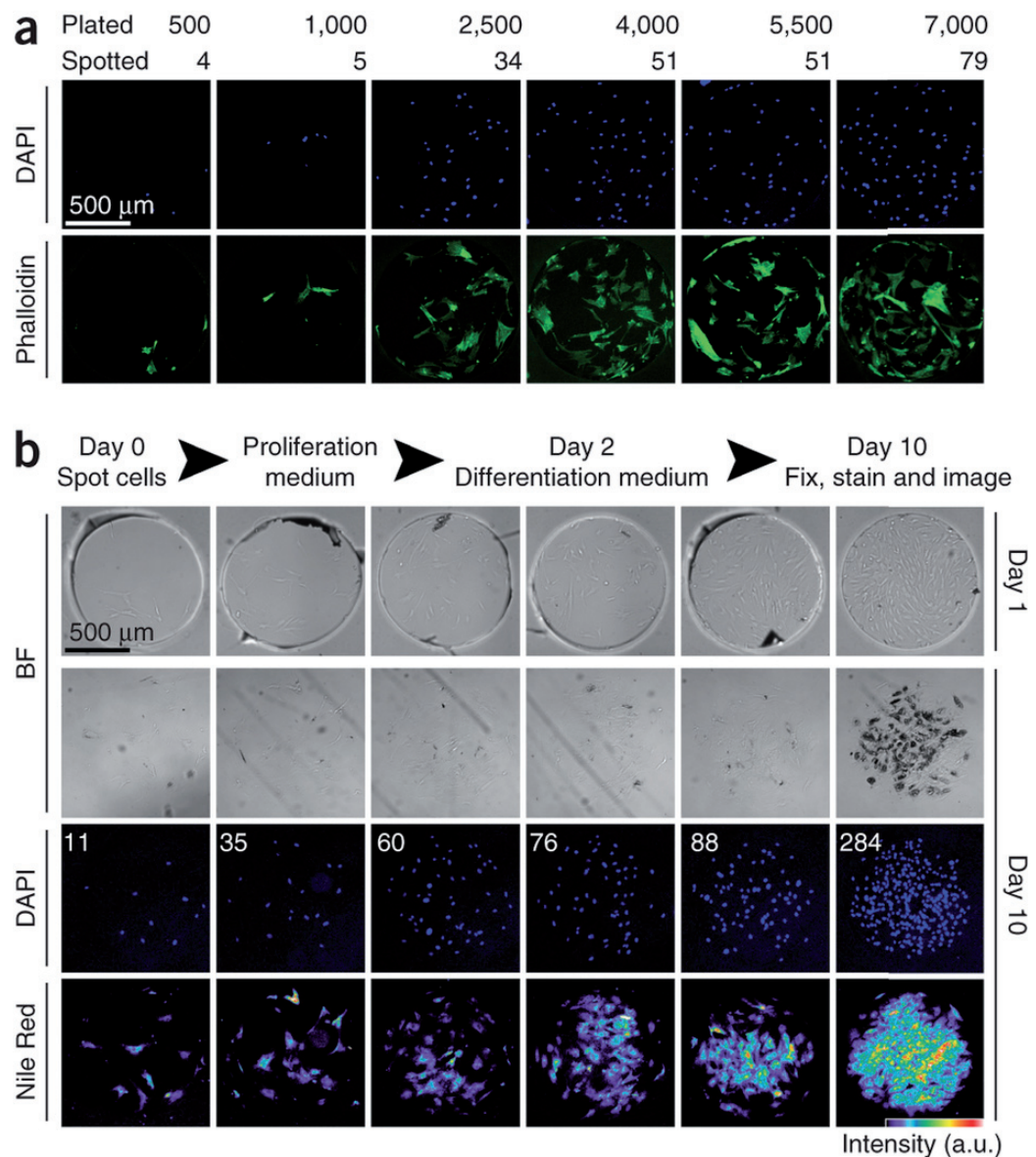


**Figure 2.11.** Human mesenchymal stem cell array. (a) DAPI and phalloidin stains of hMSCs spotted into the 48-well PDMS array from sample wells containing 500-7,000 cells. (b) hMSC differentiation scheme and micrographs of individual nanowells from the PDMS array. Bright-field (BF), DAPI and Nile Red stains are shown. On the DAPI micrographs, total cell numbers are indicated. In the Nile Red pseudocolor scale, the highest adipogenic differentiation is indicated by red and white pixels.

### 2.3.6 Primary cells on the LMCAs

We also spotted hMSCs at different densities in a controlled fashion, which resulted in a cell-transfer efficiency similar to that observed with standard cell lines (Fig. 2.11a). We could

spot ~5 cells into the nanowells when using a sample well containing as few as 500 cells, and up to ~80 cells when using samples of 7,000 cells (Fig. 2.12).

We repeatedly used each sample well to spot 4 nanowells, which resulted in fewer cells deposited into each subsequent nanowell. We investigated the adipogenic differentiation potential of hMSCs cultured on arrays for up to 10 d. We spotted the hMSCs at a variety of densities and incubated the array in proliferation medium for 2 d. Then we placed the array into differentiation medium for 8 d. At the end of the 10-d period, we fixed the array, stained it with DAPI and Nile Red, and imaged it. Wells that initially contained larger numbers of cells exhibited pronounced adipogenic differentiation, as measured by Nile Red staining (Fig. 2.11b). These cells produced large lipid vesicles that appeared as dark spots in brightfield. In contrast, wells seeded at lower densities contained cells that differentiated to a lesser extent and produced fewer and smaller lipid vesicles.

## 2.4 Conclusion

In summary, we generated high-density LMCAs with a variety of mammalian cell types using contact spotting. This method requires only a standard contact microarrayer and a nanowell array that can be easily fabricated<sup>96</sup> or commercially acquired (ALine, Inc.). The cell arrays could also be used in conjunction with arrays of hydrogels and biomolecules or for screening of artificial extracellular matrix<sup>6,97</sup>. The high-throughput approach to cell handling will enable the parallel culture and analysis of large libraries of mammalian cells.

### 2.4.1 Acknowledgments

We thank D. Hacker (Laboratory of Cellular Biotechnology, Institute of Bioengineering, Ecole Polytechnique Fédérale de Lausanne) for kindly providing GFP-expressing CHO and HEK cells, and V.M. Mangoua, A. Ranga and A. Negro for help with the project. The work was funded by a Marie Curie fellowship (FP7-PEOPLE-2009-IEF 252457), by a SystemsX.ch Research, Technology and Development grant: DynamiX (2008/005), a Swiss National Science Foundation Pro-Doc grant (PDFMP3 137065), a European Young Investigator grant PE002-117115/1 to M.P.L. and the Ecole Polytechnique Fédérale de Lausanne.

### 2.4.2 Author contributions

L.M.F., K.W., M.P.L. and S.J.M. designed experiments and developed the method. L.M.F. and K.W. performed experiments. S.G. assisted with cell culturing and image processing and provided transfection reagents. L.M.F., K.W., M.P.L. and S.J.M. wrote the paper. S.J.M. conceived the idea.

### 2.4.3 Competing financial interests

The authors declare no competing financial interests.

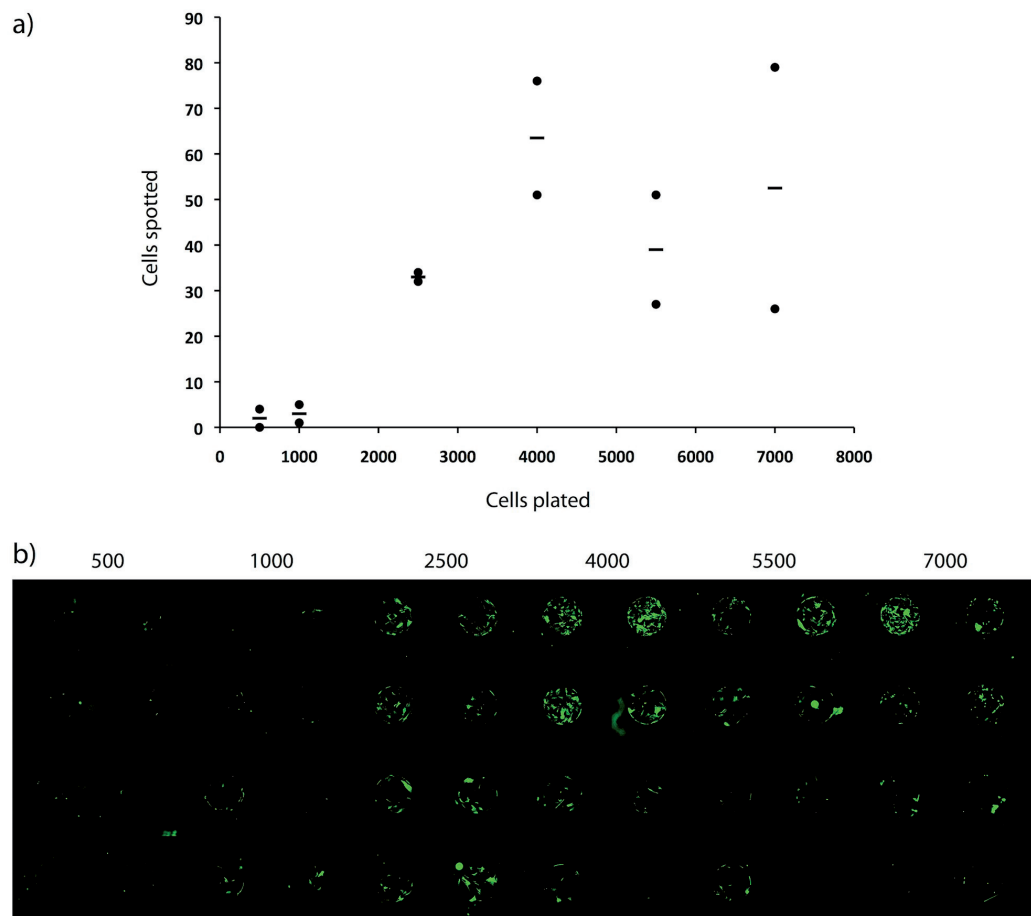


**Figure 2.12.** (a) Quantitation of the MSC array shown in (b). The number of hMSCs spotted into the array can be tuned by adjusting the number of cells in the well plate sample. Two separate well plate preparations were tested for each cell concentration (circles, with the mean value represented by the bar). hMSCs were spotted into the 48 well array at increasing densities from left to right. The number of cells in each sample well ranges from 500 to 7,000. Each sample in the well plate was used to spot 4 nanowells (one column), resulting in decreased cell density from the top to the bottom of each column. Only the top row of the spotted array was used for quantitation. (b) The hMSC cell array. Phalloidin staining was used to visualize cell shape.

## 2.5 Methods

### 2.5.1 Substrate fabrication

PDMS membranes were molded from SU8 structures fabricated on silicon wafers using standard photolithography methods<sup>98</sup>. Two layers of approximately 200  $\mu\text{m}$  thickness were spun and baked before exposure and development. Before use, the structures were silanized using 1H,1H,2H,2Hperfluorooctyl trichloro silane (Sigma) as previously described<sup>99</sup>. The wafers were spin coated with PDMS (RTV615, General electric, 60 s at 150 r.p.m. and 120 s at 350 r.p.m.). The coated wafer was degassed for 5 min and left to reflow for 25 min at room temperature before baking for 30 min at 80 °C. This process resulted in a perforated membrane of ~200  $\mu\text{m}$  thickness. The membrane had 48 wells of 1 mm of diameter with a pitch of 2.25 mm.

The patterned PDMS was cut from the wafer and transferred to glass microscope coverslips. Separately, an array of BSA that matched the pitch of the membrane was spotted onto an epoxy covered microscope slide. The membrane wells on the coverslip were manually aligned to the BSA spots on the slide using a stereoscope, providing a simple method to ensure alignment between the arraying robot and the microfabricated substrate. For some samples, a PDMS frame surrounding the membrane was manually cut and bonded to the coverslip using oxygen plasma. This frame provided an efficient medium container around the membrane and enabled high-resolution imaging of the coverslip-supported cell array. Samples were UV light-sterilized after assembly and coated with fibronectin (Sigma) either by spotting a concentrated suspension (1 mg/ml) or by 1-h incubation in a dilute solution (50  $\mu\text{g}/\text{ml}$ ).

The 675-well array plastic substrates were purchased from ALine, Inc. The arrays consisted of a 500  $\mu\text{m}$  acrylic layer and a 50  $\mu\text{m}$  silicone adhesive layer. They had wells of 1 mm diameter with 1.5 mm pitch and were adhered to glass microscope slides by passing them slowly through lamination rollers at 60 °C. Arrays were not treated with fibronectin before cell spotting.

### 2.5.2 Cell culture

Cells were cultured in Dulbecco's modified Eagle medium (DMEM) supplemented with 10% FBS and 1% penicillinstreptomycin at 37 °C and 5% CO<sub>2</sub>. For long-term assays, medium supplemented with antibiotic-antimycotic was used. Cells were passaged every 2 d using TrypleE express or trypsin. All culture reagents were acquired from Gibco (Life Technologies). NIH-3T3 fibroblasts stably expressed GFP or tdTomato fluorescent protein, whereas CHO and HEK293 cells expressed GFP (100% and 50% of the cells expressing fluorescent protein, respectively). Other cell lines used included Hep G2 cells, human MSCs and wildtype CHO cells.



### 2.5.3 Cell spotting

Cells were collected from T75 or T25 flasks and washed. After cells were adjusted to the desired concentration, they were transferred to 500  $\mu\text{L}$  Eppendorf tubes in 20- $\mu\text{L}$  aliquots. These aliquots were centrifuged at 300g for 3 min and resuspended in a Percoll standard solution (700  $\mu\text{L}$  Percoll (Sigma), 100  $\mu\text{L}$  10x PBS (Gibco) and 200  $\mu\text{L}$  Milli-Q water). For longer spotting programs, 10x PBS was replaced with 10x DMEM. Cells resuspended in Percoll were plated in 5- $\mu\text{L}$  aliquots onto conical-well, poly(propylene) 384-well plates (Arrayit). Cells were spotted using a pin with a 100- $\mu\text{m}$ -wide channel, a 1.25  $\mu\text{L}$  uptake volume and a nominal 1.5 nl transfer volume (WCMP, Arrayit). Spotting parameters were 2 x 1 s inking time, 2 x 1 s print time per well. The washing protocol consisted of four alternating washes with ethanol and water. The first three washes were 2 s each, and the last wash was 5 s, with 5 s of drying after the last wash. Including spotting and washing, the total time per sample was approximately 30 s, and therefore an array of 48 different samples was completed in under 25 min. Before spotting, the 48-well PDMS arrays were prefilled by manual pipetting  $\sim$ 0.5  $\mu\text{L}$  of 0.7x culture medium into each well. For the 675-well arrays, wells were prefilled by submerging the entire array in 0.7x medium. Air bubbles were removed from wells by pipetting. The array was then slowly removed from the medium, and excess liquid was wiped from the surface. The same printing conditions used for the 48-well array were used for the 675-well array, but only with one 1.5 s water wash and 3 s of drying. During spotting, the humidity in the chamber was set to 70% to reduce evaporation of medium from the wells without causing the printing malfunction that is observed at higher humidity.

### 2.5.4 Array culture

Immediately after spotting, substrates were placed in a petri dish that contained warm Milli-Q water to prevent evaporation during transport to the incubator and during cell attachment. To preserve the integrity of the array, the samples were placed on a PDMS block adhered at the center of the dish, ensuring that the water contained in the dish did not come in contact with the sample. After incubation at 37  $^{\circ}\text{C}$  (1 h for the 48-well array and 3 h for the 675-well array) the cell arrays were covered in medium for culture. To this end, either the coverslip was detached from the epoxy slide and placed in a different petri dish or, for samples with a PDMS frame, medium was directly added to the array.

To prepare arrays for freezing, LMCAs were placed in small plastic containers containing 90% FBS and 10% DMSO. The container was then placed into a cryobox with isopropanol, and frozen at -80  $^{\circ}\text{C}$  overnight. The arrays were thawed by submersion in a beaker of PBS contained in a 37  $^{\circ}\text{C}$  water bath. Once thawed, arrays were washed three times in culture medium to remove residual DMSO.

For primary cell arrays, hMSCs were spotted onto a 48-well PDMS array following the procedure used for other cell types. hMSC proliferation medium consisted of alpha-minimum essential medium (Invitrogen), 10% FBS (Hyclone), 1 ng/ml fibroblast growth factor 2 (FGF2;

R&D Systems), 2 mM l-glutamine (Sigma-Aldrich) and 1% penicillin-streptomycin (Invitrogen). Adipogenic differentiation medium contained low-glucose DMEM (Invitrogen), 20% FCS (Hyclone), 0.5 mM 3-isobutyl-1-methylxanthine (IBMX; Sigma-Aldrich), 60  $\mu$ M indomethacin (Fluka) and 1  $\mu$ M dexamethasone (Sigma-Aldrich). The arrays were fixed in 4% paraformaldehyde for 15 min at room temperature. The PDMS membrane was removed before cell staining. Nuclei were stained with a 10  $\mu$ g/ml solution of DAPI (SigmaAldrich) in PBS. Lipid vesicles were stained with a 1  $\mu$ g/ml solution of Nile Red (Sigma-Aldrich) in PBS. The cell cytoskeleton was visualized by staining with phalloidin–Alexa Fluor 488 (Invitrogen) according to the manufacturer's instructions.

### 2.5.5 Transfection

For the reverse-transfection approach, glass slides coated with poly(l-lysine) (Electron Microscopy Sciences) were used. We diluted 0.37  $\mu$ L DNA (at 1.8  $\mu$ g/ $\mu$ L into 11.13  $\mu$ L of a dextran solution. We added 2  $\mu$ L Fugene (Roche), and the mixture was incubated for 15 min. Then, 46  $\mu$ L polyvinyl alcohol (PVA) was added, and the mixture was spotted into the nanowells using a pin with a 500- $\mu$ m-wide channel, a 1.25  $\mu$ L uptake volume and a 15–25 nl transfer volume (WCMPL, Arrayit). Arrays were allowed to dry, after which cells were introduced into the nanowells by manual pipetting. Spotting conditions for the lipid-DNA mixture were identical to those used for cells except that only one water wash (1 s) with 3 s drying was used between samples, and three stamps per well were implemented. Dextran ( $M_r$ ~40,000, Sigma) was prepared at 45 mg/ml and PVA (molecular weight, 25,000; Polysciences) was prepared at 0.5% (v/v) as described<sup>95</sup>. For regular transfection, cells were spotted as previously described. Two hours after spotting, a lipid-DNA mixture was prepared and spotted into the nanowells as described above, with the modification that fibronectin (1 mg/ml) was used instead of PVA. Regular transfection arrays were not submerged in medium until 20 h after initial cell spotting.

### 2.5.6 Array imaging

Imaging of the 48-nanowell array was performed on a Nikon Ti automated microscope using custom-written software to determine the positions to image trigonometrically and acquire the multichannel images. Images were typically acquired using 10x magnification to capture an entire well in the field of view. Array images were collaged using ImageJ. ImageJ was also used for cell counting. First, images were thresholded and inverted. Then, single cells were counted using the particle analysis functions. Cells that were aggregated or too close for direct counting were counted by measuring their area and calculating the number using a proportion obtained from manual counting of a group of cells from the same sample. DAPI-stained hMSCs were counted using the count nuclei program of Metamorph. Imaging of the 675-nanowell array was performed on a Nikon TI automated microscope using NIS Elements. Each well was imaged with a 4x objective in brightfield and fluorescence mode. The resulting 675 images were first brightness-adjusted and converted to jpeg format from tiff format, and then stitched together using the Grid/Collection Stitching plugin in Fiji<sup>100</sup>.

# 3 A high-throughput microfluidic platform for mammalian cell transfection and culturing

Article published in Scientific Reports, 2016

**Authors:**

Kristina Woodruff & Sebastian J Maerkl

**Contribution:**

KW developed the method, designed and performed experiments, and wrote the paper.

**Bibliographic reference:**

Woodruff, K. & Maerkl, S. J. A High-Throughput Microfluidic Platform for Mammalian Cell Transfection and Culturing. *Sci. Rep.* 6, 23937 (2016). DOI: 10.1038/srep23937

Permission to reproduce the article is granted by Nature Publishing Group.

## Chapter 3. A high-throughput microfluidic platform for mammalian cell transfection and culturing

---

### 3.1 Abstract

Mammalian synthetic biology could be augmented through the development of high-throughput microfluidic systems that integrate cellular transfection, culturing, and imaging. We created a microfluidic chip that cultures cells and implements 280 independent transfections at up to 99% efficiency. The chip can perform co-transfections, in which the number of cells expressing each protein and the average protein expression level can be precisely tuned as a function of input DNA concentration and synthetic gene circuits can be optimized on chip. We co-transfected four plasmids to test a histidine kinase signaling pathway and mapped the dose dependence of this network on the level of one of its constituents. The chip is readily integrated with high-content imaging, enabling the evaluation of cellular behavior and protein expression dynamics over time. These features make the transfection chip applicable to high-throughput mammalian protein and synthetic biology studies.

### 3.2 Introduction

Reverse transfection assays have the potential to analyze the entire proteome in the natural cellular context. Unlike protein microarrays, this method does not require individual purification of each protein<sup>16,34,35</sup>. Instead, reverse transfection arrays utilize purified cDNA samples<sup>33</sup>. The array is seeded with cells, which upon transfection converts the cDNA into protein. Arrays can also be made of siRNA to perform loss-of-function studies. With a pitch of approximately 400  $\mu\text{m}$ , more than 5,000 samples can be printed on a single glass microscope slide<sup>33,36</sup>. A recent study was able to further increase this density, printing spots just 150  $\mu\text{m}$  apart<sup>37</sup>. This throughput is especially important in light of ongoing efforts to screen genome-wide RNAi libraries<sup>38</sup> and cDNA libraries<sup>39</sup>. With the accumulation of data from cDNA microarrays and whole genome sequencing, there is a need to validate protein function and characterize therapeutic targets.

Reverse transfection could also serve as a valuable tool for synthetic biology. Synthetic biology is often performed in prokaryotic models because of the ease with which prokaryotes can be genetically modified and interrogated. Engineering mammalian systems remains more difficult, but mammalian synthetic biology is posed to impact biotechnology such as protein production and provide novel therapies through stem cell engineering<sup>40,42</sup>. However, the lack of high-throughput tools to efficiently deliver genetic material to mammalian cells is slowing down progress. Mammalian synthetic systems can be complex and require multiple constructs to be simultaneously delivered at precise ratios, necessitating painstaking optimization of the transfection conditions<sup>43,44</sup>. Reverse transfection could provide a solution to this problem, but to date it has not been adapted for this purpose.

Although reverse transfection has applications in many fields and is easily scalable, the method involves manual cell seeding and culturing. Moreover, spots on the live cell array are not physically separated from one another. These conditions preclude precise control over the cell

environment and increase the likelihood of cross-contamination, to the extent that attempts have been made to separate DNA spots with silicon gaskets and cell-repellent coatings<sup>49,50</sup>. The integration of transfected cell arrays with microfluidics could eliminate these concerns, enabling long-term experiments and studies using poorly adherent or highly migrant cell types. Nevertheless, microfluidic transfection devices have yet to reach the impressive throughput of the original reverse transfection microarrays. In a recent method developed by Schudel et al., a separate microfluidic channel was required to introduce each lipid-DNA sample, allowing a maximum of 8 unique transfections to be performed on chip<sup>56</sup>. In another study, a lipid-DNA array was generated and aligned to an 8-chamber chip<sup>57</sup>. However, this system was not designed to replenish medium in the transfection chambers, thus prohibiting long-term experiments or flow manipulation.

In this article, we present a platform that combines reverse transfection with microfluidics. Up to 280 independent transfections can be performed per chip, with transfection efficiencies of up to 99% and minimal cross-contamination. The use of a microarrayer to deposit DNA constructs significantly increases throughput, while the microfluidic environment permits transfection, long-term culturing and manipulation of transfected cells. The setup can be continuously imaged, enabling time-lapse studies. We thoroughly characterized our new integrated microfluidic reverse transfection array and applied it to synthetic gene circuits.

## 3.3 Results

### 3.3.1 Device design and cell loading/culturing

Standard reverse transfection has been used by various groups with transfection efficiencies ranging from 13 to 80%<sup>51-53</sup>. We sought to create a highly reproducible and efficient reverse transfection microfluidic platform that supports more complex experiments. Our high-throughput chip design (Fig. 3.1a, 3.2a) measures 1.6 x 5.8 cm and contains 280 cell-culturing/transfection chambers. A low-throughput chip containing 80 chambers was also used (Fig 3.2b). The chips are aligned to DNA arrays so that each of the cell chambers contains a unique transfection reaction. Cell loading takes no more than 10 min and consists of two steps: first, a suspension of HEK 239T cells is flowed through the channels, and second, the channels are segmented into individual chambers by valves (Fig. 3.3). Up to 600 cells can be cultured in each chamber (diameter: 500  $\mu\text{m}$ , and height: 30  $\mu\text{m}$ ; Fig. 3.1b).

To achieve both high cell viability and uniform cell density throughout the chip, we loaded segments of the chip sequentially and at low flow velocity. In contrast, an un-segmented chip requires high loading speed to prevent clogging, and this velocity has been shown to decrease cell viability<sup>101</sup>. Our layout permits the loading of 5 columns at a time (Fig. 3.1c). Each of these subsections can be addressed individually, making it possible to load the device with different cell densities or even different cell types. A loading rate of 7.2  $\mu\text{L}/\text{min}$  (volume of medium

### Chapter 3. A high-throughput microfluidic platform for mammalian cell transfection and culturing

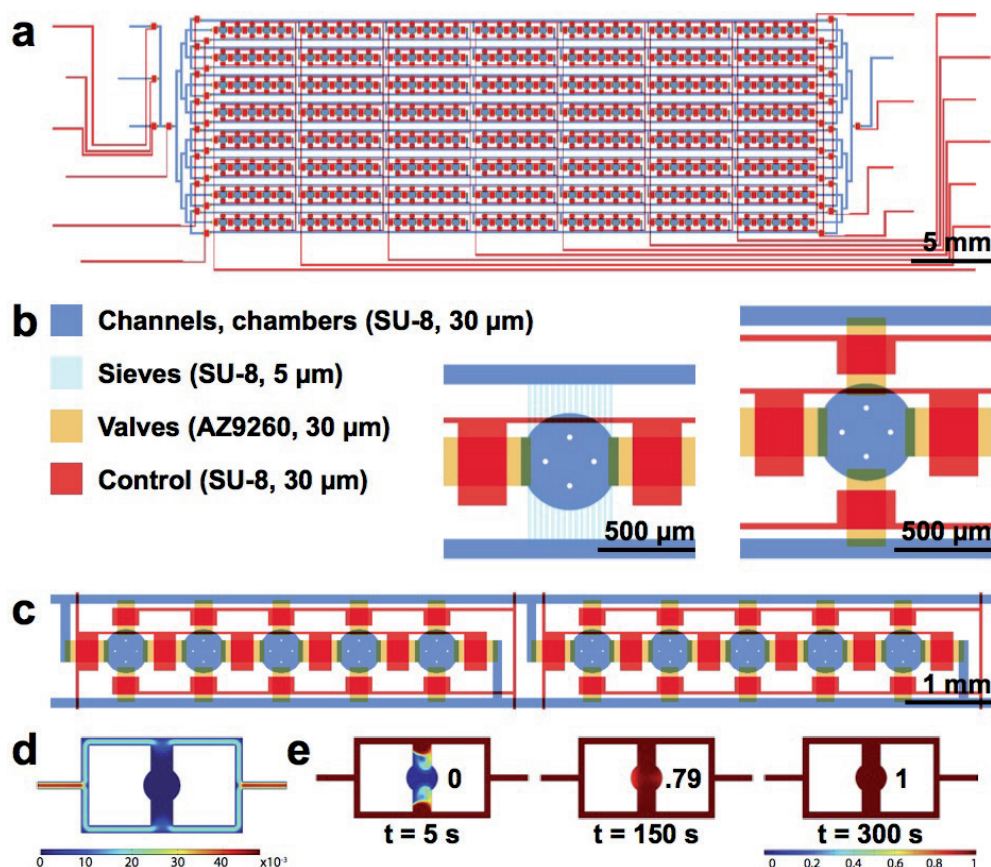


**Figure 3.1.** High-throughput microfluidic cell culturing and transfection chip. (a) Schematic of the 280-chamber valve perfusion chip. (b) The different layers of the device were patterned in photoresist. Close-up images show the sieve design (left) and the valve design (right). (c) The chip is loaded in segments of 5 chambers. (d) COMSOL model showing the flow velocity profile of the valve design (Scale: m/s). (e) COMSOL model showing the diffusion of nutrients into the center of the chamber using a 13.4 kDa protein with a diffusion coefficient of  $1.14 \times 10^{-6} \text{ cm}^2/\text{s}$  as an example. The extent of diffusion (0-1) is indicated.

exiting the chip over time) is used for the low-throughput chip. Due to an increased number of features, the high-throughput chip requires a flow rate of  $27.3 \mu\text{L}/\text{min}$  in order to achieve the same linear velocity through the channels.

Cell culturing is performed in a shear-free manner to reduce cross-contamination, minimize cell stress, and increase compatibility of the device with weakly or non-adherent cells. Although shear-free microfluidic perfusion systems have been designed<sup>64,102,103</sup>, most are limited in throughput because chambers are not separated from one another. In our 80 and 280-chamber devices, we perfused medium at a rate of 8-17  $\mu\text{L}/\text{min}$  through supply channels that run parallel to the cell chambers, eliminating shear stress (Fig. 3.1a). 5  $\mu\text{m}$  high sieves or

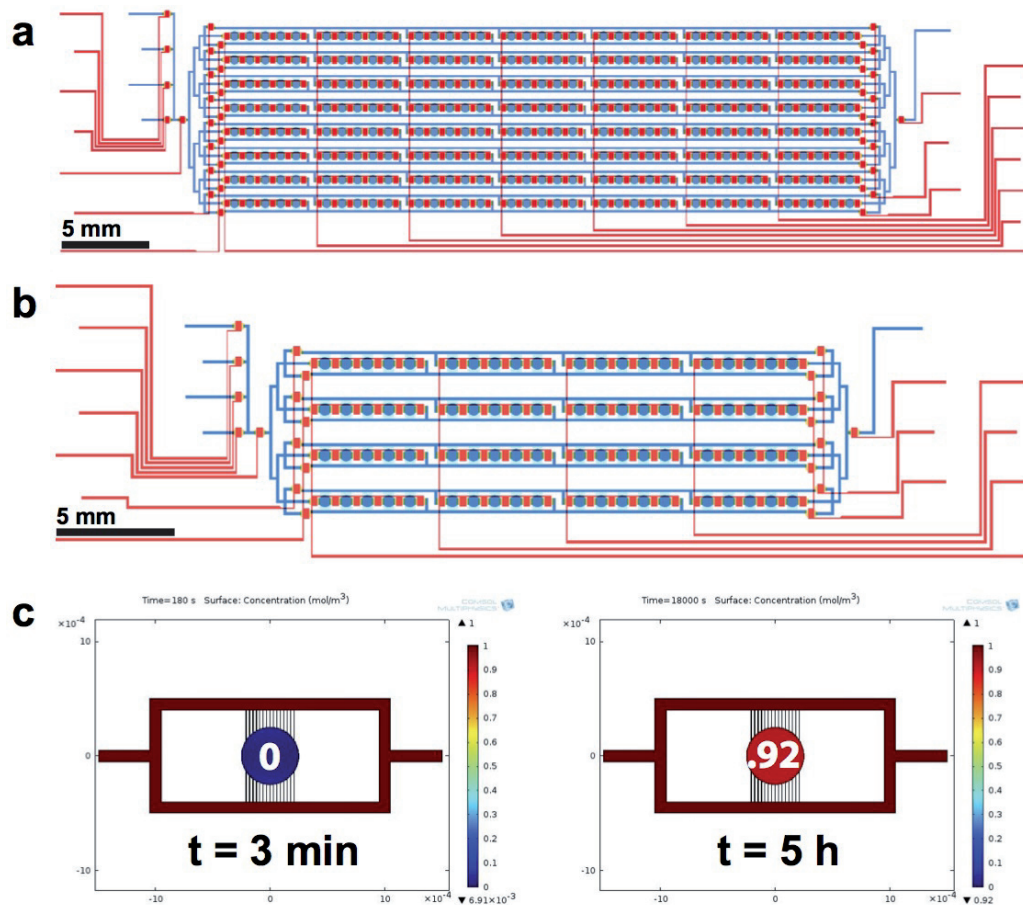


**Figure 3.2.** Design of the high-throughput cell culturing and transfection chip (sieve version). (a) Design of the 280-chamber chip with sieves for medium perfusion. The chip measures 1.5 x 5.7 cm. Refer to Figure 3.1b for legend. (b) Design of the 80-chamber chip with sieves for medium perfusion. The chip measures 1.2 x 4.1 cm. Refer to Figure 3.1b for legend. (c) COMSOL modeling shows that diffusion of nutrients into the center of the cell chamber is 92% complete after 5 h. A 13.4 kDa protein with a diffusion coefficient of  $1.14 \times 10^{-6} \text{ cm}^2/\text{s}$  was used as an example.

30  $\mu\text{m}$  high valves connect the flow channels and culturing chambers, preventing cell escape from the chambers during medium perfusion (Fig. 3.1b). Diffusion through the sieves or valves (when opened) introduces nutrients and eliminates waste from the chambers.

COMSOL modeling verified that flow through the chambers was nonexistent (Fig. 3.1d). According to the model, near-complete diffusion of medium from the side channels to the center of the chambers occurs after 5 h for the sieve design (Fig. 3.2c) and 5 min for the valve design (Fig. 3.1e). Since we were working with adherent HEK 239T cells, we chose to use the valve design for most experiments. After pulse perfusing<sup>104</sup> (see methods) for one hour, cells adhere inside the chambers and the valves can remain open for optimal diffusion of nutrients. Nevertheless we also tested transfection with the sieve chip, which can be used for weakly

### Chapter 3. A high-throughput microfluidic platform for mammalian cell transfection and culturing

or non-adherent cells without the need for a pulse perfusion system. We found that due to limited diffusion into the chambers of the sieve chip, the FBS used to prepare the culture medium should be as fresh as possible (Fig. 3.4).

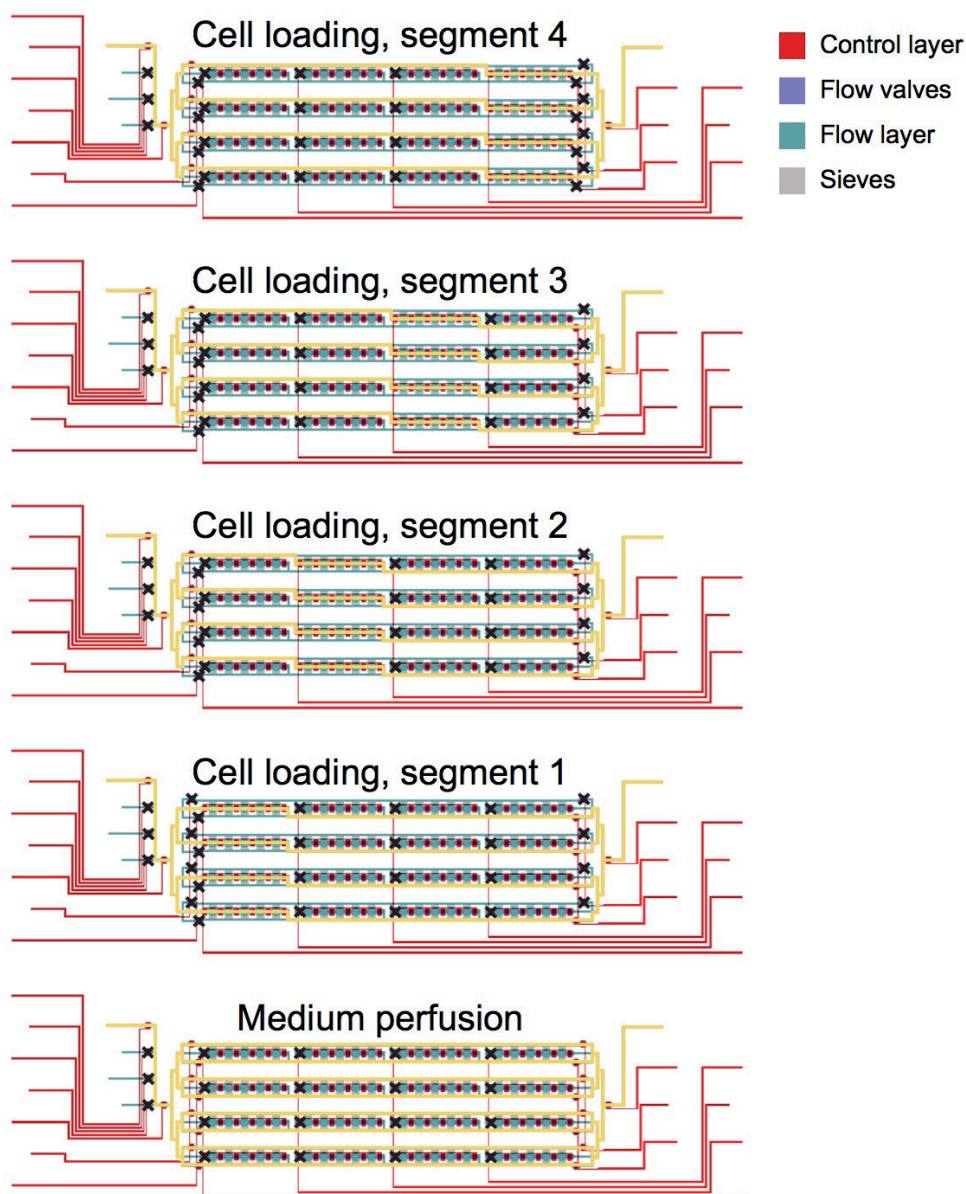


**Figure 3.3.** Schematic of cell loading and culturing on the low-throughput chip. Segments of chambers containing 5 columns are loaded sequentially. Yellow indicates the trajectory of flow through the chip. Black crosses indicate valves that are closed. For the chip design containing valves in the place of sieves (Fig. 3.1b), these valves remain closed during cell loading and are opened during medium perfusion. The high-throughput chip is loaded in a similar manner, the main difference being the number of chamber segments (7 instead of 4).



### 3.3.2 Device assembly

Initial microfluidic cell culturing experiments were performed using low-throughput PDMS chips that were bonded to glass slides by baking at 80 °C. For high-throughput chips with densely packed features, the decreased surface area of PDMS available for bonding resulted in frequent delamination of the chip from the glass. To resolve this issue, we investigated whether oxygen plasma could be used to mediate binding between PDMS and DNA-glass arrays. To our knowledge, oxygen plasma has not been used on glass slides patterned with biological substances such as lipid-DNA complexes because the oxygen plasma could potentially destroy the spotted material. We thus tested the effect of plasma on DNA arrays that were completely exposed to plasma and also on arrays where the DNA spots were protected with a PDMS block (Fig. 3.5). The plasma-treated arrays were seeded with cells and measured for transfection efficiency. We found that 7 s plasma treatment, with or without the protective PDMS block, did not affect the spotted DNA, as transfection efficiency was comparable to an array that was not plasma treated (Fig. 3.5). The strong glass-PDMS bond resulting from plasma treatment can sustain increased medium perfusion speeds and drastically enhances the structural stability of the assembled device, which is critical for performing long-term experiments.

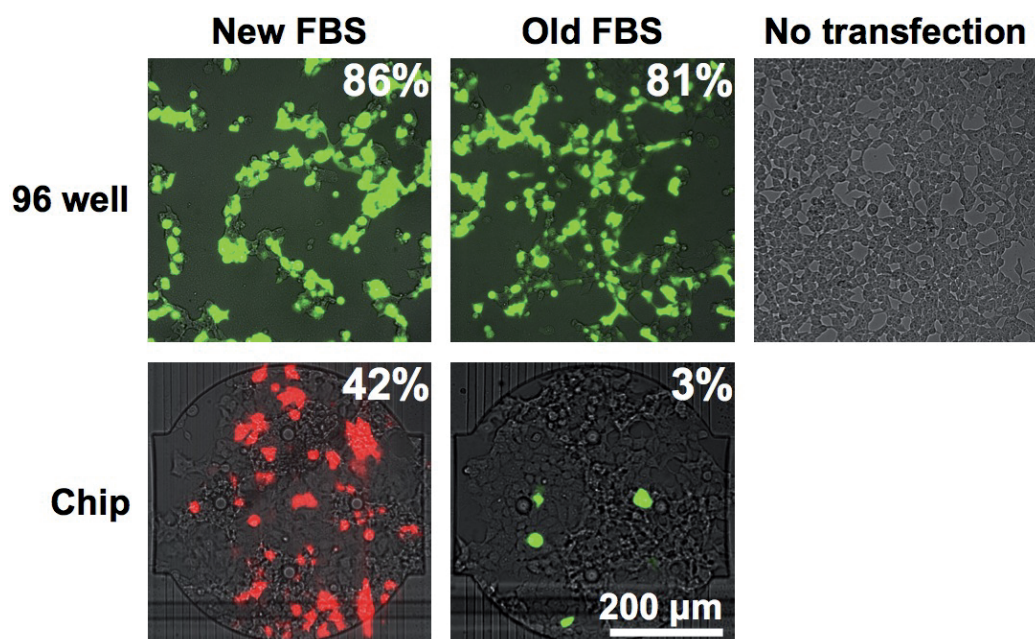


**Figure 3.4.** The effect of serum quality on transfection efficiency with the sieve device. Old (freeze-thawed 3 times) FBS was used for transfection experiments on a 96 well plate and on the sieve design chip. Transfection efficiencies of eGFP and tdTomato are indicated in the composite fluorescent images. Cells proliferate faster when no transfection reagent is present.

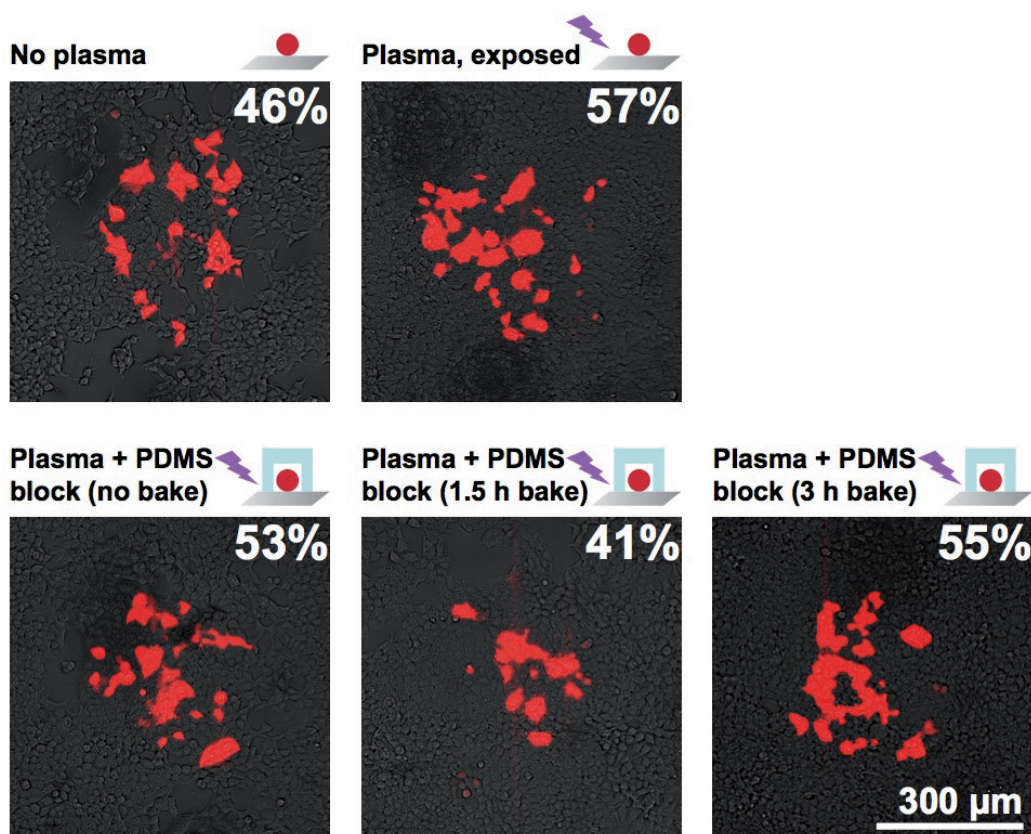


**Figure 3.5.** Plasma treatment of lipid-DNA microarrays. tdTomato transfection arrays were treated with oxygen plasma for 7 s before being seeded with cells. For some arrays, the lipid-DNA spots were protected by a PDMS block that had been adhered to a glass slide immediately before plasma treatment (no bake) or during an 80 °C bake (1.5 or 3 h). tdTomato transfection efficiency is indicated for each composite fluorescence image.

### 3.3.3 Generating a microfluidic-compatible reverse transfection array

Reverse transfection requires an arraying substrate that retains DNA, such as gamma-amino propyl silane (GAPS) or poly-L-lysine (PLL). However, these surfaces are positively charged and do not bind robustly to hydrophobic PDMS microfluidic chips. To develop a PDMS-compatible substrate, we first arrayed PLL, followed by arraying lipid-DNA complexes onto the PLL spots (Fig. 3.6a). Arraying of PLL and lipid-DNA is automated and takes between 30 min and 2 h to complete.

Depending on the exact application, PLL-coated glass slides are fabricated using solutions containing 25 μg/ml to 1 mg/ml PLL and various buffers<sup>105–109</sup>. Due to the large discrepancies in protocols, we tested a range of PLL concentrations for microarraying (Fig. 3.6b). PLL arrays were spotted with a standard lipid-DNA mixture and seeded with cells to test for transfection efficiency. We obtained optimal results when depositing a 333 μg/ml PLL solution 4 times per spot, resulting in spots containing ~22 ng/mm<sup>2</sup> of PLL (Fig. 3.6b). The time delay between

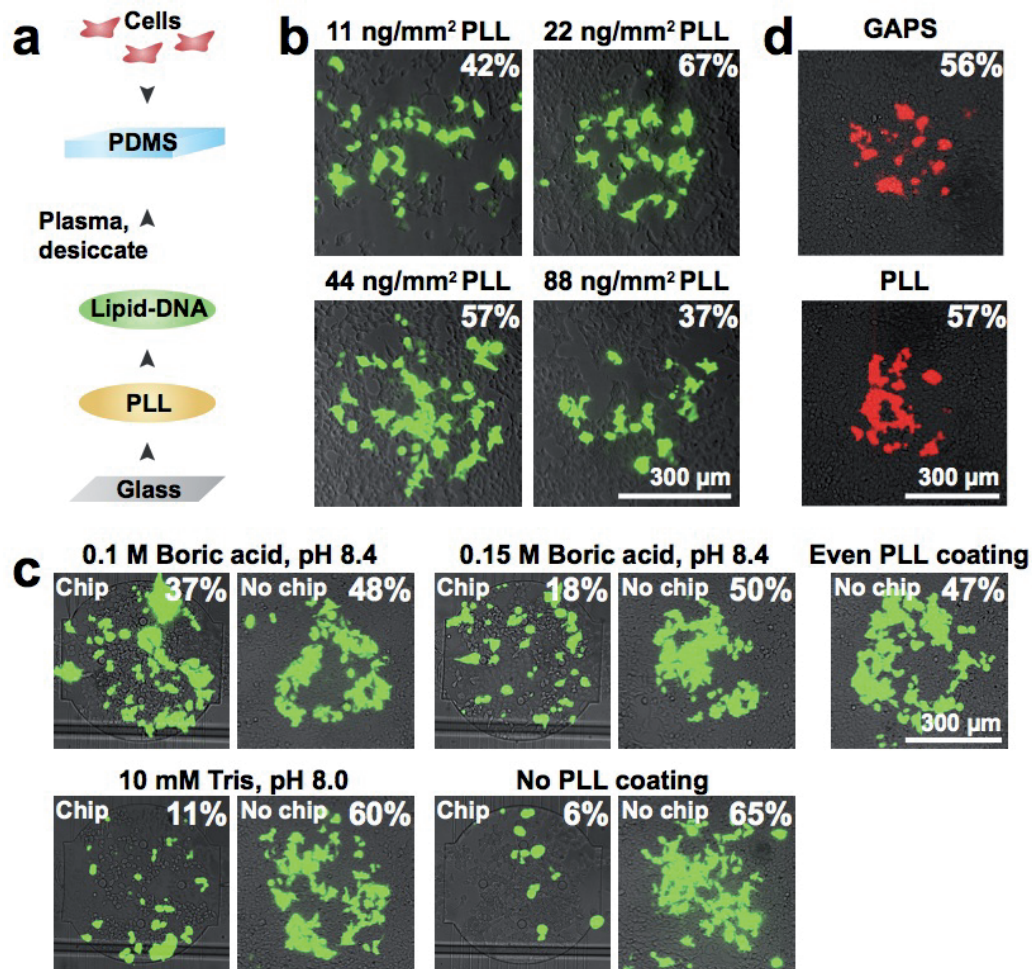


**Figure 3.6.** Generation of a microfluidic-compatible reverse transfection array. (a) Workflow to fabricate the transfection device. (b) Optimization of the amount of PLL deposited during microarraying. eGFP transfection efficiency is indicated for each composite fluorescence image. (c) Effect of the composition of the PLL spotting mixture on eGFP transfection efficiency. The images on the left of each set represent the full assembly (PLL spotted array + DNA array + chip). The images on the right of each set represent the assembly without the chip (PLL spotted array + DNA array). A standard reverse transfection array (evenly coated PLL + DNA array) was also tested. eGFP transfection efficiency is indicated for each composite fluorescence image. (d) Comparison of tdTomato transfection efficiency using a standard GAPS slide or our spotted PLL slide. Transfection efficiencies are indicated for the composite fluorescence images.

each of the 4 spotting cycles did not considerably alter transfection efficiency (Fig. 3.7a). Arrays were washed after arraying to remove excess PLL, and the time elapsed between array completion and washing did not significantly affect array quality (Fig. 3.7b).

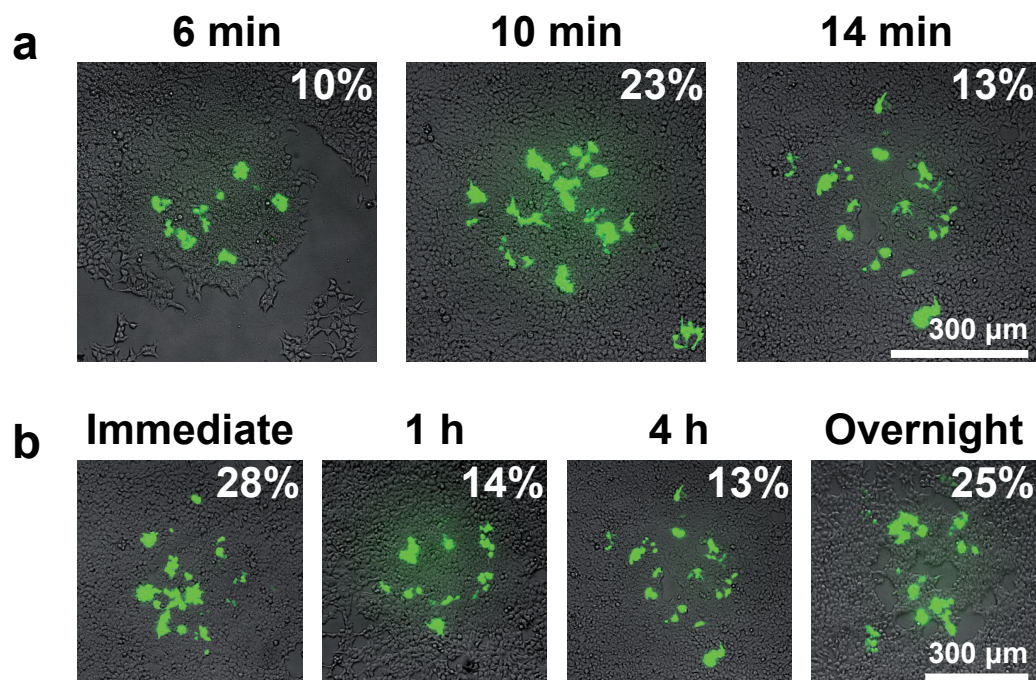


**Figure 3.7.** Optimization of PLL spotting. (a) The amount of time elapsed between each of the 4 PLL spotting cycles has little effect on eGFP transfection efficiency, as indicated by the composite fluorescent images. (b) The amount of time elapsed between array completion and array rinsing to remove excess PLL has little effect on eGFP transfection efficiency, as shown on the composite fluorescent images.

We next optimized the chemical composition of the PLL spotting solution, testing recipes derived from oligonucleotide microarraying protocols as well as tissue adhesion protocols<sup>109,110</sup> (Fig. 3.6c). To examine the differences between standard and microfluidic transfection, we ran a control array that lacked the microfluidic chip. Arrays made with a water-PBS mixture that is typically used to prepare microarrays yielded very low transfection efficiency. When we spotted PLL diluted in pH-adjusted 0.1 M boric acid, we achieved moderate transfection efficiency on chip (37%) that corresponded well to the efficiency of the control array lacking a chip (48%) (Fig. 3.6c). These results were also comparable to the 47% efficiency obtained when spotting DNA on an evenly coated PLL slide, which is the standard substrate for reverse transfection.

In addition to identifying the optimal buffer-PLL mixture for on-chip transfection, these experiments also revealed differences in the nature of on-chip vs. standard array setups. The control array lacking a chip yielded efficiencies of 48-65% for all PLL mixtures spotted (Fig. 3.6c). On chip, depending on which buffer-PLL mixture was used, transfection efficiency ranged from 11 to 37% (Fig. 3.6c). There was also a stark difference between the chip and control arrays for positions where no PLL was deposited beneath the lipid-DNA. On the control array, this spot yielded a transfection efficiency of 65% (Fig. 3.6c). In contrast, the same array

aligned to a chip had just 6% efficiency (Fig. 3.6c). These findings indicate that the presence of PLL is crucial for the success of on-chip reverse transfection.

We also tested our optimized PLL arrays alongside commercial GAPS (gamma-amino propyl silane) slides, which are the standard substrate for reverse transfection, and found that both PLL and GAPS substrates performed equally well (Fig. 3.6d). Compared to the manual batch coating method, our PLL arraying method is simple and precise because an automated microarrayer is used to deposit the PLL. This method is also cost-effective since it requires 100 times less PLL than traditional coating. Moreover, when optimized, in-house coated PLL slides have been shown to support higher and more consistent DNA retention than commercially available slides<sup>111</sup>.

### 3.3.4 Microarraying and composition of transfection complexes

After optimizing the PLL arraying, we optimized transfection efficiency by varying the composition of the lipid-DNA mixture. We first used the standard gelatin-containing recipe to prepare lipid-DNA complexes for reverse transfection<sup>33,52,53,112</sup>. When this mixture was deposited on the PLL arrays and used in combination with a PDMS chip, 13% efficiency was achieved (Fig. 3.8a). We next included fibronectin, which has been previously reported to increase transfection efficiency<sup>48</sup>. When used with the PLL arrays, the fibronectin-containing transfection mixture resulted in 77% efficiency (Fig. 3.8b, Table 3.1). When the gelatin-fibronectin mixture was used in combination with optimized DNA concentration and PLL arrays, we were able to obtain a very high transfection efficiency of 99% (Fig. 3.8c, Table 3.1). Moreover, different types of cells can be cultured and transfected on the chip. Using an array optimized for HEK cells, we were able to transfect CHO cells at a rate of 25% (Fig. 3.9a). The transfection efficiency can likely be improved by optimizing the protocol for specific cell types.

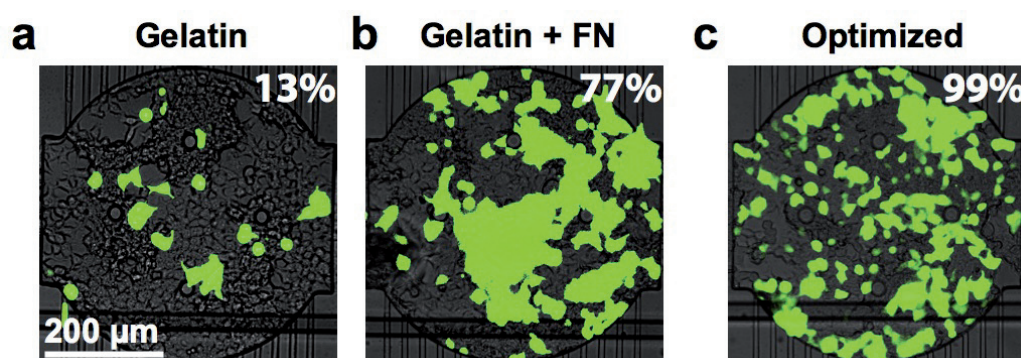


**Figure 3.8.** Optimization of the lipid-DNA composition. (a) Microfluidic transfection arrays were prepared using mixtures containing eGFP plasmid DNA, Effectene, and gelatin. eGFP transfection efficiency is indicated for the composite fluorescence image. (b) As in (a), but including fibronectin in the transfection mixture. (c) As in (a), but using a higher DNA concentration and an optimized PLL array.

### Chapter 3. A high-throughput microfluidic platform for mammalian cell transfection and culturing

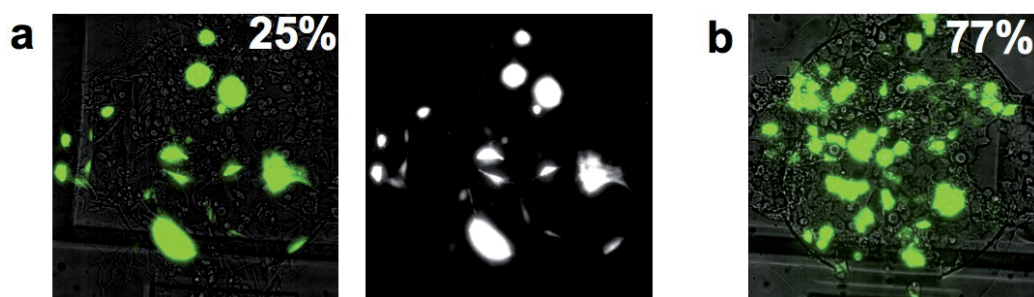


**Figure 3.9.** Adapting the microchip to different cell types and transfection methods. (a) CHO cells are transfected with eGFP on chip at high efficiency when using conditions that were optimized for HEK cells. Transfection efficiency is indicated on the composite fluorescent image (left). The fluorescence image is shown on the right. (b) HEK cells are transfected with eGFP on chip at high efficiency when using the gelatin-DNA method. Transfection efficiency is indicated on the composite fluorescent image.

Sample	DNA	Buffer	Effectene	Gelatin	Fibronectin	PLL	Non-optimal component
Fig. 3.6b	0.5 $\mu$ g	6.5 $\mu$ l EC buffer 1.2 $\mu$ l 1.5 M sucrose 10 $\mu$ l water	2 $\mu$ l Enhancer 2 $\mu$ l Effectene	6 $\mu$ l, 1%	0	25 $\mu$ l PLL + 50 $\mu$ l water, spotted as indicated in figure	DNA, Buffer, Effectene, Gelatin, Fibronectin, PLL
Fig. 3.6c	0.5 $\mu$ g	15 $\mu$ l EC buffer 4.5 $\mu$ l 1.5 M sucrose	1.5 $\mu$ l Enhancer 5 $\mu$ l Effectene	11.85 $\mu$ l, 0.5%	11.85 $\mu$ l, 1 mg/ml	25 $\mu$ l PLL + 50 $\mu$ l of 0.15 or 0.225 M boric acid, pH 8.4 or 15 mM tris, pH 8.0, spotted at approximately 22 ng/mm <sup>2</sup>	DNA, Buffer, PLL
Fig. 3.6d	1.5 $\mu$ g	15 $\mu$ l EC buffer containing 0.2 M sucrose	1.5 $\mu$ l Enhancer 5 $\mu$ l Effectene	12.7 $\mu$ l, 0.5%	12.7 $\mu$ l, 1 mg/ml	25 $\mu$ l PLL + 50 $\mu$ l 0.225 M boric acid, pH 8.4, spotted at approximately 22 ng/mm <sup>2</sup>	
Fig. 3.8a	0.5 $\mu$ g	15 $\mu$ l EC buffer 4.5 $\mu$ l 1.5 M sucrose	1.5 $\mu$ l Enhancer 5 $\mu$ l Effectene	23.7 $\mu$ l, 0.5%	0	25 $\mu$ l PLL + 50 $\mu$ l 0.15 M boric acid, pH 8.4, spotted at approximately 22 ng/mm <sup>2</sup>	DNA, Buffer, Gelatin, Fibronectin, PLL
Fig. 3.8b	0.5 $\mu$ g	15 $\mu$ l EC buffer 4.5 $\mu$ l 1.5 M sucrose	1.5 $\mu$ l Enhancer 5 $\mu$ l Effectene	11.85 $\mu$ l, 0.5%	11.85 $\mu$ l, 1 mg/ml	25 $\mu$ l PLL + 50 $\mu$ l 0.15 M boric acid, pH 8.4, spotted at approximately 22 ng/mm <sup>2</sup>	DNA, Buffer, PLL
Fig. 3.8c	1.5 $\mu$ g	15 $\mu$ l EC buffer 4.5 $\mu$ l 1.5 M sucrose	1.5 $\mu$ l Enhancer 5 $\mu$ l Effectene	11.85 $\mu$ l, 0.5%	11.85 $\mu$ l, 1 mg/ml	25 $\mu$ l PLL + 50 $\mu$ l 0.225 M boric acid, pH 8.4, spotted at approximately 22 ng/mm <sup>2</sup>	Buffer

**Table 3.1.** Detailed composition of transfection mixtures used for optimization experiments.

In addition to generating lipid-DNA arrays, we also tested the gelatin-DNA reverse transfection technique. For this method, we deposited spots containing a mixture of DNA, gelatin, and fibronectin. Effectene transfection reagent was introduced on chip, and transfection complexes were allowed to form before cells were loaded. This method yielded high efficiency of 77% (Fig. 3.9b) and conserves reagent. For the gelatin-DNA method 25  $\mu$ l Effectene is required for the entire 280-chamber chip or 90 nl per sample, whereas the lipid-DNA method requires 5  $\mu$ l per sample spotted. A similar amount is consumed by standard reverse transfection arrays, while well plate transfections require significantly more reagent (Table 3.2). Moreover, well

	12 well plate	RT array (lipid-DNA)	Chip (lipid-DNA)	RT array (gelatin-DNA)	Chip (gelatin-DNA)
Effectene reagent ( $\mu\text{l}$ )	6	5	5	25 per array (1000s of reactions)	25 per chip (100s of reactions)
DNA ( $\mu\text{g}$ )	0.3	1.5	1.5	1.5	1.5

**Table 3.2.** Comparison of reagent requirements for various transfection methods. RT, reverse transfection.

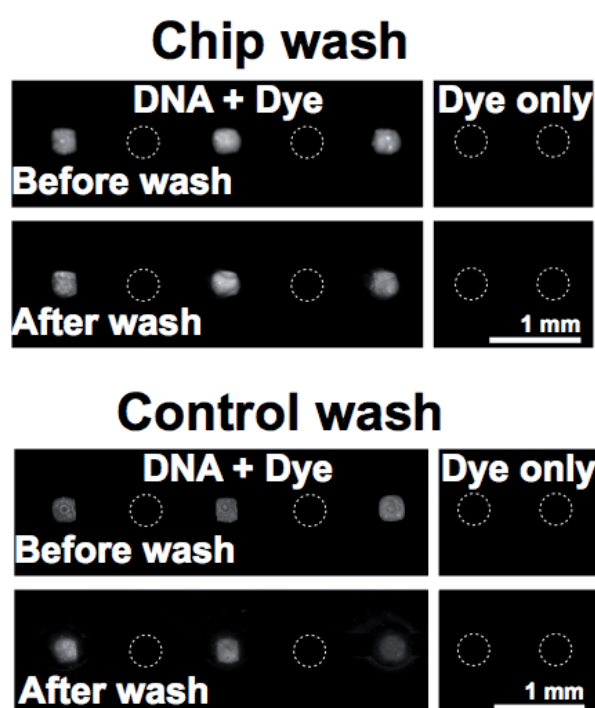


**Figure 3.10.** Investigating DNA cross-contamination on the transfection arrays. Testing DNA cross-contamination by staining with Sybr Green dye. DNA + dye or dye alone were included in the transfection mixture and spotted on a PLL array. Fluorescence scans were obtained before and after washing the arrays with PBS on chip (chip wash) or immersing the arrays with PBS in batch (control wash). Dashed circles indicate positions where nothing (DNA + Dye section) or dye only was spotted.

plate transfection requires three reagent mixing steps to be performed separately for each sample and manual addition of the samples to the wells. Microfluidic transfection using the gelatin-DNA method requires just one manual dilution; arraying of the samples and addition of the Effectene is automated. Despite this advantage, existing microfluidic and biochip transfection systems have thus far not taken advantage of the gelatin-DNA method<sup>57,113</sup>.

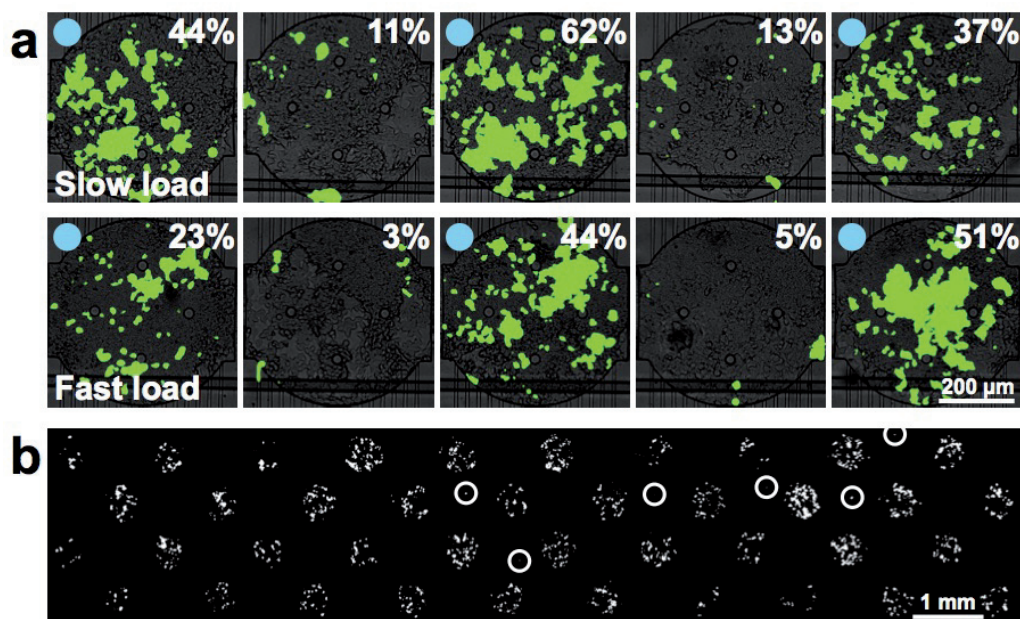


**Figure 3.11.** Determining the source and extent of contamination on the transfection arrays. (a) Cells were loaded into a transfection chip either at a slow flow speed of  $0.8 \mu\text{L}/\text{min}$  (upper) or a fast flow speed of  $5.2 \mu\text{L}/\text{min}$  (lower). Blue circles indicate that DNA was spotted in the chamber. eGFP transfection efficiencies are indicated on the composite fluorescence images. (b) Fluorescence micrograph of a chip in which tdTomato transfection mixture was spotted in every other chamber. White circles indicate contaminating cells.

### 3.3.5 Quantification of cross-contamination

During culturing of the transfection chip, constant flow of medium parallel to the chambers decreases the probability of cross-contamination or communication between chambers (Fig. 3.1d). However, cell loading requires direct flow through adjacent chambers (Fig. 3.3), and during this process lipid-DNA complexes could be detached from their original arraying position and deposited in a chamber further downstream. To test this possibility we stained the DNA with fluorescent dye, spotting every other chamber of the array with DNA (Fig. 3.10). One portion of the array was spotted with dye only. The control consisted of an array that was gently immersed in PBS. The test array was aligned to a low-throughput chip and cell loading (flow speed of  $5.2 \mu\text{L}/\text{min}$ ) was simulated with PBS. For both the control and on-chip PBS washes, the fluorescent DNA spots were still visible on the arrays. Fluorescence was not observed in adjacent positions where DNA was not spotted, indicating that high levels of DNA cross-contamination did not occur. Our PLL arraying procedure is thus sufficient to strongly anchor the DNA to the glass surface.

Although these findings imply that lipid-DNA does not detach in significant quantities from the arrays, these experiments were performed in PBS without cells. It is possible that cells take up lipid-DNA complexes as they traverse upstream chambers and ultimately settle in



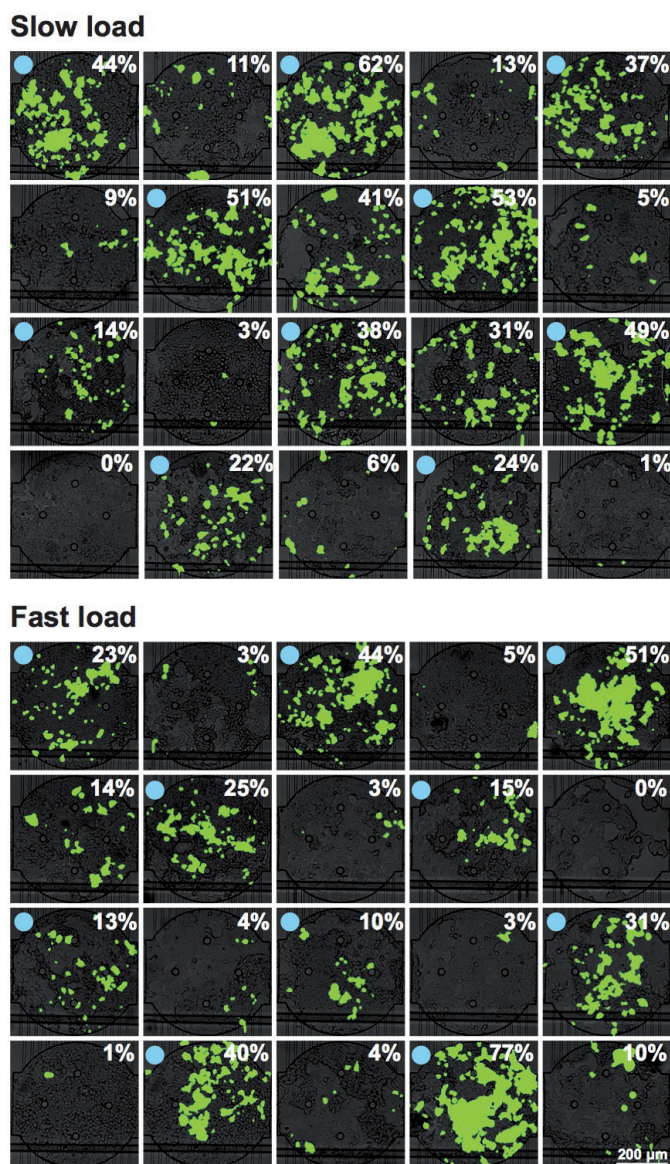


**Figure 3.12.** Cell loading speed and cross-contamination. The relationship between cell loading speed and cross-contamination was tested using the bottom two rows of a low-throughput chip. The left half of the rows (20 chambers) was loaded at a low speed of  $0.8 \mu\text{L}/\text{min}$ , and the right half of the rows (20 chambers) was loaded at a higher speed of  $5.2 \mu\text{L}/\text{min}$ . Transfection efficiencies are indicated for the composite fluorescence images. Blue circles indicate that DNA was spotted in the chamber.

chambers further downstream. To test this possibility we generated a low-throughput array in which every other chamber was spotted with eGFP DNA. When loading at a low speed of  $0.8 \mu\text{L}/\text{min}$ , average transfection efficiency across all chambers was 39% in the DNA-spotted chambers and 12% in the non-spotted chambers (Fig. 3.11a, 3.12). Loading at a higher speed of  $5.2 \mu\text{L}/\text{min}$  resulted in transfection efficiency of 33% in the DNA-spotted chambers and 5%

### Chapter 3. A high-throughput microfluidic platform for mammalian cell transfection and culturing

in the non-spotted chambers. It is likely that at slow loading speeds, cells have more time to interact with the DNA spots and acquire more DNA while in transit. Using a loading speed of 7.2  $\mu\text{L}/\text{min}$  we obtained extremely low cross-contamination when every other chamber was patterned with tdTomato DNA (Fig. 3.11b). Of the 40 chambers not patterned with DNA, 6 were contaminated. Two chambers contained two tdTomato-expressing cells, and the other 4 chambers contained one tdTomato-expressing cell.

We also performed transfection on the high-throughput chip, transfecting each cell-loading segment with either eGFP or tdTomato. We observed that all 280 chambers were transfected, and at similar efficiencies (Fig. 3.13a, 3.14). Average transfection efficiency for all chambers on the chip was 65% (Fig. 3.14). 10 eGFP chambers were contaminated with 1-3 tdTomato cells (Fig. 3.13b). eGFP contamination in tdTomato-spotted chambers was slightly higher. However,

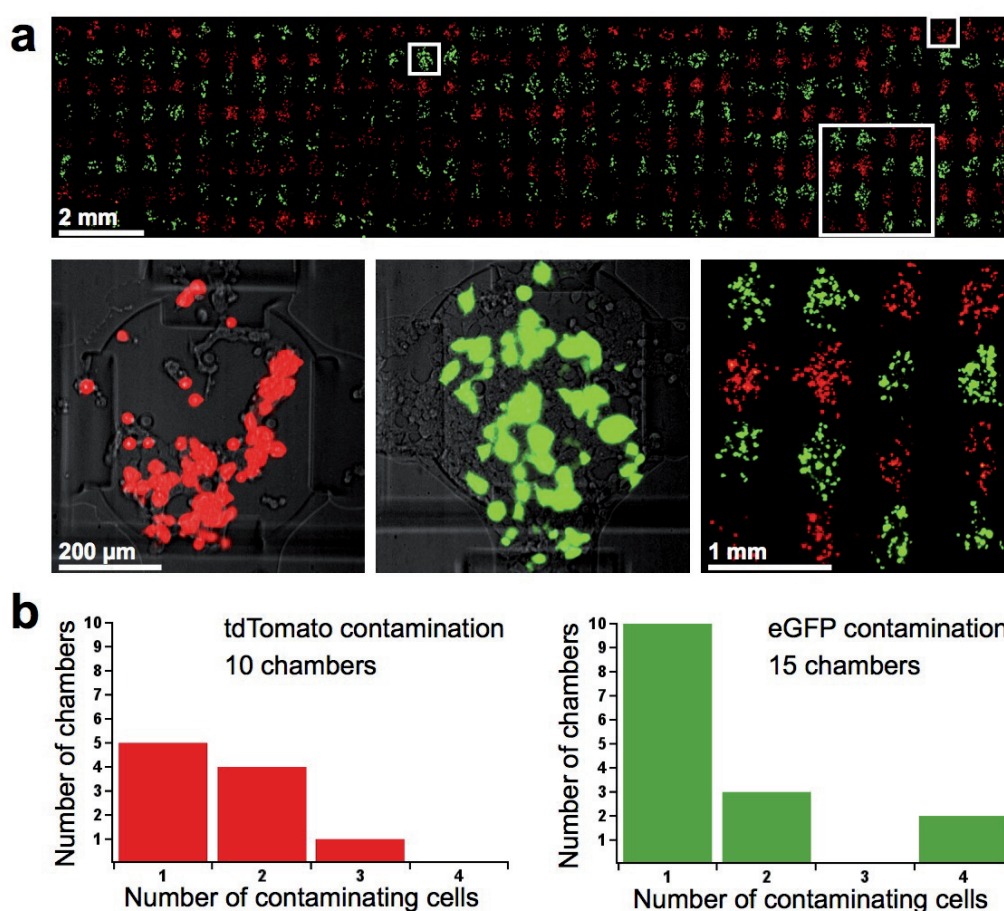


**Figure 3.13.** Transfection on the high-throughput chip. (a) Fluorescence micrograph of the entire transfected 280-chamber chip (upper) and close-up (lower right). Close-up composite fluorescence images indicate tdTomato and eGFP transfection efficiencies. (b) Histograms showing the extent of contamination on the transfected high-throughput chip. eGFP counts were calculated using intensity-adjusted images.

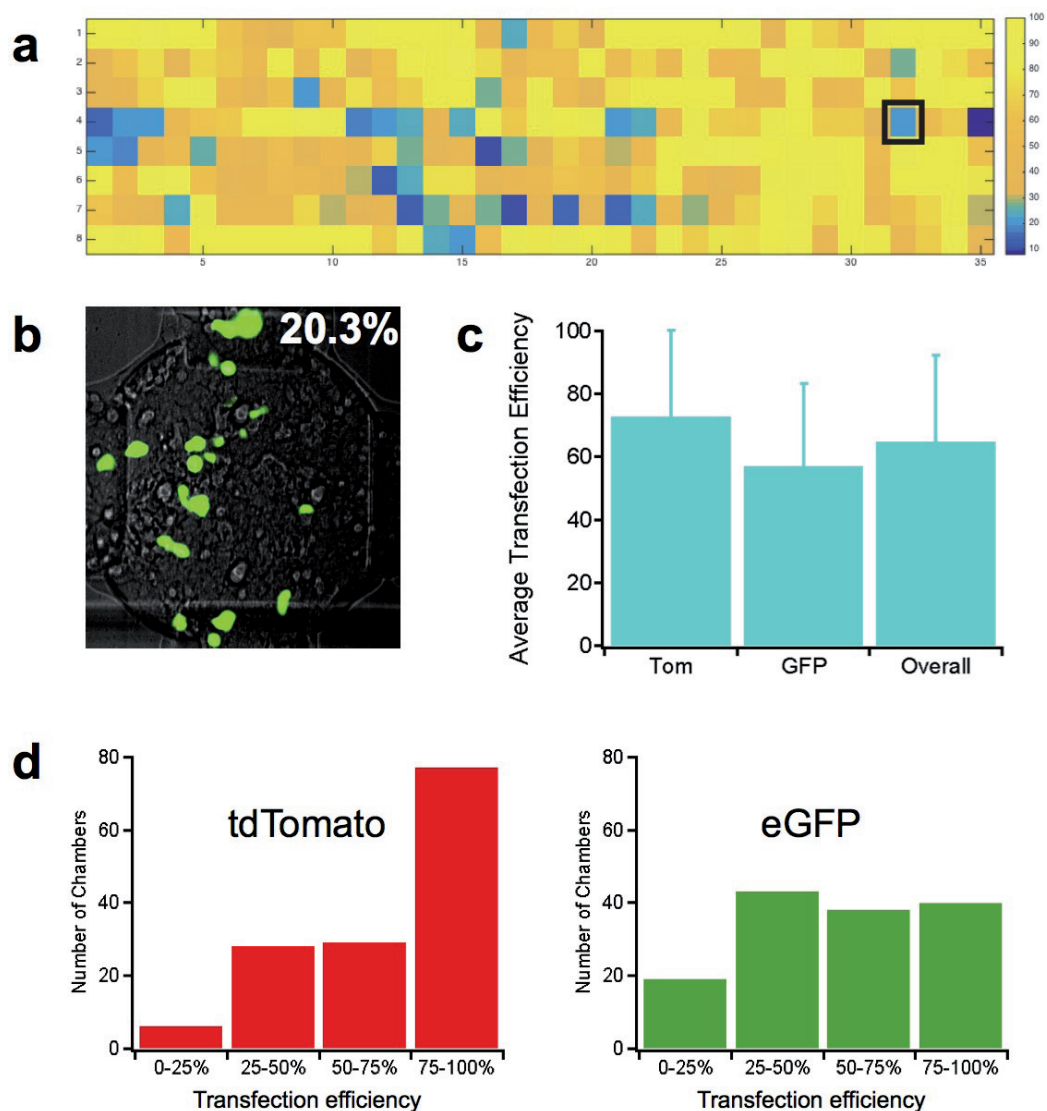


**Figure 3.14.** Transfection efficiencies on the high-throughput chip. (a) Heatmap showing the distribution of transfection efficiencies for each chamber of the chip presented in Figure 3.13a. (b) Close-up composite fluorescence image of a chamber from (a) with low eGFP transfection efficiency (row 4, column 32). Although a moderate number of cells express eGFP, overall transfection efficiency is low due to the large number of cells in the chamber. (c) Average transfection efficiencies for the chip presented in Figure 3.13a. (d) Distribution of transfection efficiencies amongst tdTomato and eGFP chambers.

the expression level of eGFP in the contaminating cells was extremely faint compared to the normal level of protein expressed by a transfected cell (Fig. 3.15a). The eGFP contamination histogram shown in Figure 3.13b has been adjusted to reflect this (Fig. 3.15b). The adjusted count reveals that 15 chambers were contaminated by eGFP cells, the majority of which contained a single cell.

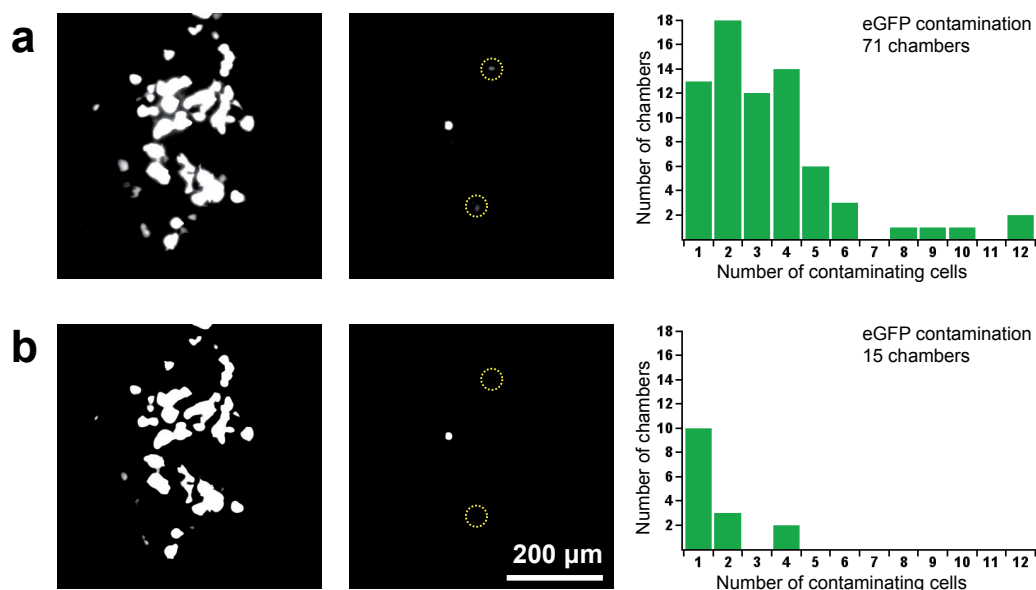


**Figure 3.15.** Quantification of eGFP contamination on the high-throughput transfection chip. (a) Unadjusted images showing representative chambers transfected with eGFP (left) and contaminated with eGFP (center) from the chip shown in Figure 3.13. Dashed yellow circles indicate the positions of two weakly fluorescent eGFP cells. The histogram on the right indicates the total contamination count when including weakly fluorescent cells. (b) Same as (a), but after adjusting the threshold to exclude weakly fluorescent eGFP cells.

### 3.3.6 Simultaneous delivery of multiple plasmids

Massively parallel transfection on chip should be useful for optimizing and characterizing synthetic systems implemented in mammalian cells. Sophisticated gene circuits contain many components placed on several plasmids that should be co-expressed at different levels, thus the quantities of the different plasmids must be extensively and painstakingly optimized<sup>44,114</sup>. To determine if our device could be used to optimize and characterize synthetic systems, we used our high-throughput chip to transfect cells with tdTomato and eGFP DNA mixed at different ratios. In all experiments the total amount of DNA was kept constant, since it has been well-established that there is a specific concentration of DNA that supports maximal transfection efficiency<sup>20,115</sup>. We tested each ratio in a total of 10 chambers, using two 5-chamber segments of the chip (Fig. 3.1c) and analyzing them separately.

First, we evaluated the number of cells that were transfected with eGFP alone, tdTomato alone, or both plasmids. As expected, we found that the transfection efficiency of each plasmid correlated with its concentration in the co-transfection mixture (Fig. 3.16a). The number of cells expressing both tdTomato and eGFP progressively increased as the Tom:GFP ratio increased from 1:4 to 2:1, reaching a peak of 82% at the 4:1 ratio and decreasing at the 8:1 ratio (Fig. 3.16a,e). This experimental setup can be used to find the DNA ratio that maximizes the number of cells expressing both plasmids.

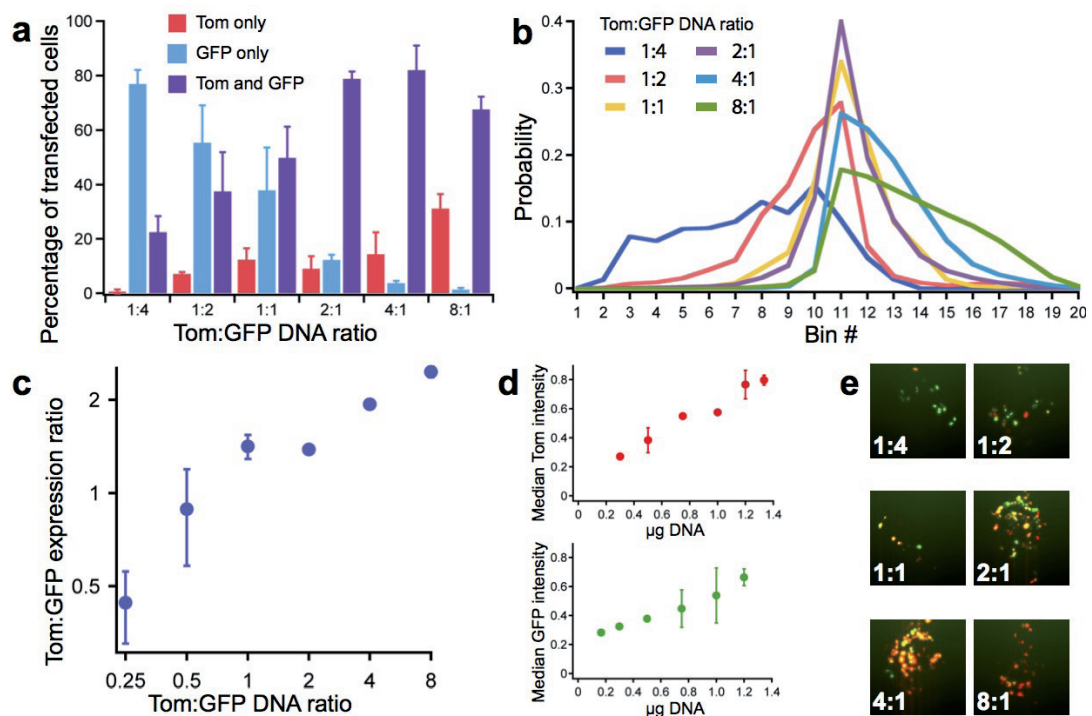


**Figure 3.16.** Ratios of protein expression and transfection efficiency during co-transfection on the high-throughput chip. (a) Transfection efficiencies as a function of the Tom:GFP co-transfection ratio. Each sample represents the average from 10 chambers patterned with a specific Tom:GFP DNA ratio. Error bars show standard deviation. (b) Distribution of Tom:GFP expression ratios. Bin edges span from Tom:GFP expression ratios of 1/6 (left) to 6/1 (right), with increments of 1/0.5 or 0.5/1 (e.g. 1/6, 1/5.5, 1/5 ... 5/1, 5.5/1, 6/1). Samples prepared as in (a). (c) Plot indicating the median Tom:GFP expression ratio from each sample shown in (b). Error bars show standard deviation. (d) Protein expression (measured by fluorescence intensity) as a function of the amount of DNA transfected. Samples were prepared as in (a). Error bars show standard deviation. (e) Sample images for each Tom:GFP co-transfection DNA ratio.

Next, we considered only the cells that expressed both proteins and evaluated their protein expression levels by measuring the fluorescence intensities of tdTomato and eGFP. We observed that protein expression ratios were dependent on the ratio of plasmid DNA used (Fig. 3.16b,c). There was also considerable agreement between the two 5-chamber segments that served as replicates of one another (Fig. 3.17). At more extreme ratios, we observed a weaker correlation between the input DNA ratio and the actual protein expression ratio. For example, the 8:1 sample resulted in a 2.46:1 expression ratio while the 2:1 sample yielded a more predictable value of 1.38:1 (Fig. 3.16c). Measured protein expression ratios are only relative values and likely skewed from the true values since they are based on measured intensity, and the tdTomato and eGFP fluorophores have different intrinsic brightness. Nevertheless, these findings show that it is possible to tune the expression ratios of proteins inside transfected cells.

### Chapter 3. A high-throughput microfluidic platform for mammalian cell transfection and culturing

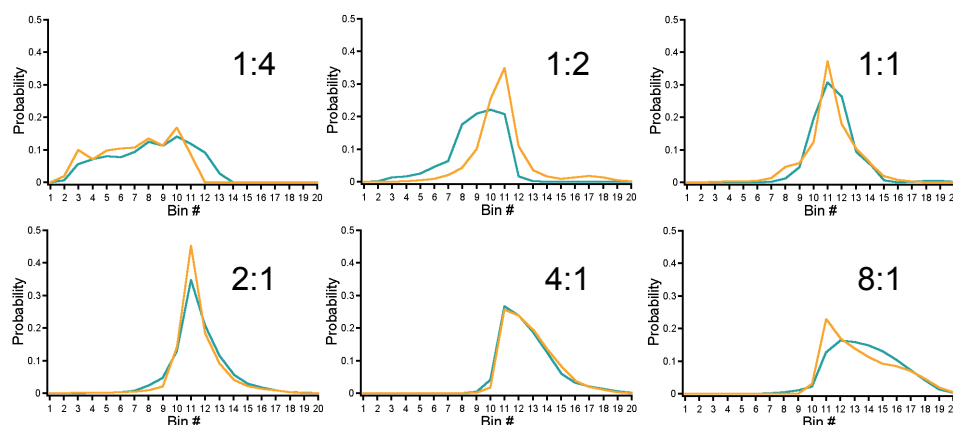


**Figure 3.17.** Ratios of protein expression and transfection efficiency for microfluidic co-transfection. Distribution of Tom:GFP expression ratios for co-transfection ratios ranging from 1:4 to 8:1. Bins span from Tom:GFP ratios of 1/6 (left) to 6/1 (right), with increments of 1/0.5 or 0.5/1 (e.g. 1/6, 1/5.5, 1/5 ... 5/1, 5.5/1, 6/1). Each curve represents the averages from one 5-chamber segment of this chip (Fig. 3.1c). The average of these two data sets was used to generate the curves shown in Figure 3.16

When we processed the tdTomato and eGFP data separately, we observed a similar correlation between the amount of DNA used for transfection and the level of protein expression. Increasing the quantity of DNA used for transfection directly increases the fluorescence intensity in a manner that is similar for both tdTomato and eGFP (Fig. 3.16d). Therefore in addition to co-transfection the transfection device can be used to produce precise levels of a single protein, provided that a second empty plasmid is added to keep the total amount of DNA transfected at the optimal level of 1.5  $\mu\text{g}$ .

These on-chip results corroborated well with the data obtained from performing the same experiment in 96 well and 6 well plate format (Fig. 3.16, 3.18, 3.19, 3.20). In contrast to the reverse transfection array technique used on chip, for the well plates the transfection mixture was added in solution to cells that had already been seeded. The ability of the on-chip results to match the trends displayed by the well plate results assures that this technology can be used interchangeably with standard cell culturing and transfection methods.

In addition to validating that on-chip transfection is comparable to well plate transfection, we also validated our image analysis approach. To do so, we implemented the standard 6 well plate transfection method followed by flow cytometry analysis. The flow cytometry-derived distribution of eGFP-only, tdTomato-only, and co-transfected cells displayed the same dependency on DNA ratios that was seen with the data obtained by image analysis (Fig. 3.16, 3.18, 3.19, 3.20). The relationship between co-transfection DNA ratio and protein expression ratio was also similar, with flow cytometry performing better at more extreme ratios (Fig. 3.16, 3.19, 3.20). Image analysis thus can serve as a less complicated alternative to flow cytometry, as there is no need to harvest and prepare each cell sample.

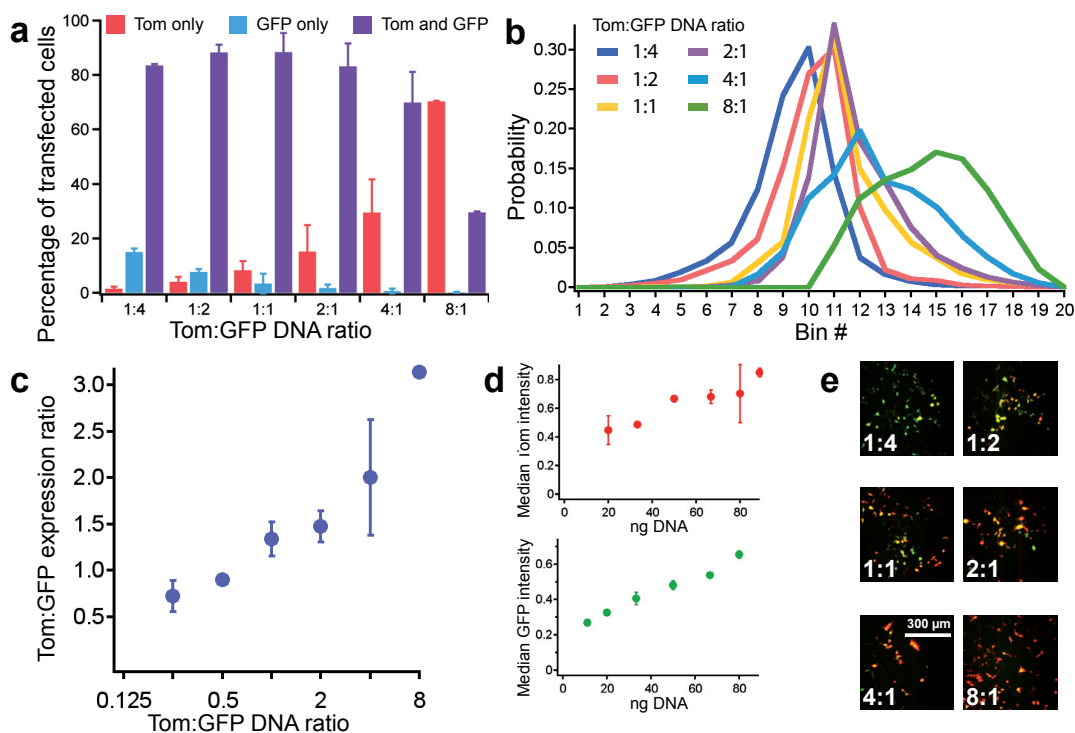


**Figure 3.18.** Ratios of protein expression and transfection efficiency for 96-well plate co-transfection. (a) Transfection efficiencies as a function of the Tom:GFP co-transfection ratio. Each sample represents the average from 2 wells (each imaged at 3 different positions) transfected with a specific Tom:GFP DNA ratio. Error bars show standard deviation. (b) Distribution of Tom:GFP expression ratios. Bin edges span from Tom:GFP expression ratios of 1/6 (left) to 6/1 (right), with increments of 1/0.5 or 0.5/1 (e.g. 1/6, 1/5.5, 1/5 ... 5/1, 5.5/1, 6/1). Samples prepared as in (a). (c) Plot indicating the median Tom:GFP expression ratio from each sample shown in (b). Error bars show standard deviation. (d) Protein expression (measured by fluorescence intensity) as a function of the amount of DNA transfected. Samples were prepared as in (a). Error bars show standard deviation. (e) Sample images for each Tom:GFP co-transfection DNA ratio. Variance of the 96-well plate data from the on-chip data may be due to slightly different imaging conditions (on-chip exposure times: 50 ms Tom, 70 ms GFP; well plate exposure times: 50 ms Tom, 50 ms GFP).

### 3.3.7 Transfection of synthetic genetic circuits

Many different co-transfection ratios can be tested in parallel on the chip, facilitating optimization and enabling high-throughput mammalian synthetic biology. To test the device with a recently reported synthetic system, we implemented the two-component signaling (TCS) system developed by Hansen et al<sup>114</sup>. The pathway consists of prokaryotic proteins DcuS and DcuR<sup>116,117</sup> that have been codon-optimized for expression in mammalian cells and are constitutively expressed from a CMV promoter. Upon stimulation by C4-carboxylates present in the cell culture medium, the membrane-localized histidine kinase (DcuS) autophosphorylates its cytoplasmic domain (Fig. 3.21a). The phosphate is then transferred to DcuR, a

### Chapter 3. A high-throughput microfluidic platform for mammalian cell transfection and culturing

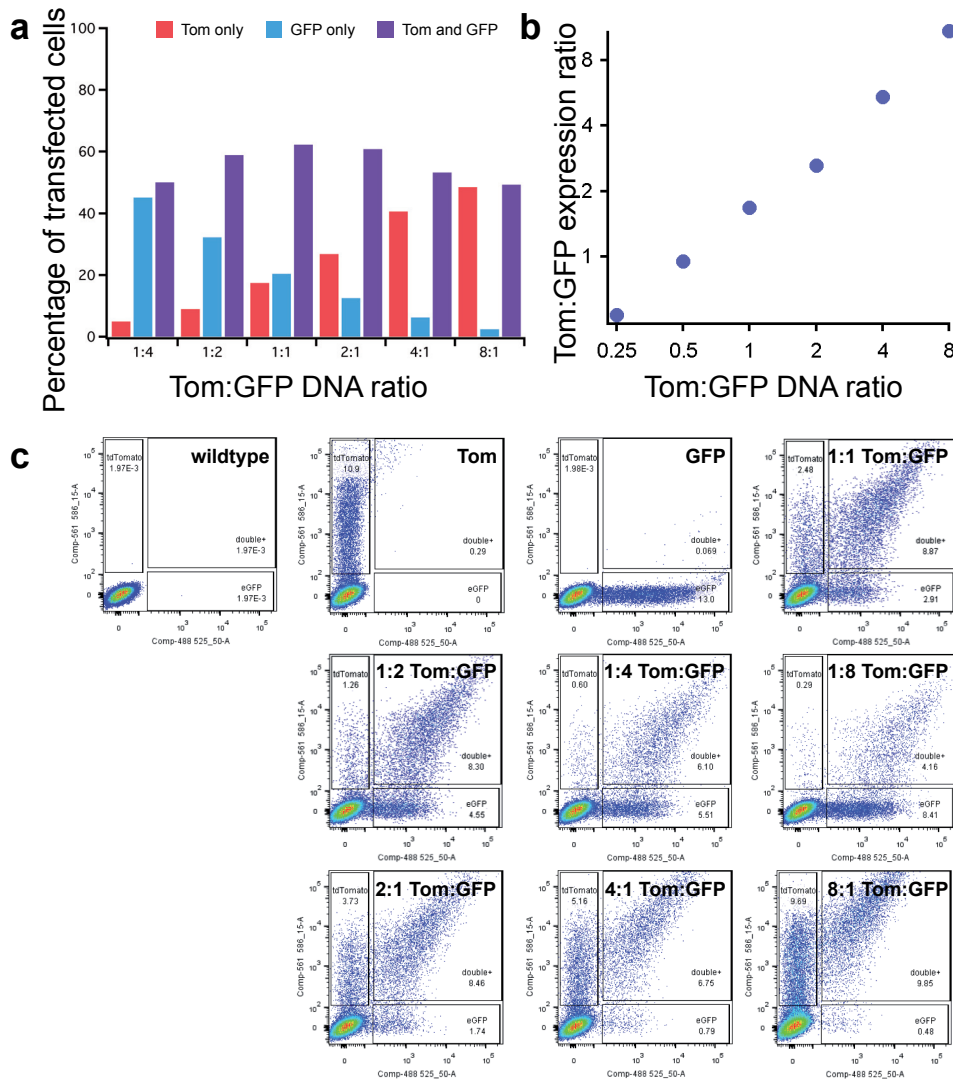


**Figure 3.19.** Flow cytometry analysis for 6-well plate co-transfection. (a) Transfection efficiencies as a function of the Tom:GFP co-transfection ratio. Each sample represents 50,000 cells transfected with a specific Tom:GFP DNA ratio. (b) Plot indicating the median Tom:GFP expression ratio from each co-transfection ratio shown in (a). (c) Flow cytometry plots.

transcriptional regulator that has been modified to contain three minimal VP16 transactivating domains at the C terminus. Upon activation by phosphorylation, DcuR binds to the promoter of the reporter plasmid and activates transcription of AmCyan. Various ratios of the three plasmids were used for transfection on the high-throughput chip, and a fourth plasmid (expressing tdTomato) was used as a transfection control. Activation of AmCyan expression was observed for all ratios tested (Fig. 3.21b). Transfections lacking any one element of the synthetic circuit did not produce AmCyan fluorescence and only expressed the tdTomato transfection control. We next tested the sensitivity of the system to changes in DcuS while



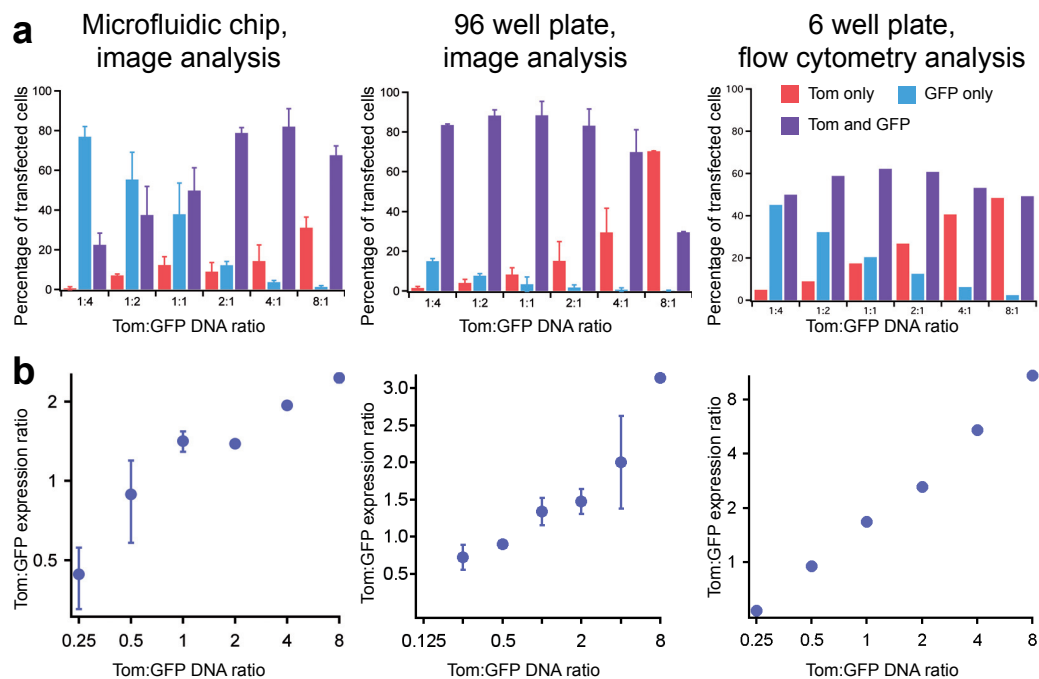


**Figure 3.20.** Comparison of ratios of protein expression and transfection efficiency for various co-transfection and analysis methods. (a) Transfection efficiencies as a function of the Tom:GFP co-transfection ratio, as previously shown in Figure 3.16a, 3.18a, 3.19a. (b) Plots indicating the median Tom:GFP expression ratio from each sample shown in (a).

keeping DcuR and the AmCyan reporter at fixed quantities.

We found that maximal AmCyan induction occurs when DcuS represents 2% of the total 3-plasmid transfection mixture and decreases below the optimal DcuS concentration (Fig. 3.21c). This finding is in agreement with the original study, which implemented transfections in 12-well plates followed by flow cytometry analysis of protein expression. We additionally performed the experiment in 96-well plate format followed by image analysis of protein expression and obtained similar results (Fig. 3.22). Our microfluidic transfection and image analysis method is thus capable of reproducing the results obtained from standard transfection and flow cytometry techniques.

We also performed time-lapse experiments to visualize the changes in protein expression over the course of transfection. Expression of the tdTomato transfection control began immediately post transfection (Fig. 3.21d,e, Supplementary Movie 1). AmCyan expression was first detected 12 h post transfection (Fig. 3.21d,e, Supplementary Movie 2). Assuming that tdTomato and AmCyan have similar maturation times<sup>118,119</sup>, this time lag can be explained by the fact that DcuS and DcuR must first be transfected and expressed before they can activate expression of AmCyan (Fig. 3.21a). For both tdTomato and AmCyan, protein expression levels continued to increase steadily until 53 h post transfection (Fig. 3.21d,e, Supplementary Movies 1, 2).

### Chapter 3. A high-throughput microfluidic platform for mammalian cell transfection and culturing

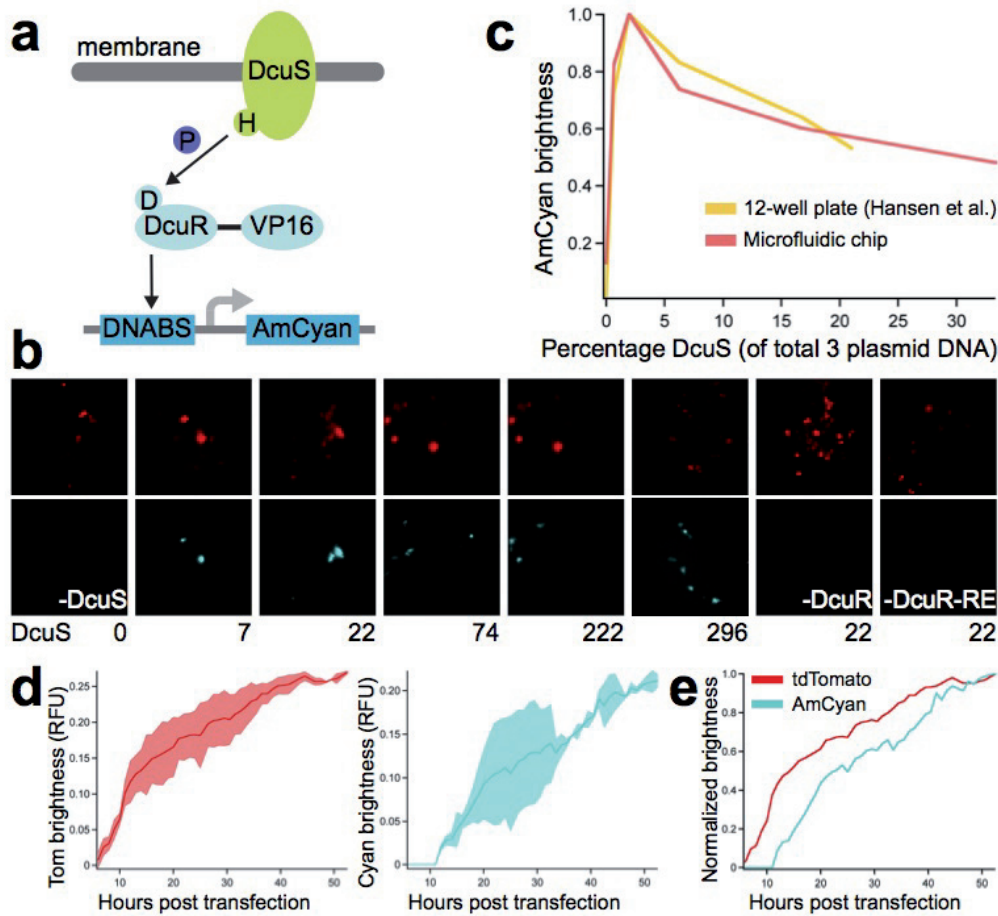


**Figure 3.21.** Measuring the dynamics of synthetic gene circuits on the high-throughput chip. (a) Schematic of the two-component signaling pathway. The histidine kinase (DcuS) is activated by ligand binding and transmits the signal to DcuR, a DNA-binding protein. P, phosphate; VP16, VP16 transactivator domain, DNABS, DNA binding sites. (b) Representative fluorescence images with DcuS amounts indicated in ng. Reactions included 296 ng tdTomato and, aside from the negative controls, 444 ng DcuR and 665 ng DcuR-RE. (c) Brightness of the reporter as a function of histidine kinase concentration for the original 12-well setup<sup>114</sup> and for the microfluidic setup. For the microfluidic data, points are the average of 10 chambers. Brightness is normalized so that the maximum occurs at 1. (d) Dynamics of tdTomato and AmCyan protein expression over time. The sample contained 296 ng tdTomato, 59 ng DcuS, 444 ng DcuR 665 ng DcuR-RE. The average brightness of two 5-chamber segments of the chip was calculated separately, and shaded areas represent the standard deviation between these two values. Maximum brightness is 1. (e) As in (d), but with brightness normalized so that the maximum occurs at 1.

These results support the standard practice of acquiring images after 48 h, when transfection efficiency and protein expression are high. Because our microfluidic technology is compatible with high-content imaging, samples can be monitored continuously, allowing significantly

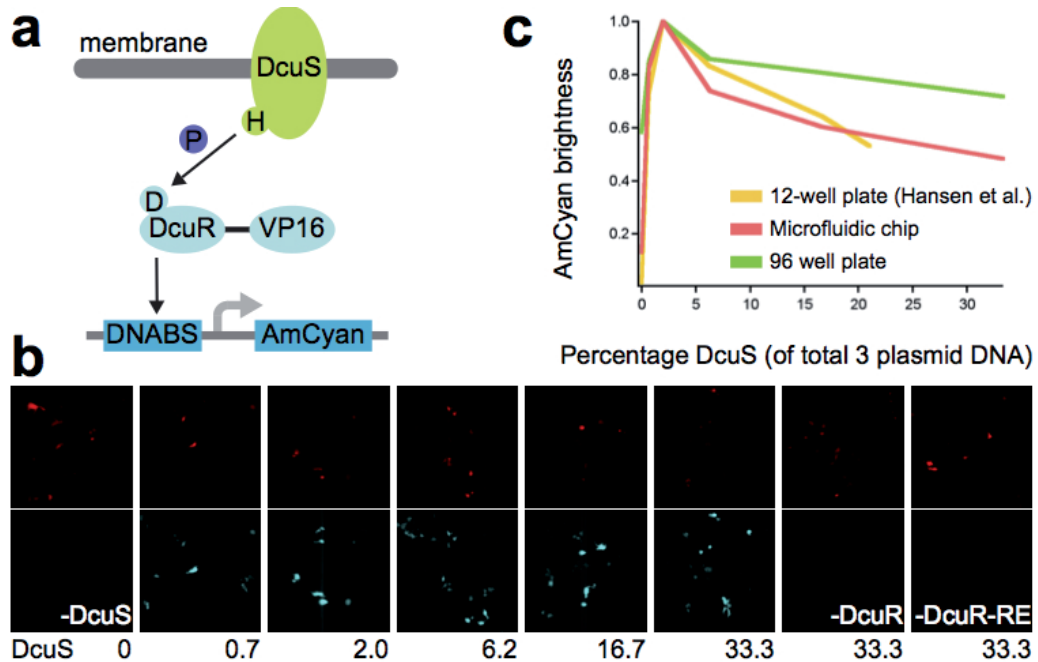


**Figure 3.22.** Measuring the dynamics of synthetic gene circuits for 96-well plate transfections. (a) Schematic of the two-component signaling pathway. The histidine kinase (DcuS) is activated by ligand binding and transmits the signal to DcuR, a DNA-binding protein. P, phosphate; VP16, VP16 transactivator domain, DNABS, DNA binding sites. (b) Representative fluorescence images with DcuS amounts indicated in ng. Each well of a 96-well plate was transfected with 13 ng tdTomato DNA and, aside from the negative controls, 38 ng DcuR and 56 DcuR-RE DNA. (c) Brightness of the reporter as a function of histidine kinase concentration for the original 12-well setup<sup>114</sup>, for the microfluidic setup, and for the 96-well plate setup. For the microfluidic data, points are the average of 10 chambers. For the 96-well plate data, points are the average of 6 images originating from 2 wells. Brightness is normalized so that the maximum occurs at 1. Variance of the 96-well plate data from the on-chip data may be due to slightly different imaging conditions (on-chip exposure times: 100 ms Tom, 100 ms cyan; well plate exposure times: 50 ms Tom, 50 ms cyan).

more data to be collected compared to end-point methods such as FACS.

### 3.3.8 Supplementary Movies

Supplementary movies (53 h continuous monitoring of tdTomato expression, AmCyan expression, and growth in brightfield) are available at: <http://www.nature.com/articles/srep23937>

## 3.4 Discussion

We developed a high-throughput microfluidic platform capable of 280 independent transfections at up to 99% efficiency with HEK 293T cells. In comparison, other biochip platforms

### **Chapter 3. A high-throughput microfluidic platform for mammalian cell transfection and culturing**

---

obtained between 13% and 80% transfection efficiency<sup>51-53</sup>, while throughputs ranged between 1 to 96 reactions per device<sup>54-57</sup>. The transfection reactions on our chip are confined to separate chambers, decreasing the risks of cross-contamination and communication between different positions on the array. This segregation, combined with the chip's ability to automate long-term cell culture, has the potential to overcome the limitations of reverse transfection microarrays. Microfluidic platforms are easily adapted to high-content imaging<sup>88-90</sup>, and the reduced sample requirement enables the study of cells that are available in limited quantities. The behavior of cells over time can further be monitored in response to fluidic stimuli such as change of the culturing medium or introduction of a drug<sup>58</sup>. By implementing a recently developed synthetic two-component system we show that our integrated microfluidic transfection platform can be used to optimize and study synthetic circuits. Overall, the high-throughput microfluidic transfection and cell-culturing platform we demonstrate here should be a useful tool for mammalian cell engineering.

#### **3.4.1 Acknowledgments**

We thank Zuzana Tatarova (CDTSO, School of Life Sciences, Ecole Polytechnique Fédérale de Lausanne) for providing the HEK cells and for advice regarding cell culturing and microfabrication. We thank Valérian Ruhaut (CMi, Ecole Polytechnique Fédérale de Lausanne) for advice regarding microfabrication. We thank Loïc Tauzin and Valérie Glutz (FCCF, Ecole Polytechnique Fédérale de Lausanne) for assistance with flow cytometry. We thank Yaakov Benenson for providing the DcuS/R system. The work was funded by a Swiss National Science Foundation Pro-Doc grant (PDFMP3 137065).

#### **3.4.2 Author contributions**

K.W. performed experiments. K.W. and S.J.M. designed experiments and wrote the paper.

#### **3.4.3 Competing financial interests**

The authors declare no competing financial interests.

### **3.5 Methods**

#### **3.5.1 Microarray printing and slide treatment**

Prior to arraying, glass slides were washed by shaking in a 57% Ethanol, 10% w/v NaOH solution for 2 h. The slides were thoroughly washed with Milli-Q water and dried before proceeding to microarray printing. Glass slides etched with microwells in the positions of the cell chambers were also explored in attempts to decrease cross-contamination, however the microwells were difficult to align with the microarrayer. The spotting pin tended to come in contact with the

sides of the wells rather than the bottom, preventing sufficient amounts of transfection mixture from being deposited into the bottoms of the wells. A QArray2 microarrayer (Genetix GmbH) was used to array samples contained in conical-well, poly(propylene) 384-well plates (Arrayit). Most solutions were spotted using a pin with a 300  $\mu\text{m}$  spot diameter and 3.3 nl delivery volume (946MP9, Arrayit). For the 2-component system, a 500  $\mu\text{m}$  spotting pin was used (946MP15, Arrayit). Spotting parameters for both lipid-DNA mixtures and PLL were 1 s inking time, 500 ms printing time. Between samples, the pin was washed with water for 500 ms and dried for 500 ms. Lipid-DNA was stamped once per spot. As has been previously reported<sup>52</sup>, we found that stamping multiple times per spot resulted in imprecisely localized spots due to spreading of excess DNA. Following microarraying, lipid-DNA arrays were immediately stored in a desiccator.

PLL was stamped 4 times per spot in a cyclic fashion, with approximately 8 min between cycles. 2 h after the arraying was complete, PLL arrays were thoroughly washed with filtered water, dried, and stored in a desiccator. PLL slides were used between 2 and 8 weeks post-coating, since the quality of the PLL has been shown to decrease significantly beyond this time period<sup>111</sup>.

#### 3.5.2 Microarraying mixture preparation

The PLL sample was prepared by adding 25  $\mu\text{L}$  of 0.1% PLL solution (Sigma) to 50  $\mu\text{L}$  of a solution of 0.225 M boric acid, pH 8.4. Evenly-coated PLL slides were prepared according to standard protocols<sup>109</sup>. The lipid-DNA method developed by Ziauddin et al.<sup>33</sup> was used to prepare transfection mixtures containing Effectene (Qiagen). First, 1.5  $\mu\text{g}$  of supercoiled plasmid DNA was diluted in 15  $\mu\text{L}$  of EC buffer in which sucrose had been dissolved at a concentration of 0.2 M. In the case of co-transfection, this mixture was vortexed for 10 s and allowed to incubate for 15 min. Next, 1.5  $\mu\text{L}$  Enhancer was added and the mixture was vortexed for 1 s and incubated at room temperature for 5 min. Next, 5  $\mu\text{L}$  Effectene was added and the mixture was vortexed gently for 10 s and incubated for 10 min. Lastly, 12.7  $\mu\text{L}$  of a 0.5% gelatin solution (prepared from G9391, Sigma) and 12.7  $\mu\text{L}$  of a 0.1% fibronectin solution (F0895, Sigma) were added and the samples were transferred to a 384-well plate for microarraying. Human plasma fibronectin could be replaced with bovine plasma fibronectin (Sigma-Aldrich F4759, powder dissolved in water at 1 mg/ml) with no decrease in transfection efficiency.

Samples for the gelatin-DNA transfection method were prepared similarly and contained a mixture of 1.5  $\mu\text{g}$  DNA and buffer EC (total of 25.4  $\mu\text{L}$ ), 12.7  $\mu\text{L}$  gelatin, and 12.7  $\mu\text{L}$  fibronectin. A mixture of 16  $\mu\text{L}$  Enhancer, 150  $\mu\text{L}$  EC buffer, and 25  $\mu\text{L}$  Effectene was flowed on chip for 30 min using the same conditions used for medium perfusion. Medium was flowed on chip for 20 min before cell loading.

Co-transfection mixtures were prepared by modifying the ratios of each plasmid and keeping total DNA content at 1.5  $\mu\text{g}$  for each mixture. Attempts to co-transfect by co-spotting (sequential spotting of separately prepared transfection mixtures) and to achieve stable protein

## **Chapter 3. A high-throughput microfluidic platform for mammalian cell transfection and culturing**

---

production via lentiviral transduction were unsuccessful (see Appendix).

### **3.5.3 Standard transfections**

96-well plate transfections were performed by first seeding each well with 10,000 cells the day before transfection. Each well was transfected with 0.1 µg DNA diluted in EC buffer, 0.8 µL Enhancer, and 2.5 µL Effectene (prepared according to manufacturer's instructions). Images were acquired and processed in the same manner used for on-chip experiments. 6-well plate transfections were performed by first seeding each well with 200,000 cells the day before transfection. Each well was transfected with 0.4 µg DNA diluted in EC buffer, 3.2 µL Enhancer, and 10 µL Effectene (prepared according to manufacturer's instructions). Cells were harvested and subjected to analysis by flow cytometry.

### **3.5.4 DNA staining**

A 100x dilution of YOYO-1 dye (Life Technologies) was prepared in DMSO (Sigma). The YOYO dilution was added to the complete lipid-DNA transfection mixture to result in a final 10,000 fold dilution. The transfection-dye mixture was incubated for 60 min before microarraying. The stained arrays were visualized by using an ArrayWorx scanner (Applied Precision).

### **3.5.5 Cell culture**

All culture reagents were acquired from Gibco (Life Technologies). Cells were cultured at 37 °C and 5% CO<sub>2</sub> in Dulbecco's modified Eagle medium (DMEM) supplemented with 10% FBS and antibiotic-antimycotic. Cells were passaged every 2-3 days using TrypleE express. For on-chip experiments, cells were grown in CO<sub>2</sub> independent medium supplemented with GlutaMAX, 10% FBS and antibiotic-antimycotic. Microfluidic chips were cultured on the stage of a microscope contained within an incubation chamber (Life Imaging Services) maintained at 37 °C.

### **3.5.6 Flow cytometry**

48 h after transfection, cells were trypsinized and resuspended in PBS. For analysis, a BD LSRII was used with the following settings: for eGFP, a 488 nm laser and a 525/50 filter with a photomultiplier tube (PMT) voltage of 225, for tdTomato: a 561 nm laser and 585/15 filter with a PMT voltage of 379. 50,000 events were measured per sample.

### **3.5.7 Imaging**

Imaging of the microfluidic transfection arrays was performed on a Nikon Ti-E Eclipse automated microscope using NIS Elements. Images were acquired with an Ixon DU-888 camera

(Andor Technology), using 20x magnification to capture an entire chamber in the field of view. Each chamber was imaged in brightfield and fluorescence mode. Three HC filter cubes were used: TexasRed (HC 562/40, HC 624/40, BS 593) for tdTomato, FITC (HC 482/35, HC 536/40, BS 506) for eGFP, and CFP (HC 438/24, HC 483/32, BS 458) for AmCyan (all from AHF Analysentechnik AG). Images were stitched together using the Grid/Collection Stitching plugin in Fiji<sup>100</sup>. Cells were counted using the “Load Images”, “Crop”, “Identify Primary Objects”, and “Measure Image Area Occupied” modules of CellProfiler<sup>120</sup> or by using a custom written Matlab script (see Appendix).

Transfection efficiency was calculated as the area occupied by fluorescent cells in the entire chamber (500  $\mu\text{m}$  diameter) divided by the area occupied by cells within the 300  $\mu\text{m}$  diameter spot where the lipid-DNA was deposited. This normalization is necessary because following cell loading into the chambers, only some of the cells have access to the transfection mixture (a 300  $\mu\text{m}$  spot within a 500  $\mu\text{m}$  chamber). Some cells that initially settle in the lipid-DNA area migrate to different parts of the chamber after 48 h (when images are captured), resulting in the dispersed pattern visible in the images.

#### 3.5.8 COMSOL modeling

COMSOL Multiphysics was used to build a 2D representation of the microfluidic cell culturing chambers. The modules laminar flow and transport of diluted species were used. Cytochrome C, a 13.4 kDa protein with a diffusion coefficient of  $1.14 \times 10^{-6} \text{ cm}^2/\text{s}$ , was used to model the transport of diluted species.

#### 3.5.9 Microfluidic device fabrication

Microfluidic devices were designed in Clewin (WieWeb software, Netherlands). Two molds were designed: one for the control layer, which contains the valves, and another for the flow layer, which contains the channels and chambers necessary for reagent introduction and cell culturing. The control layer was scaled by 101.5% to account for PDMS shrinkage during curing.

The molds were fabricated using standard photolithography methods. The control layer mold was patterned with SU-8 photoresist (Gersteltec, Switzerland) to a height of 30  $\mu\text{m}$ . The flow layer mold for the sieve chip design (Fig. 3.2a) was fabricated in five steps. First, to create alignment marks, AZ1512 positive photoresist (MicroChemicals GmbH) was spin coated to a height of 1  $\mu\text{m}$ , then exposed and developed. The alignment marks were etched to a depth of 4  $\mu\text{m}$  using inductively coupled plasma. The AZ1512 hard mask was then removed using oxygen plasma. Second, a dummy layer of SU-8 was spin coated to a height of 2  $\mu\text{m}$ , then flood exposed and developed. Third, sieves were created by spin coating SU-8 to a height of 5  $\mu\text{m}$ , followed by exposure and development. Fourth, flow channels were generated by spin coating SU-8 to a height of 30  $\mu\text{m}$ , followed by exposure and development. Lastly, valve

### **Chapter 3. A high-throughput microfluidic platform for mammalian cell transfection and culturing**

---

regions were patterned by spin coating AZ9260 (MicroChemicals GmbH) to a height of 30  $\mu\text{m}$ , then exposing and developing. The AZ9260 was annealed at 120  $^{\circ}\text{C}$  for 25 s to generate the rounded profile that is required for complete valve closure. The valve chip design (Fig. 3.1a) was fabricated by performing only steps four and five of the protocol detailed above.

Polydimethylsiloxane (PDMS; Sylgard 184, Dow Corning Corp., USA) was cast onto the molds and multilayer soft lithography techniques were used to assemble the chip<sup>121</sup>. A thick layer of PDMS (5:1 ratio of parts A:B) was poured onto the control layer, whereas the flow layer was spin coated with PDMS (20:1 ratio of parts A:B) with a ramp of 15 s and a spin of 35 s at 650 rpm. The molds were baked for 30 min at 80  $^{\circ}\text{C}$ . The control layer chips were then cut, removed from the mold, and punched with inlet holes. The control layer chips were aligned to the flow layer, and the assembly was baked for 90 min at 80  $^{\circ}\text{C}$ . The aligned devices were then cut, removed from the mold, and punched with inlet and outlet holes. The PDMS chips were bonded to the glass arrays by using 7 s of oxygen plasma treatment, followed by baking for 1 h at 80  $^{\circ}\text{C}$ . Transfection devices were stored in a desiccator prior to use.

#### **3.5.10 Microfluidic device operation**

The pressures of the flow and control layers of the chip were controlled by using a custom built pneumatic setup. The valves of the control layer were first primed with filtered water at 5 psi. Once all air had been removed from the control lines, the control layer pressure was increased to 22 psi. Medium was flowed through the chip prior to cell loading. A sample containing 800,000 cells in 20  $\mu\text{L}$  PBS was purged through the chip inlets. After purging, the cells were loaded into the first set of columns at a speed of 7.2  $\mu\text{L}/\text{min}$  for the low-throughput chip and 27.3  $\mu\text{L}/\text{min}$  for the high-throughput chip. Flow rate was determined by measuring the volume of liquid exiting the chip over a period of time. Columns were loaded in sets sequentially, and the chamber-segmenting valves were actuated once loading for each set was complete. For the sieve design, medium was immediately perfused at a rate of 1 ml/h (16.7  $\mu\text{L}/\text{min}$ ). For the valve design, medium was pulse perfused for the first hour. Medium was flowed with chamber valves closed (5 min) followed by stopping the flow and opening the chamber valves (5 min). After cycling between these two states for the first hour, the chamber valves were opened during continuous medium flow of 1 ml/h. PTFE tubing was used for all fluidic connections because we observed some cell toxicity when using Tygon tubing, as has been previously reported<sup>103</sup>.



# 4 A microfluidic module for real-time generation of complex multi-molecule temporal concentration profiles

Article submitted to Analytical Chemistry, May 2017

**Authors:**

Kristina Woodruff & Sebastian J Maerkl

**Contribution:**

KW designed and performed experiments and wrote the paper.

**Bibliographic reference:**

Woodruff, K. & Maerkl, S. J. A microfluidic module for the real-time generation of complex multi-molecule temporal concentration profiles. Manuscript submitted and in revision (Analytical Chemistry).

## Chapter 4. A microfluidic module for real-time generation of complex multi-molecule temporal concentration profiles

---

### 4.1 Abstract

We designed a microfluidic module that generates complex, dynamic concentration profiles of multiple molecules over a large concentration range using pulse-width modulation (PWM). Our PWM device can arbitrarily combine up to 6 different inputs and select between three downstream mixing channels as required by the application. The module can produce arbitrary concentrations with a dynamic range of up to 3-5 decades. We created complex concentration profiles of 2 molecules, with each concentration independently controllable, and show that the PWM module can execute rapid concentration changes as well as long-timescale pharmacokinetic profiles. Concentration profiles were generated for molecules with molecular weights ranging from 560 Da to 150 kDa. Our PWM module produces robust and precise concentration profiles under a variety of operating conditions, making it ideal for integration with existing microfluidic devices for advanced cell and pharmacokinetic studies.

### 4.2 Introduction

In order to perform complex and biologically relevant experiments on microfluidic platforms, there is a need for accurate and automated methods to manipulate molecular concentrations on chip. Microfluidic devices are generally connected to a small number of input solutions. Consequently, most experiments involve one or more step function changes, switching rapidly from one molecule to another or from one concentration to another. In contrast, naturally occurring changes in concentrations of molecules are rarely instantaneous step-functions. Physiologically relevant changes, such as pharmacokinetic drug concentration profiles, occur over minutes to hours and follow a complex, continuous rise and fall pattern. Complex temporal concentration profiles of one or more substances could be used to study the influence of changing antibiotic concentrations on bacteria, the effects of drugs on mammalian cells, and stem cell differentiation. The ability to rapidly generate arbitrary and complex temporal concentration profiles is thus of general interest and a useful experimental method.

One technique to create concentration profiles from two inputs involves lateral diffusion-based gradients<sup>70,71</sup>. Two fluids are simultaneously flowed parallel to one another along the length of a channel or chamber, establishing a gradient that is perpendicular to the direction of the flow. This principle has been used to design microfluidic devices capable of preparing up to 81 chemical combinations<sup>69</sup>. However, the total possible outputs are highly dependent on the number of inputs (16 stock solutions are needed to produce 81 different solutions) and because this approach is diffusion-based, it offers poor spatio-temporal resolution. Several active mixing techniques<sup>72</sup> including mechanical micromixers<sup>73</sup>, microstructures<sup>74</sup>, integrated peristaltic pumps<sup>75</sup>, and serial dilution schemes<sup>76</sup> have been developed to provide fast concentration changes. As with the gradient-based technique, the number of possible concentrations on these devices is also limited and defined by the number of solution inputs.

To generate small changes in concentration over a large dynamic range, dynamic strategies

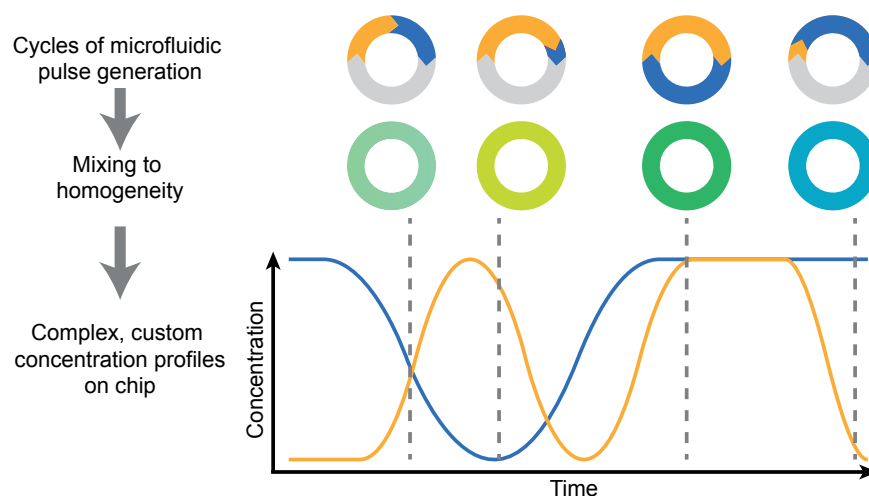


**Figure 4.1.** Schematic of microfluidic PWM. Circles represent one full pulse cycle. Yellow and blue represent molecules of interest, gray represents diluting buffer.

such as pulse-width modulation (PWM) are necessary. PWM is based on the concept of controlling the duty cycle of a load to control voltage and current in electrical engineering. The microfluidic equivalent controls the flow of buffer and substrate reservoirs (Fig. 4.1). A microfluidic device that supports fast switching times can generate alternating pulses of buffer and substrate. When directed through a channel, these pulses diffuse to homogeneity. Total cycle time (time to execute one pulse of buffer and one pulse of substrate) is kept constant. Different concentrations are created by varying the duty cycle, which refers to the fraction of time occupied by the substrate pulse in comparison to the total cycle time.

PWM has been incorporated into microfluidic diluters in the past<sup>85–87,122</sup>. For a single molecule of small size, previous examples have prepared solutions of specific concentrations with high accuracy. The compatibility of these devices with proteins and substances larger than small dye molecules has not been tested. Moreover, current PWM devices have not demonstrated that complex patterns can be generated for multiple molecules simultaneously. Another drawback is the large, non-standard dimensions of the mixing infrastructure; these elements require additional cleanroom fabrication steps and occupy a significant amount of space on the chip. Lastly, previously reported PWM chips have performed experiments lasting from a few minutes to 1.5 hours. It is unknown whether these devices are capable of sustaining concentrations for extended time periods, as experiments spanning several hours or days would be required for studies involving bacteria or mammalian cells.

Long-term concentration manipulation on microfluidic devices would also be interesting for pharmacokinetic and pharmacodynamic (PK/PD) studies. These assays are central to drug discovery and development<sup>80,81</sup>. Typical *in vitro* PK/PD models, while able to properly reproduce the pharmacokinetics of drugs *in vivo*, provide only bulk measurements<sup>82</sup>. This simplified setup poorly represents the complex *in vivo* environment and is not compatible

## Chapter 4. A microfluidic module for real-time generation of complex multi-molecule temporal concentration profiles

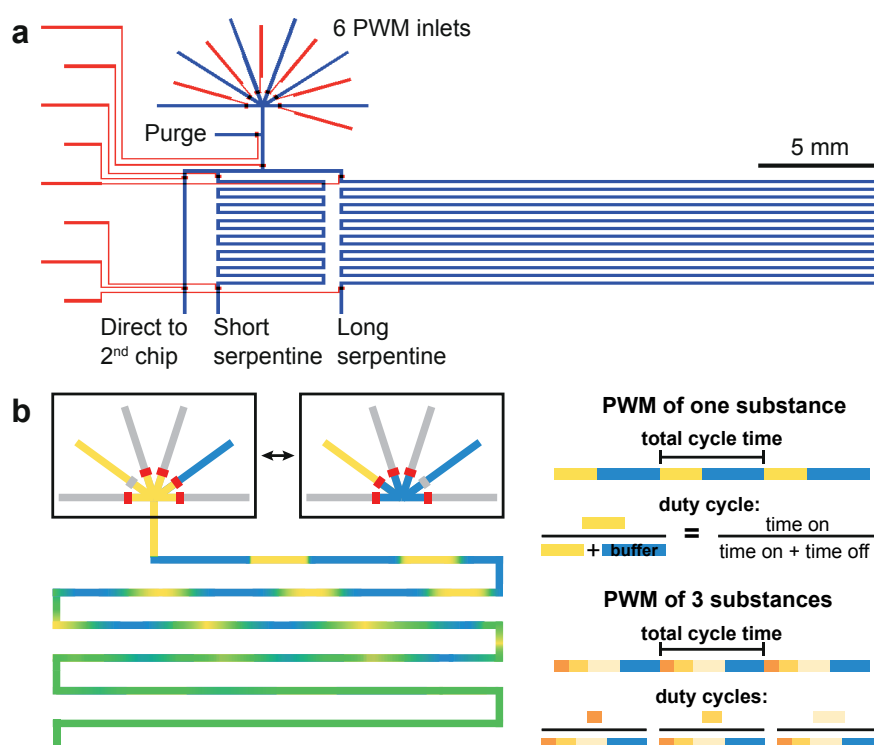


**Figure 4.2.** The PWM platform. (a) Design of the PWM mixing chip. Red, control layer for valve actuation; blue, flow layer for fluid manipulation. (b) Schematic of the PWM technique. Pulses are created by alternating the opening and closing of inlets. The pulsed flow pattern diffuses to homogeneity in the serpentine channels.

with techniques that probe single cell phenotypes. Although microfluidic chips have been designed to address this need<sup>83,84</sup>, these devices lack the ability to simulate the gradually rising and falling concentrations of drugs in plasma. Ideally, a device should be able to create realistic PK/PD profiles for multiple substances at once.

We have developed a microfluidic device that improves upon previous PWM-based chips, making it compatible with a broad range of applications. Our device successfully implements concentration changes over both short and long time scales, making it capable of producing complex PK/PD profiles. The device occupies minimal space and its features can be fabricated in one photolithographic layer. These characteristics facilitate integration of the module into existing chip designs. We also show that the PWM device can function as an independent module connected upstream of a second chip. The ability to easily modify total cycle times and choose between 3 mixing channel options (short serpentine, long serpentine, and tubing connection to a second chip) ensure that our chip can function with a variety of molecule sizes and flow rates. Two substances can be manipulated in parallel, and the chip supports a dynamic range of nearly 3 orders of magnitude in output concentrations. These qualities make our chip an attractive tool for chemical and biological research requiring complex profiles and

will enable studies that were previously inaccessible because of technical limitations.

## 4.3 Results

### 4.3.1 PWM chip design and technique

We designed a microfluidic module (Fig. 4.2a) that performs PWM to mix up to 6 different input solutions. The device measures 1.2 x 2.8 cm and was fabricated using standard photolithography and soft lithography techniques. The valves controlling the flow of these inputs were engineered for fast actuation (<30 ms, Fig. 4.3) in order to accurately dispense short pulses of each input solution. The input channels merge into a common channel, and the flow can be directed into one of three paths depending on the application. A short serpentine channel (53 mm length, 0.074  $\mu$ L capacity) facilitates diffusion-based mixing of small molecules and most proteins as they travel along the channel. The long serpentine channel (255 mm length, 0.356  $\mu$ L capacity) provides for the mixing of complex solutions or large proteins with small diffusion coefficients. Lastly, flow can be directed into a short channel (8 mm length) and subsequently connected to another chip via flexible tubing. Merging of the pulses will occur in the tubing, delivering a homogeneous solution to the connected chip.

To adjust the concentration generated on chip, we modified the amount of time that each solution was flowed to produce pulses of different lengths. Only one solution was flowed at a time, and both the flow rate and the total cycle time (time to complete one round of pulses) were kept constant (Fig. 4.2b). Of the 6 inputs, at least one was a buffer used for dilution. The other 5 can be either 5 different substances (to prepare a complex mixture), the same substance diluted to 5 different concentrations (to enable an expansive dynamic range), or any combination of these two cases. We wrote a program that selects which inputs to use and executes valve opening and closing to create pulse patterns that reflect the programmed profile.

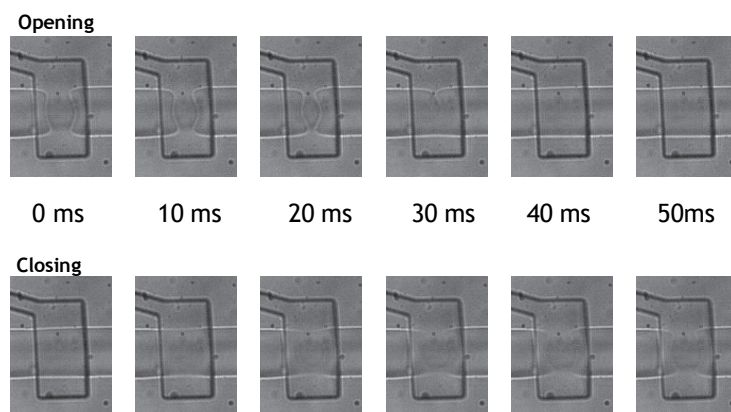


**Figure 4.3.** Timing of valve switching.

## Chapter 4. A microfluidic module for real-time generation of complex multi-molecule temporal concentration profiles

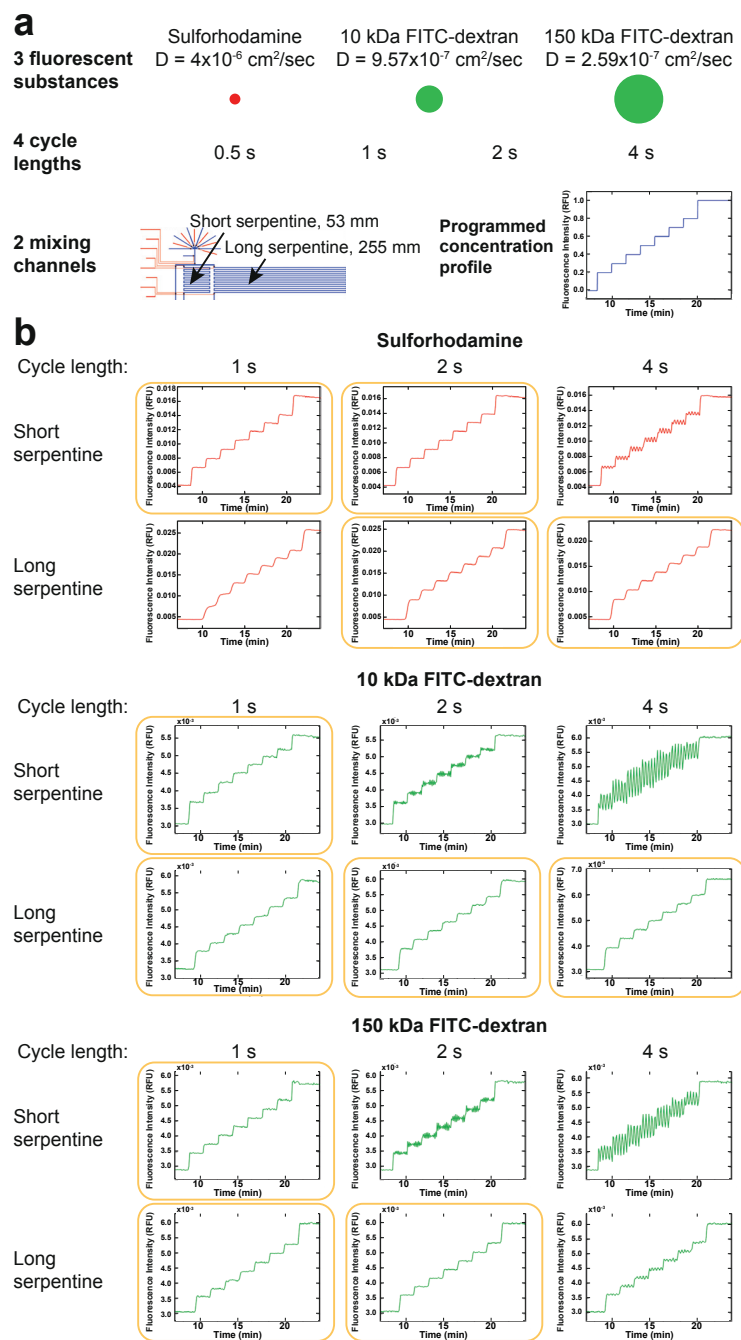


**Figure 4.4.** Determining optimal PWM conditions. (a) Schematic of experimental conditions tested and programmed concentration profile. (b) Experimental results. Images were acquired every 5 s at the end of the serpentine channels and analyzed for fluorescence intensity. Rightward shift of the data compared to the expected profile is caused by the time required for the solutions to travel from the PWM area to the end of the channel. Yellow boxes indicate optimal conditions.

### 4.3.2 Optimizing PWM total cycle length

To determine the optimal operating conditions for the PWM chip, we conducted experiments with 2 inputs. Since we aimed to engineer a chip that would be functional for low and high molecular weight proteins in addition to small molecules, we tested 10 kDa FITC-dextran, 150 kDa FITC-dextran, and 559 Da sulforhodamine as substrates (Fig. 4.4a). 9 different duty cycles were consecutively implemented on chip using total cycle times of 0.5, 1, 2, and 4 s (Fig. 4.4a). Both the short and long serpentine channels were tested, with flow rates of 24  $\mu\text{L}/\text{h}$  and 19  $\mu\text{L}/\text{h}$ , respectively. The fluorescence intensity of the fluid was measured at the end of the mixing channels and analyzed.

We observed repeated and random experimental failures when using a 0.5 s cycling time (Fig. 4.5). This result could possibly arise from the inability of the automated setup (a LabVIEW-controlled relay board and solenoid valves) to perform accurately over extended periods of time with such high switching rates. Alternatively, the 30 ms valve opening/closing time may be non-negligible in comparison to the short pulse lengths. All other cycle times (1-4 s) yielded an excellent linear correlation between programmed duty cycle and mean fluorescence intensity for both the short and long serpentine and for all 3 fluorescent substances (Fig. 4.4b). The concentrations produced on chip (Fig. 4.4b) closely match the programmed profile (Fig. 4.4a).

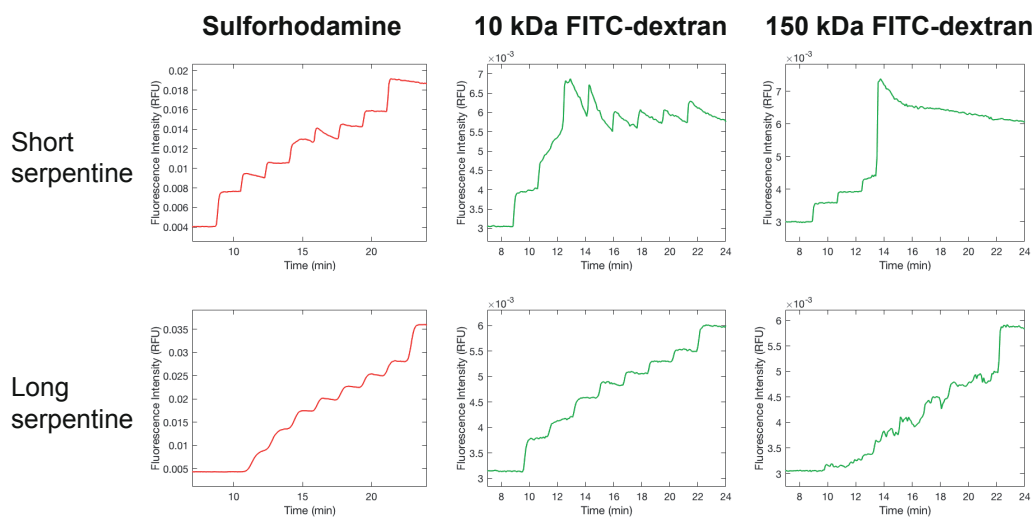


**Figure 4.5.** Plot of fluorescence intensity over time for a 0.5 s total cycle time. Experiment was performed as in Figure 4.4b.

## Chapter 4. A microfluidic module for real-time generation of complex multi-molecule temporal concentration profiles

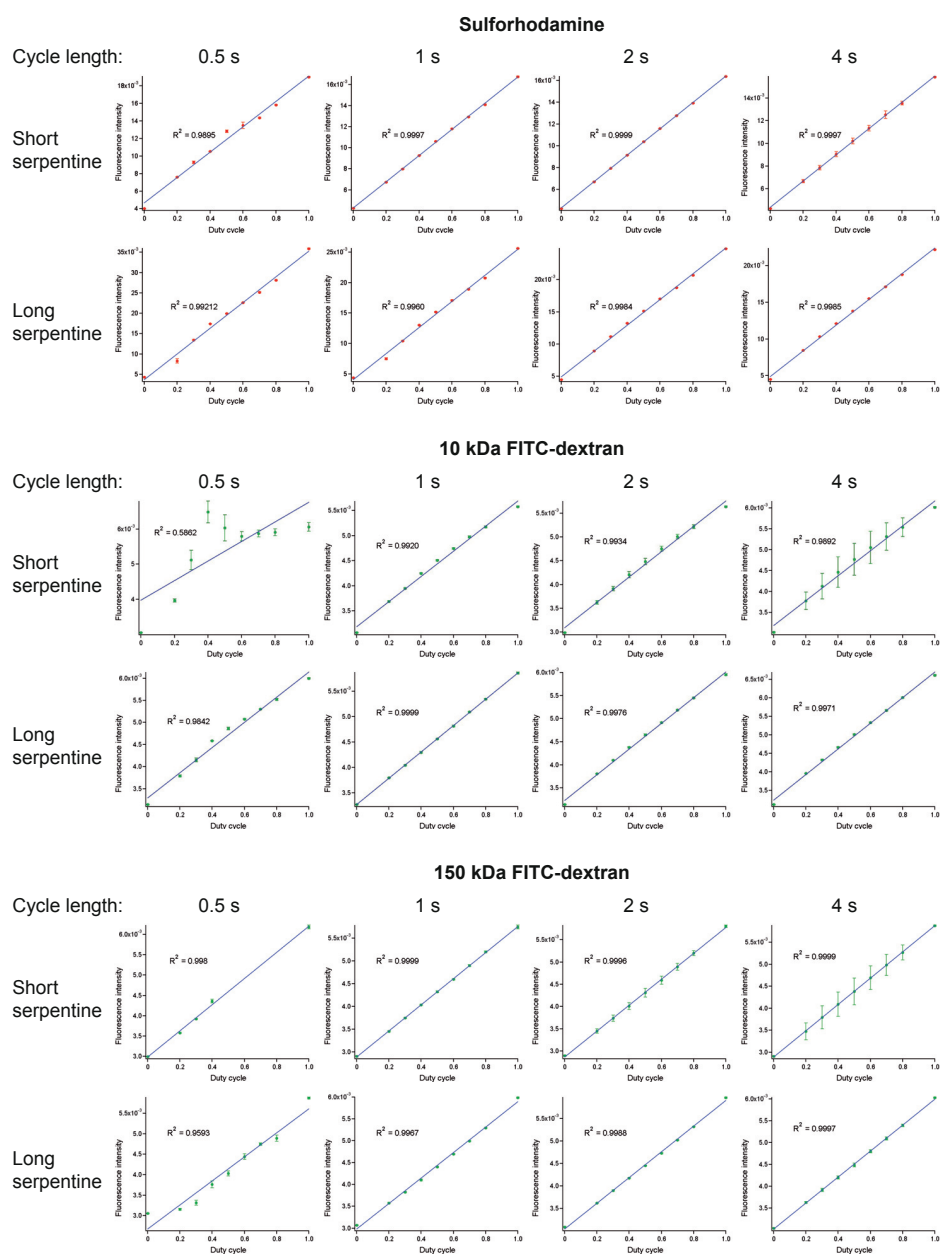


**Figure 4.6.** Different cycles times on the PWM chip: Mean fluorescence intensity as a function of programmed duty cycle, derived from the data presented in Fig. 4.4b. Errors bars represent standard deviation. Means were calculated from ~15-20 RFU measurements each and did not include the data points that fell between two concentrations (during ramp up).

In addition to establishing that concentration can be precisely regulated, we tested conditions that gave rise to the most homogeneous solutions. In cases of insufficient diffusion, the pulses generated at the inlet are not completely mixed by the time they reach the measurement area. These pulses manifest as spikes of alternating high and low intensity on the raw data



graphs (Fig. 4.4b) and equate to sizeable standard deviations on the extrapolated duty cycle graphs (Fig. 4.6). Mixing is presumably more restricted for larger substrates, shorter mixing channels, or longer pulses created by longer cycle times. We observed these trends in our data; distinct pulses were especially perceptible for the 10 and 150 kDa dextrans flowed through the short serpentine at increased (2-4 s) cycle lengths (Fig. 4.4b). By testing this matrix of various operating conditions, we identified the combinations of molecule size, mixing channel, and cycle length for optimal performance.

### 4.3.3 Characterizing response time

We next conducted experiments to determine the response time of our PWM module, defined as the amount of time needed to switch from 10 to 90% of the maximum concentration. We used a flow rate of 36  $\mu\text{L}/\text{h}$  for the short mixing channel and 30  $\mu\text{L}/\text{h}$  for the long channel. When performing PWM with a 1 s total cycle time, we obtained response times as low as 5 s (Fig. 4.7a,b). Depending on which substance was used, response times for the long mixing channel were 2.3-3x greater than those of the short channel. Descending from 90 to 10% concentration required slightly more time than rising from 10 to 90%. As anticipated, response time increased as substrate molecular weight decreased; for large diffusion coefficients, steep ramps became spread out due to extensive diffusion (Fig. 4.7a). Accordingly, the short serpentine is better suited for experiments that call for sudden and extreme changes of diffusion-sensitive small molecules. However as shown in Figures 4.4b and 4.6, the longer serpentine can be successfully used for larger molecules and to create profiles that entail more gradual changes.

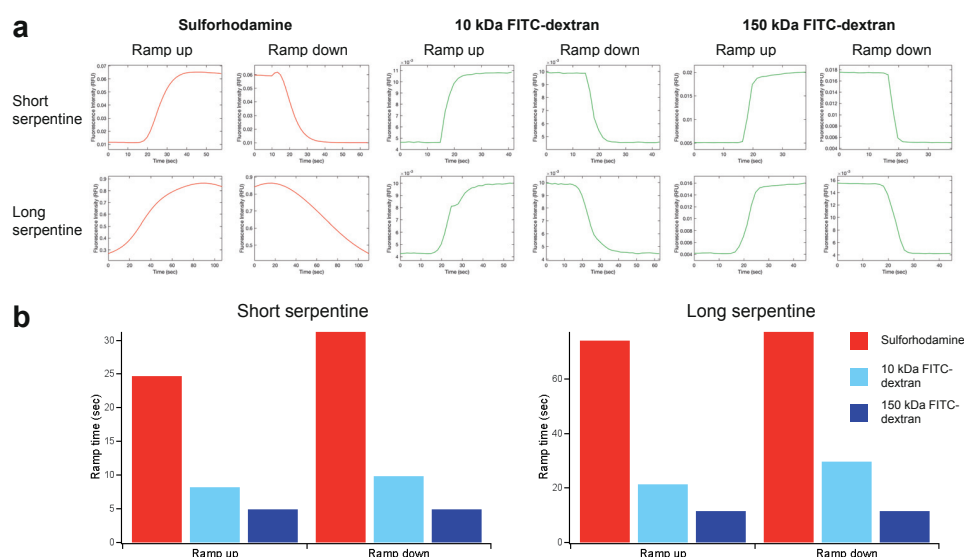


**Figure 4.7.** Response times required to switch between 10 and 90% of the maximum concentration. (a) Plots showing the time needed to ramp up and down. (b) Summary of results.

## Chapter 4. A microfluidic module for real-time generation of complex multi-molecule temporal concentration profiles

### 4.3.4 Testing different flow rates on the PWM module

The data presented in Figures 4.4, 4.6, and 4.7 attests to the precision and quick response time of our chip when operated with typical flow rates. For these experiments, we used flow rates of  $\sim 24\text{-}36\ \mu\text{L}/\text{h}$  for the short channel and  $\sim 19\text{-}30\ \mu\text{L}/\text{h}$  for the long channel, generated by pressurizing the flow inputs with 4 or 10 psi, respectively. These pressures are within

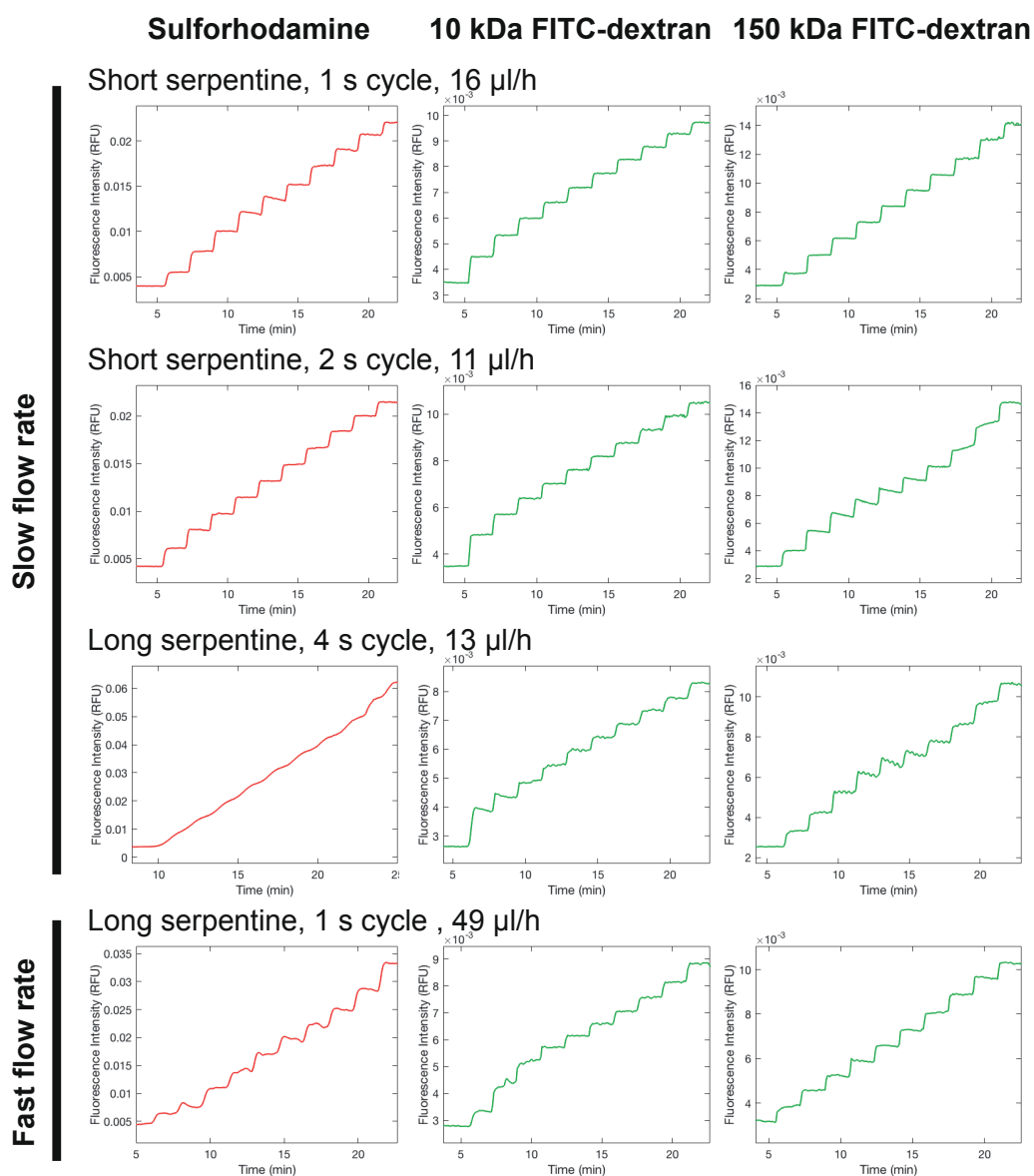


**Figure 4.8.** Different flow rates on the PWM chip: Measured fluorescence intensity resulting from step-wise duty cycle increases over time. Images were acquired at the end of the serpentine channels every 5 s and analyzed for fluorescence intensity.

the standard range used for microfluidic chips of similar dimensions<sup>123,124</sup>. To ensure the compatibility of our chip with a greater variety of applications, we also tested the chip with faster and slower flow velocities.

Slow flow rates (11-16  $\mu\text{L}/\text{h}$ ) worked best when the short mixing channel was used with a total cycle length of 1-2 s (Fig. 4.8, 4.9). Using a long mixing channel with a slow flow rate bears the risk that the fluid will spend too much time in the channel. Subsequently, extensive diffusion will obscure the programmed concentration steps. We mitigated this effect in the long channel by extending the total cycle time to 4 s in order to create large pulses that would homogenize more slowly. This strategy would work best for small ( $\sim 10$  kDa) proteins; the 150 kDa FITC-dextran pulses did not completely combine, and the sulforhodamine concentration steps were blended as a consequence of diffusion (Fig. 4.8, 4.9).

When coupling faster flow rates (49  $\mu\text{L}/\text{h}$ ) with the short mixing channel, pulses passed through the channel too quickly and exited still intact. Only the long channel promoted complete

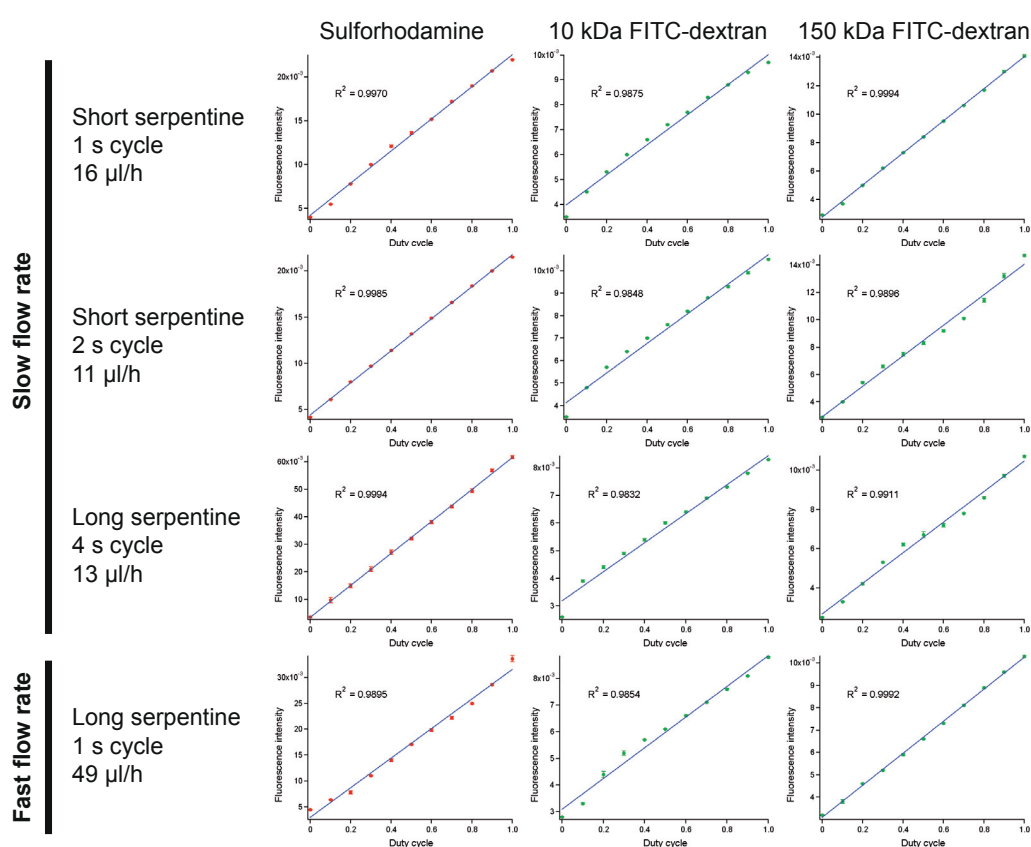


**Figure 4.9.** Different flow rates on the PWM chip: Mean fluorescence as a function of programmed duty cycle, derived from the data presented in Figure 4.8. Errors bars represent standard deviation. Means were calculated from  $\sim 15$ -20 RFU measurements each and did not include the data points that fell between two concentrations (during ramping up).

## Chapter 4. A microfluidic module for real-time generation of complex multi-molecule temporal concentration profiles

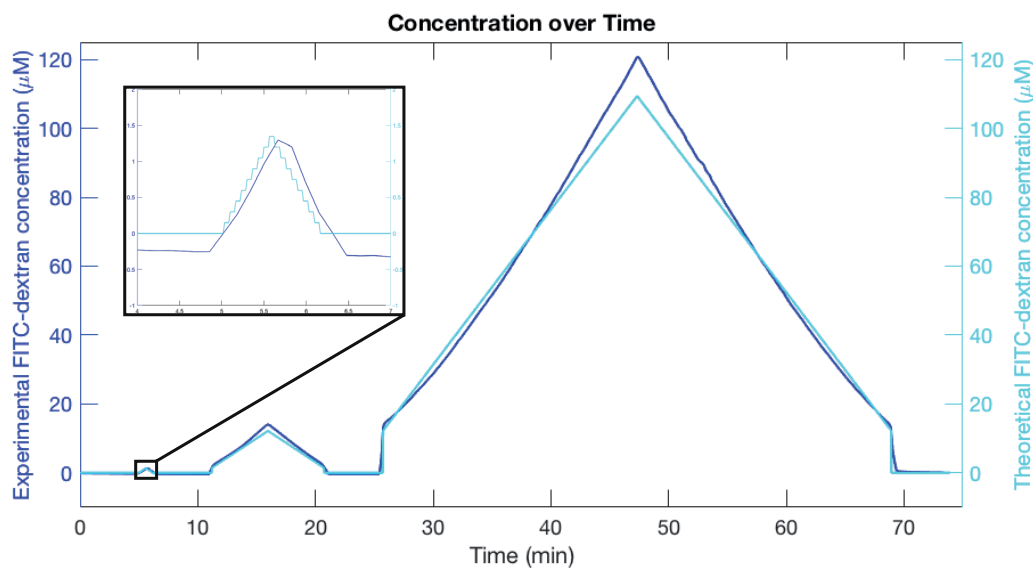


**Figure 4.10.** PWM dynamic range and control of on chip concentration. Experimental result superimposed with programmed values for 10 kDa FITC-dextran. Images were acquired at the end of the long serpentine channel every 10 s, analyzed for fluorescence intensity, and converted to absolute concentration using calibration images.

diffusion for fast flow rates owing to the increased passage time (Fig. 4.8, 4.9). Additionally, we applied the shortest possible total cycle time (1 s) to generate short pulses that would homogenize faster and expedite the mixing process. Comparing the fast flow data to the slow flow data reveals that our chip can support more than a 4-fold change in flow rates. These flow rates (11-49  $\mu\text{L}/\text{h}$ ) are compatible with those used for low to medium throughput microfluidic studies of bacteria<sup>125,126</sup> and mammalian cells<sup>103,127,128</sup>. The faster flow rates necessary for high-throughput culturing devices<sup>129</sup> could be achieved by scaling up the features of the PWM chip, which would decrease fluidic resistance.

### 4.3.5 Characterizing the dynamic range

For all experiments we used a minimum duty cycle of 0.1 and maximum of 0.9 to ensure that the valve opening and closing times (30 ms, Fig. 4.3) were not too substantial compared to pulse lengths. Cycle times greater than those tested in this work equate to longer pulsing lengths and can most likely support more extreme duty cycles. In order to broaden the dynamic range of output concentrations while keeping duty cycles between 0.1 and 0.9, we connected the chip to multiple preparations of the same substance at different concentrations. A series of 9-fold dilutions was performed to prepare 3 stock solutions of 10 kDa FITC-dextran. Our automated platform selects which stock solution to use based on the desired output concentration.

We performed this experiment using standard PWM conditions (1 s cycle length, long serpen-

tine channel, and a 27  $\mu\text{L}/\text{h}$  flow rate). The chip was programmed to create concentrations that fell within low (0.15–1.35  $\mu\text{M}$ ), medium (>1.35–12.15  $\mu\text{M}$ ), and high (>12.15–109.35  $\mu\text{M}$ ) ranges. The difference between the maximum (109.35  $\mu\text{M}$ ) and minimum (0.15  $\mu\text{M}$ ) concentration values is ~3 orders of magnitude, or a 729-fold change. We also acquired reference images of each stock solution, allowing us to convert fluorescence intensities at the outlet of the mixing channel to absolute concentrations. We found that the generated concentration profiles closely matched the programmed values for all 3 inlet pairs (Fig. 4.10). Diffusion of FITC-dextran in the serpentine channel converts the step-wise profile of the input file into a smooth contour.

Due to the limited sensitivity of fluorescence detection on our setup, we tested only 3 serial dilutions. The 729-fold concentration range presented in Figure 4.10 is for example well within the typical difference between the minimum and maximum serum concentration of antibiotics measured in clinical studies<sup>130,131</sup>. However if all 6 inlets of the chip were to be utilized (5 stock solutions prepared as 9-fold serial dilutions and 1 buffer), a 59049-fold range of output concentrations could be produced. These results suggest that our technology can accurately replicate complex *in vivo* concentration profiles.

#### 4.3.6 Connecting the PWM module to a second chip

The PWM module can be easily integrated into chips fabricated by multilayer soft lithography<sup>132</sup> due to its small size and the standard dimensions of its channels. To extend the use of the PWM module, we tested whether the PWM module could be connected to a second chip, bypassing the need to re-fabricate existing chips and allowing the PWM module to work with a wide variety of microfluidic devices fabricated with different techniques and materials. We constructed this setup by using flexible PEEK tubing to join the outlet of the short, straight channel (Fig. 4.2a) of the PWM module to the inlet of a second chip. The PEEK tubing has a 50.8  $\mu\text{m}$  inner-diameter, equating to a ~1.5x larger cross-section than the microfluidic mixing channels. Faster flow rates were required to prevent excessive diffusion and delayed response times. The geometry of the PEEK tubing also leads to lower fluidic resistance compared to the microfluidic channels, allowing one to obtain higher flow rates with less pressure.

We successfully produced programmed concentration profiles in the second chip when using 10 cm of connective PEEK tubing, a medium flow velocity (47  $\mu\text{L}/\text{h}$ ), and a 4 s total cycle length (Fig. 4.11a,b). A faster flow rate of 80  $\mu\text{L}/\text{h}$  was achieved when the cycle was shortened to 2 s (Fig. 4.11a,b). Compared to the minimum flow rate of 11  $\mu\text{L}/\text{h}$  we previously demonstrated (Fig. 4.8), this signifies that a 7.3-fold range of flow rates can be used with our platform. The

## Chapter 4. A microfluidic module for real-time generation of complex multi-molecule temporal concentration profiles

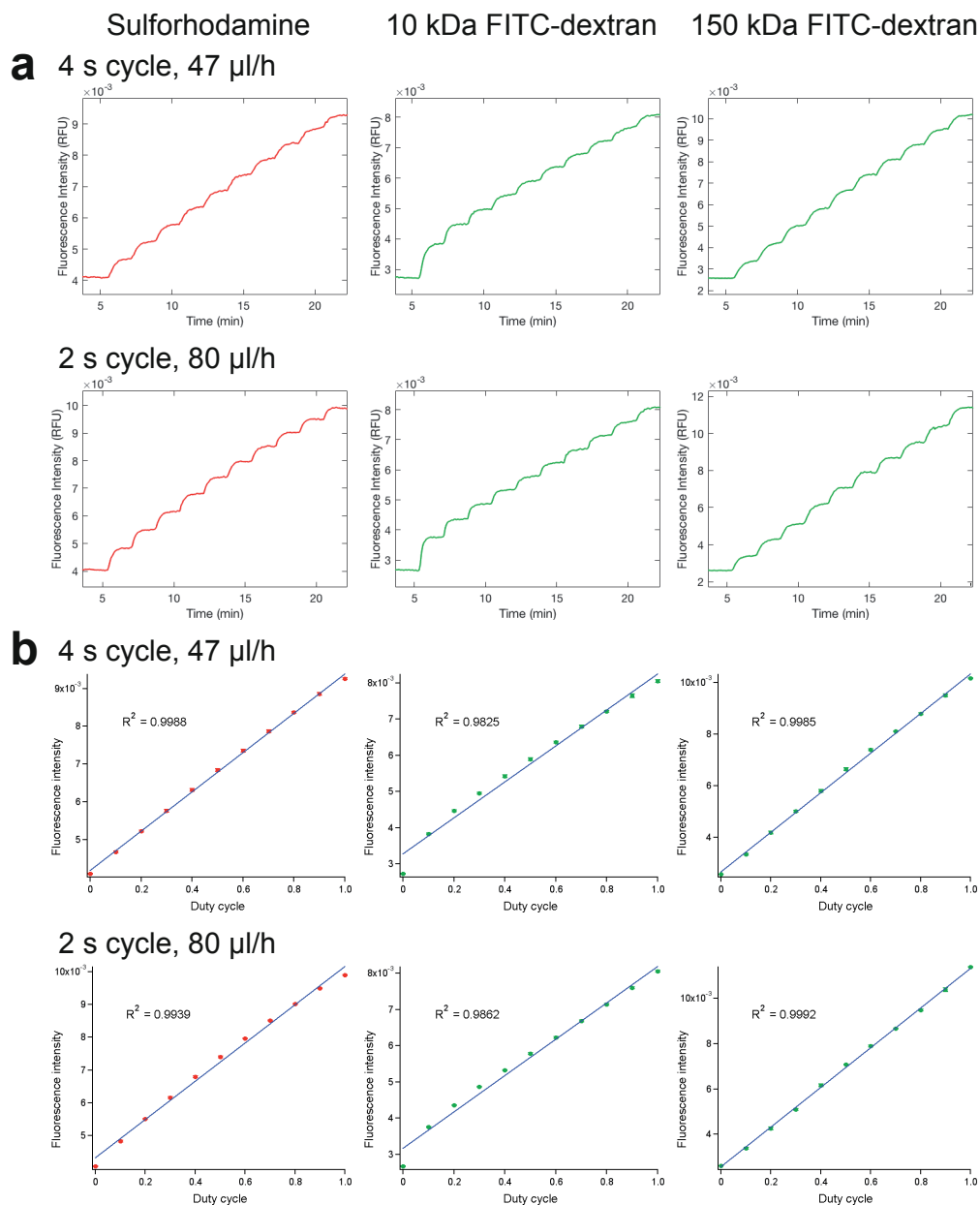


**Figure 4.11.** PWM chip used upstream of a second device. (a) Measured fluorescence intensity resulting from step-wise duty cycle increases over time. Images were acquired near the inlet of the second chip every 5 s. (b) Mean fluorescence intensity as a function of programmed duty cycle. Error bars represent standard deviations. Means were calculated from 10-15 RFU measurements and did not include the data points that fell between two concentrations (during ramping up).

ability to support higher flow rates ensures that our PWM module can be used in conjunction with more high-throughput applications such as microfluidic chemostats<sup>90,133,134</sup>. The 2-chip

setup can likely be used with an even greater range of flow rates so long as the total cycle time is adjusted accordingly to provide control over diffusional mixing.

#### 4.3.7 Complex, long-term and PK/PD concentration profiles

Complex concentration profiles can also be implemented when a PWM module is connected upstream of a second chip. Using a flow rate of 47  $\mu\text{L}/\text{h}$ , a 4 s cycling time, and 6 cm of PEEK tubing to connect the two chips, we simultaneously changed the concentrations of two substances, generating sine curves of changing periods for sulforhodamine and 10 kDa FITC-dextran (Fig. 4.12a). The 4 s cycle consisted of 3 components: a sulforhodamine pulse, a FITC pulse, and a buffer pulse (Fig. 4.12a). Sulforhodamine and FITC could each be pulsed for a maximum of 2 s, and pulse on/off times were selected independently for each substance. The off times for both sulforhodamine and FITC were combined into one buffer pulse. This technique allowed us to create sine curves with periods of 5, 10, 20, 30, and 45 min for FITC, and 80 and 60 min for sulforhodamine (Fig. 4.12a). Our LabVIEW interface enables the user to run custom concentration profiles encoded in text files and is not limited to simple mathematical functions. The ability to independently control the concentration of several substances at once on chip is pertinent to complex biological studies that require the simultaneous delivery of multiple factors as commonly required in stem cell differentiation or reprogramming experiments<sup>135</sup>.

We have shown that our device can implement fast concentration changes and programs lasting up to 2 h (Fig. 4.7, 4.12a). These parameters are compatible with chemical and *in vitro* studies. However, biological studies and especially those involving cell cultures call for extended experimental periods. We thus evaluated the capacity of our device to manipulate and sustain concentrations on time scales spanning up to 48 hours. Using the long serpentine channel, a flow rate of  $\sim 30 \mu\text{L}/\text{h}$ , and a 4 s cycling time, we performed PWM with sulforhodamine and 10 kDa FITC-dextran in parallel. Each substance was either stably maintained at 0.1 (10% of maximum) or gradually ramped up to, or down from, 0.9x (90% of maximum) (Fig. 4.12b). Each peak spanned 2, 4, 6, or 8 h, which are time ranges relevant for drug dosage and pharmacokinetic studies<sup>130,131</sup>. We found that for all ramping times, the desired profile was accurately generated (Fig. 4.12b). The 48 h experiment was not subject to errors or chip failure, showing the robustness of our setup.

The ability to slowly ramp concentrations over long periods of time would be relevant for on chip pharmacokinetic and pharmacodynamics (PK/PD) studies. To demonstrate the utility of our device for this application, we mimicked the 12 h concentration time-profiles in plasma for orally administered drugs<sup>136</sup> (Fig. 4.12c). Chip operating conditions were the same as those employed in Fig. 4.12b, and sulforhodamine and FITC were programmed simultaneously. Both molecules started at 0 concentration and quickly increased to 0.9 (90% intensity), corresponding to release of the drug from the formulation and absorption into the bloodstream<sup>79,137</sup>. After reaching maximum concentration, both substances decrease

## Chapter 4. A microfluidic module for real-time generation of complex multi-molecule temporal concentration profiles

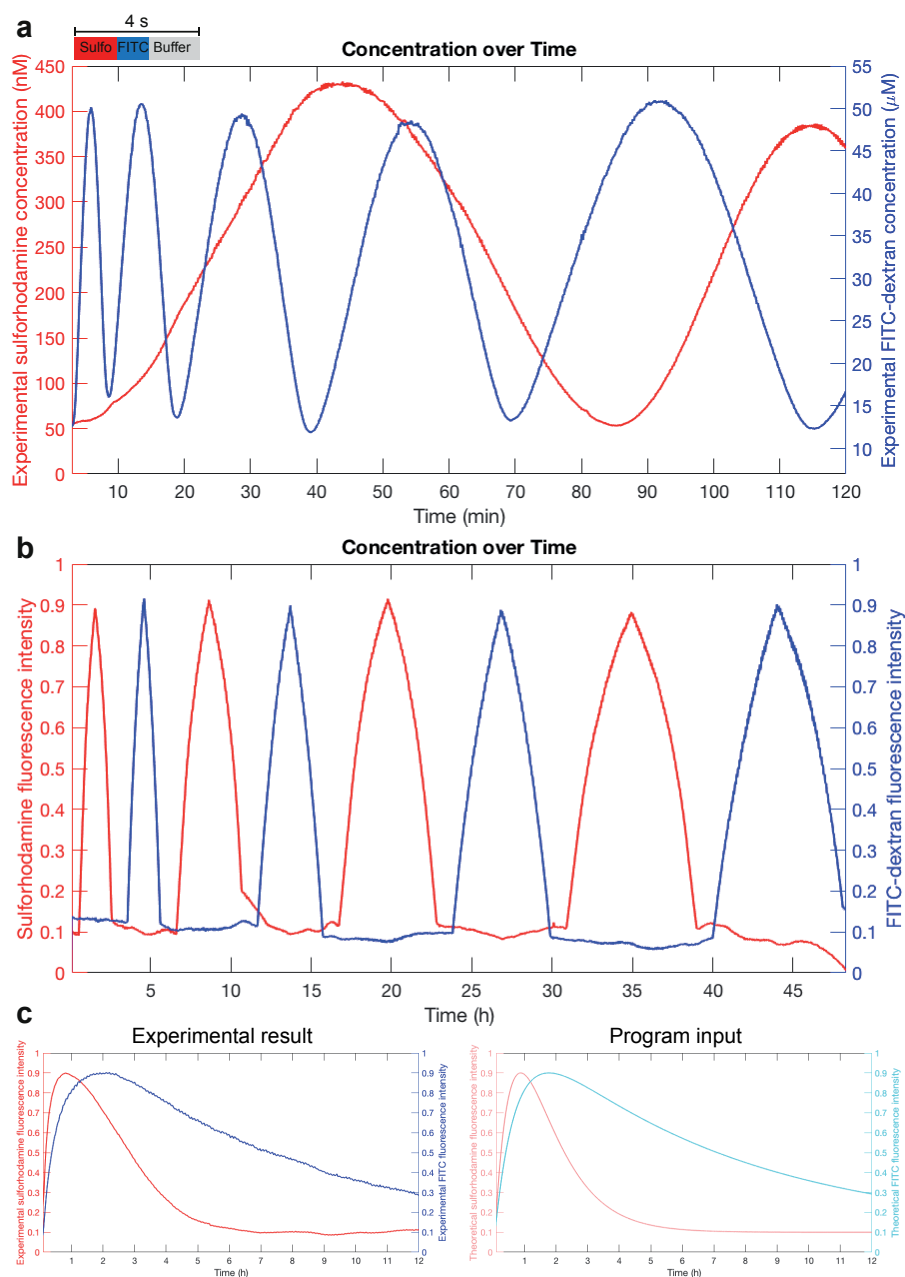


**Figure 4.12.** Complex experiments on the PWM chip. (a) PWM of sulforhodamine and 10 kDa FITC-dextran in parallel, programmed as sine curve functions with changing periods. Images were acquired near the inlet of the second chip every 10 s, analyzed for fluorescence intensity, and converted to absolute concentration using calibration images. (b) PWM of sulforhodamine and 10 kDa FITC-dextran in parallel, gradually ramped to create peaks of 2, 4, 6, or 8 h duration. Images were acquired at the end of the long serpentine channel every 2 min for 48 h, analyzed for fluorescence intensity, and normalized from 0 to 1 based on minimum and maximum fluorescence intensity. (c) Simultaneous generation of two different PK profiles using sulforhodamine and 10 kDa FITC-dextran. Images were acquired and analyzed as in (b).



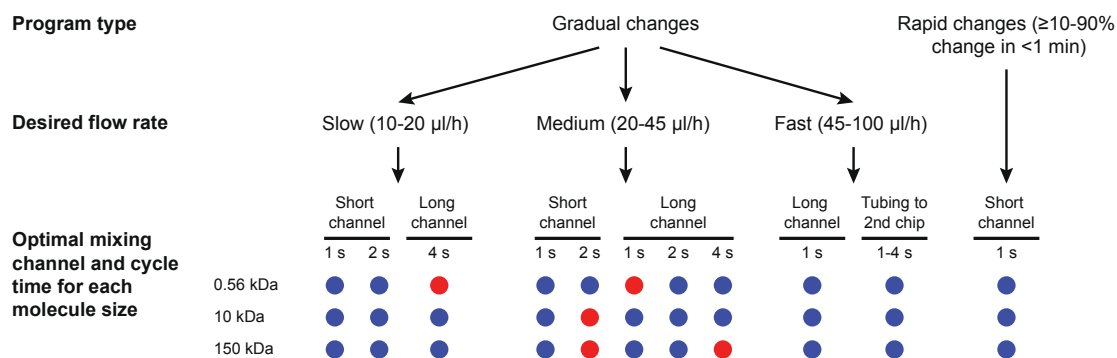


**Figure 4.13.** Guide to selecting chip operating conditions for different experimental setups. Blue, optimal; red, non-optimal.

gradually (to a final value of 0.1 for sulforhodamine and 0.29 for FITC), representing metabolism and elimination of the drug. The experimental results closely match the programmed values in both shape and concentration (Fig. 4.12c). These profiles can be custom-generated on chip to reflect different drugs, delivery methods, and formulations. This feature would be especially advantageous for studies investigating the interactions of multiple drugs to identify synergy or antagonism. When used in this manner, our PWM module could be connected upstream of existing devices to facilitate PK/PD and other dosage-dependent studies. Compared to previously developed PWM microfluidic chips<sup>85-87,122</sup>, our module enables more complex studies to be performed (Table 4.1). We have shown that our chip can be used in a variety of configurations, and a guide to selecting the optimal conditions for each desired flow rate and experiment type is presented in Figure 4.13.

## 4.4 Discussion

Our PWM module demonstrates several improvements over current microfluidic dilution methods (Table 4.1). Compared to previous chips, our platform enables long-term experiments, manipulates the concentration of multiple substances in parallel, and works with a variety of molecule sizes and flow rates. Moreover, the PWM module can easily be connected upstream of a second device. We have thoroughly characterized the platform to aid the user in selecting the optimal conditions for a given experiment (Fig. 4.13). The PWM module itself is easy to fabricate using standard multilayer soft lithography and the design files are available for download ([lbnc.epfl.ch](http://lbnc.epfl.ch)).

Microfluidics is increasingly being used as a tool to model *in vivo* conditions due to reduced sample requirements, regulation of the microenvironment, and compatibility with single-cell analysis. However, typical devices lack the ability to gradually ramp concentrations on chip and instead simply perform non-physiological step-functions by switching between on and off states for a given substance in the culturing medium. We address this limitation by allowing the user to generate arbitrary concentration-time profiles of several substances with

## Chapter 4. A microfluidic module for real-time generation of complex multi-molecule temporal concentration profiles

	Azizi et al.	Ainla et al.	Cao et al.	Zhang et al.	This work
Mixing channel dimensions	Standard and compact	Standard and space-consuming	Large and space-consuming	Large and space-consuming	Standard and compact
Molecule sizes used	<1 kDa	<1 kDa	<1 kDa	<1 kDa	<1 kDa, 10 kDa, and 150 kDa
Number of molecules used simultaneously	1	1	3 (simple patterns)	1	2 (complex patterns)
Range of flow rates	3-fold	Not tested	Not tested	Not tested	7.3-fold
Range of concentrations produced	30-fold, low precision	10-fold	33-fold	9-fold	729-fold
Ability to generate complex/arbitrary profiles	Yes, but non-continuous	No	Repeating waveforms	Repeating waveforms	Custom and complex profiles
Ability to be connected upstream of a second chip	No	No	No	No	Yes
Maximum experiment length tested	5 min	<30 min	30 min	90 min	48 h

**Table 4.1.** Comparison of the PWM module presented in this work to previous microfluidic applications of PWM.

complete control over both timing and concentration. The device can be programmed to generate PK/PD profiles, a feature that is especially relevant in light of recent developments in organ-on-chip and microfluidic stem cell technologies<sup>138,139</sup>. Overall, our PWM platform complements existing biomedical microfluidic devices and will facilitate studies that better reflect the *in vivo* environment by emulating physiologically relevant temporal changes in concentrations.

### 4.4.1 Acknowledgments

This work was funded by EPFL. We thank Nadanai Laohakunakorn and Mathieu Quinodoz for help with LabVIEW programming. We thank Gauthier Croizat for helpful discussions and assistance with fluidic modeling.

### 4.4.2 Competing financial interests

The authors declare no competing financial interests.

## 4.5 Experimental

### 4.5.1 Chemicals

Sulforhodamine, FITC-dextran 10 kDa, and FITC-CM-dextran 150 kDa were purchased from Sigma Aldrich.

### 4.5.2 Automated pneumatic setup

Actuation of microfluidic valves was controlled by a setup consisting of a 16 channel USB relay module (Numato lab) connected to 24V solenoid pneumatic valves arranged on manifold (Pneumadyne). A custom written LabVIEW VI was used to control the opening and closing of the valves on the chip (see Appendix). To run the program, the user supplies a text file containing a list of desired concentrations over time. The LabVIEW program selects which flow inputs to use, then calculates and executes the pulsing times of each input required to achieve the desired concentration. The total cycle length can be adjusted in the program.

### 4.5.3 Imaging

Imaging of the microfluidic chip was performed on a Nikon Ti-E Eclipse automated microscope using NIS Elements. 16-bit TIFF images were acquired with an Ixon DU-888 camera (Andor Technology), using 20x magnification to capture the last ~700  $\mu\text{m}$  of the mixing channel in the field of view. For imaging fluorescence, two HC filter cubes were used: TexasRed (HC 562/40, HC 624/40, BS 593) for sulforhodamine and FITC (HC 482/35, HC 536/40, BS 506) for FITC-dextran (all filters from AHF Analysentechnik AG). Images were analyzed using a custom written Matlab script in which a box of 100  $\mu\text{m}$  length and including the entire width of the channel was selected and analyzed for mean intensity (see Appendix). High-speed imaging of valve closure was performed using a FasTec Imaging HiSpec 2G camera and FasTec imaging software.

### 4.5.4 Microfluidic device fabrication

Microfluidic chips were fabricated as previously described<sup>140</sup>. Devices were designed in Clewin (WieWeb software, Netherlands). Two molds were designed: one for the control layer, which contains the valves, and another for the flow layer, which contains the channels and chambers necessary for reagent introduction and cell culturing. The control layer was scaled by 101.5% to account for PDMS shrinkage during curing. The molds were fabricated using standard photolithography methods. The control layer mold was patterned with SU-8 photoresist (Gersteltec, Switzerland) to a height of 30  $\mu\text{m}$ , then exposed and developed. The channels on the flow layer were generated by spin coating AZ9260 to a height of 14  $\mu\text{m}$ , followed by exposure and development. The AZ9260 was annealed at 120 °C for 10 min to produce the rounded profile that is required for complete valve closure. Polydimethylsiloxane (PDMS; Sylgard 184, Dow Corning Corp., USA) was cast onto the molds and multilayer soft lithography techniques were used to assemble the chip. A thick layer of PDMS (5:1 ratio of parts A:B) was poured onto the control layer, whereas the flow layer was spin coated with PDMS (20:1 ratio of parts A:B) with a ramp of 15 s and a spin of 35 s at 3000 rpm. The molds were baked for 30 min at 80 °C. The control layer chips were then cut, removed from the mold, and punched with inlet holes. The control layer chips were aligned to the flow layer, and the assembly was baked for 90 min at 80 °C. The aligned devices were then cut, removed from the

## **Chapter 4. A microfluidic module for real-time generation of complex multi-molecule temporal concentration profiles**

---

mold, and punched with inlet and outlet holes. The chips were placed on top of a glass slide that had been coated with 20:1 PDMS (15s ramp time and 35s spin at 1500 rpm) and baked for 30 min at 80 °C. Finally, the entire assembly was placed under a weight and bonded overnight at 80 °C.

### **4.5.5 Microfluidic chip operation**

The pressures of the flow and control layers of the chip were controlled by using a custom built pneumatic setup. The valves of the control layer were first primed with filtered water at 5 psi. Once all air had been removed from the control lines, the control layer pressure was increased to 25 psi. The flow layer of the chip was washed with water before each experiment. Flow rate was determined by measuring the volume of liquid exiting the chip over a period of time. Tygon tubing was used for most fluidic connections. For experiments in which a PWM device was attached to a second device, 50.8  $\mu\text{m}$  diameter PEEK tubing (VWR) was used. One end of a 6-10 cm piece of the tubing was inserted directly into the outlet hole of the PWM chip and the other end was placed into the inlet of the second chip.

## 5 Conclusions and Outlook

### 5.1 Summary of Results

Microfluidics is increasingly being used as a tool for cell-based assays due to reduced sample requirements, higher throughput, advanced control over the microenvironment, and compatibility with single-cell analysis. In this work we developed accessible microtechnologies that enable complex, high-throughput experiments with mammalian cells. These platforms are modular and can be combined with existing technologies and assays.

In Chapter 2, we described a novel method to arrange cells into high-density nanowells (live mammalian cell arrays, or LMCAs) for culturing and high-content analysis. The well array can either be purchased or constructed using basic microfabrication protocols. Deposition of the cells into the nanowells requires a microarray printer, which is a standard machine used by many laboratories to generate DNA and protein arrays. Up to 675 different cell lines can be cultured with low cross-contamination on a single microscope slide; the well density on the LMCAs is  $\sim 2.6$  times greater than that of a 1,536-well plate. A variety of cell lines were arrayed at high viability with no detectable change in phenotype, even for sensitive cell types. For example, hMSCs (human bone marrow-derived mesenchymal stem cells) retain their adipogenic differentiation potential when cultured in the nanowells for 10 days in appropriate medium. We have furthermore refined our technique to provide control over cell seeding density, for compatibility with a variety of cell types, and integration with transfection.

Similar to the LMCAs described in Chapter 2, Chapter 3 presents another high-throughput tool for mammalian cell biology. We created a microfluidic chip that is the size of a standard microscope slide and cultures mammalian cells and simultaneously performs 280 independent transfections at up to 99% efficiency. Our technology bears advantages over the original reverse transfection method, in which a glass slide spotted with an array of transfection mixtures is seeded with cells<sup>33</sup>. On our chip the culturing environment is tightly regulated and chambers physically separate the transfection reactions, preventing cross-contamination. Co-transfection can also be achieved, with the expression ratio of co-transfected proteins precisely controlled by adjusting the composition of the transfection mixture. This principle allowed

us to perform synthetic biology experiments on the chip; in Chapter 3, we co-transfected 4 plasmids to express a two-component signaling pathway (developed by Hansen et al.<sup>114</sup>). Our platform is easily adapted to high-content imaging and cells can be continuously monitored during culturing, permitting the monitoring of temporal responses. With our platform, we can collect significantly more data than the end-point methods (e.g. FACS) that are typically used for mammalian synthetic biology.

In addition to the techniques presented in Chapters 2 and 3, there is a plethora of microfluidic devices that have been recently developed for mammalian cell studies<sup>141,142</sup>. However, typical devices lack the ability to gradually ramp concentrations on chip and instead perform step function changes, switching between on and off states for a given substance in the culturing medium. This setup poorly reflects the *in vivo* environment, in which concentrations of molecules follow a complex, continuous rise and fall pattern. In Chapter 4, we addressed this limitation by creating a device that uses pulse-width modulation (PWM) to automatically generate arbitrary concentration values by mixing 2-6 input solutions. The PWM device can produce complex, dynamic concentration profiles over timescales of up to 48 h and with a dynamic range of 3-5 orders of magnitude. Profiles for two molecules can be programmed simultaneously, with each concentration independently controllable. The device is versatile and functions with a large variety of molecule sizes and flow rates. The PWM module may moreover be connected upstream of another device, avoiding the need to re-fabricate existing chip designs.

### 5.2 Limitations

Culturing of the LMCAs presented in Chapter 2 involves immersing the entire array into medium, therefore this method is not suitable for non-adherent cell types. This culturing approach may also contribute to molecular cross-contamination. For example, cells contained within one well may secrete proteins that are received by and influence the behavior of an adjacent well containing a different type of cell. Increasing the total volume of the culturing medium may successfully dilute secreted molecules to negligible levels. However, this strategy might inhibit essential paracrine interactions that require high local concentrations of signaling molecules.

All wells on the LMCAs are cultured in the same type of medium, precluding control over culturing conditions for individual samples on the array. Customization of each well may be achieved by patterning the culturing surface with specific molecules prior to cell deposition. Surface chemistry techniques can potentially be employed to generate stable modifications such as ECM-like matrices. However, soluble and non-adhered molecules will be washed out of the wells when the array is submerged in medium for long-term culturing. Liquid-handling robotics is better suited for generating complex matrices of cell types and culturing conditions, although this equipment is more expensive and not as commonly used as the standard contact spotting approach presented herein.

Aside from its utility in novel applications such as LMCAs, contact spotting has contributed to the adaptation of routine laboratory processes to high-throughput formats (for example, reverse transfection<sup>33</sup>). The approach presented in Chapter 3 is based on reverse transfection and relies on contact spotting to deposit chemical transfection mixtures into cell culturing spaces. The lipid reagent can also be flowed into the entire chip after spotting is completed, obviating the need to add the reagent individually to each transfection mixture. However, for co-transfections plasmids must still be manually mixed, impeding synthetic biology experiments that involve complex plasmid mixtures. One possible solution would be to create a stock solution of each plasmid and perform multiple rounds of spotting to “mix” the stocks on the array, but this strategy yielded unreliable results (see Appendix).

Our microfluidic platform performs transfection at high efficiency, but the chemical-based method relies upon actively dividing cells. Electroporation may be more appropriate to study a greater variety of cell types, since delivery of genetic material is not dependent on mitosis (See Chapter 1 and Table 1.1). Another drawback of our system is that protein expression is transient and limited to a few days. For observing long-term cellular processes, stable protein expression induced by viral transduction would be desirable. Although arrays of lentiviruses have been created<sup>47</sup> and in principle could be integrated with microfluidics, individual preparation of the viruses and their concentration for printing is tedious and requires a dedicated BSL-2 working space. Ideally, lentivirus components would be produced and assembled on chip by a group of producer cells and used to transduce a group of target cells on the same chip. We attempted this approach with limited success (see Appendix), indicating that many parameters remain to be optimized.

Likewise, modifications to our PWM device would expand its utility for a larger range of applications. In Chapter 4, we demonstrated how the PWM device could be used to simultaneously manipulate two molecules of interest. The ability to program 3 or more substances in parallel is pertinent to complex biological processes such as stem cell reprogramming and differentiation. We found that performing PWM with 3 or more substances may require re-optimization of total cycle times, pulse programming methods, and possibly device dimensions. Pulsing multiple molecules in parallel increases the total cycle time, which is the sum of pulse on and off times for each substance. Pulse on/off times cannot simply be scaled down to decrease total cycle time, since these intervals must be sufficiently long to avoid infringing upon minimal valve opening/closing times. This increase in cycle time will likely necessitate longer mixing channels to promote full diffusion of the pulses (alternatively, the 2-chip setup and adjustments in the length of mixing tubing may be explored). The mixing of molecules with drastically large size differences (and thus different diffusion properties) may also require careful optimization.

Although we used standard pressures<sup>123,124</sup> to drive the flow on our PWM device, the resulting flow rates (11-80  $\mu\text{L}/\text{h}$ ) are significantly lower than those employed by high-throughput and cell culturing applications such as chemostats<sup>90,129,133,134</sup>. Increasing the pressure can to some extent accelerate the flow, but often results in mechanical deformations in the valve

pulsing area (causing inaccurate dispensing of pulses) or device delamination and failure. A more suitable option would be to scale up the dimensions of the microfluidic components, promoting higher flow rates by decreasing fluidic resistance. For example, the PEEK tubing that we used for the 2-chip setup has a cross section area that is ~1.5x larger than that of the microfluidic mixing channels and allowed us to easily generate a flow rate of 80  $\mu\text{L}/\text{h}$ , compared to the ~20-36  $\mu\text{L}/\text{h}$  flow rates of the microfluidic mixing channels.

### 5.3 Outlook

We interrogated the LMCAs introduced in Chapter 2 by microscopy, observing both cell morphology and fluorescently labeled structures of interest. Additional information may be obtained by coupling the LMCAs with microengraving. In this approach, cell arrays are sealed against a functionalized glass slide<sup>143</sup>. Secreted proteins in the medium are captured on the surface of the glass slide, creating an array of spots that corresponds to the array of cell culture wells. The glass slide is then detached from the cell array and stained to identify and quantify specific proteins. This assay facilitates the detection of different proteins secreted by cells and, in the LMCA context, could streamline the screening hybridomas and libraries of antibody-producing cell lines.

Our LMCA method is modular, and aside from microengraving it can be combined with a number of other existing technologies. LMCAs are both high-throughput and consume small amounts of sample, making them superior to standard microtiter plates for handling extensive collections of rare or primary cells. LMCAs could be used to study large libraries of cell lines, which have recently become available<sup>2,3</sup>. Alternatively, this system could be applied to elucidate the stem cell microenvironment, which plays an important role in guiding differentiation and organization<sup>5</sup>. Integrating artificial niche arrays<sup>6,97</sup> with the cell-arraying technology developed herein would enable screening of artificial cellular matrices for a vast number of cell types. Lastly, the effect of specific intracellular proteins on cells cultured in LMCAs may be interrogated via transfection. The optimized microfluidic transfection method developed in Chapter 3 could be applied to the nanowells to increase transfection efficiencies. High content screens performed with arrays cultured in the presence of a molecule of interest would uncover fundamental cell mechanisms and assist in drug discovery and development.

Similarly, the transfection technique described in Chapter 3 can investigate the impact of protein expression on cell responses to stimuli such as a change in the culturing medium or introduction of a drug. Moreover, the novel design of the microfluidic chip allows downstream manipulation to be performed without any cross-talk between different transfection chambers. For example, fluidic manipulation could be used to direct the conditioned medium produced by a chamber of transfected cells towards a group of responder cells. This setup could measure the chemotaxis of stem cells in response to a large library secreted proteins<sup>144</sup>. Other possibilities include using this technology to produce protein arrays and co-culture different types of cells in the same chamber (see Appendix).



As shown in Chapter 3, the transfection chip is applicable to synthetic biology. The automated deposition of transfection mixtures is advantageous compared to the manual transfection of multiwell plates typically used for synthetic biology experiments. Synthetic biology studies necessitate the simultaneous delivery of multiple constructs at precise ratios (see Appendix for an example of a complex synthetic system), and transfection conditions must be painstakingly optimized before synthetic circuits can be tested. The transfection chip platform could thus provide a solution to increasing throughput in synthetic biology. Subsequent work could further characterize synthetic circuits by examining their response to activating or repressing molecules introduced in the culturing medium. A microfluidic setup would serve to tightly control the concentration and timing of incubation of these molecules.

When studying molecules of interest in biological experiments, a pressing concern is the inability to generate physiological concentration curves. Standard well-plate systems rely on changes in the culturing medium to sequentially modify the concentration of a molecule. This process poorly represents the dynamic, continuously increasing and decreasing patterns of proteins such as transcription factors. The PWM platform presented in Chapter 4 offers considerably higher accuracy in mimicking biological processes, enabling experiments that were previously unachievable due to technical limitations.

The PWM device could for instance be connected upstream of a second chip to facilitate complex and physiologically relevant experiments with mammalian cells and bacteria. Upon connecting the PWM chip to the transfection chip described in Chapter 3, one could study the temporal effect of a molecule on a library of expressed proteins. The chip's capacity to generate pharmacokinetic/pharmacodynamic (PK/PD) profiles furthermore provides accurate simulations of drug concentrations *in vivo*. This feature could be used in combination with microfluidic chemostats<sup>90,133,134</sup> to elucidate mechanisms of antibiotic resistance and persistence in bacteria<sup>145</sup>. The ability to program multiple substances in parallel would shed light on the interactions of multiple drugs and help identify synergy or antagonism. The simultaneous, temporally controlled delivery of several molecules may also be applied to microfluidic experiments involving stem cell differentiation and reprogramming<sup>135</sup>.

In summary, in this work we have created microfluidic tools for high-throughput screening, mammalian cell engineering, and physiologically relevant studies on chip. These modular platforms can be integrated with recent developments in mammalian synthetic biology, organ-on-chip, and microfluidic stem cell technologies. Taken together, the developments presented in this thesis promise to increase throughput and better replicate the *in vivo* environment for cell-based assays and drug discovery.



## 6 Appendix

### 6.1 Co-spotting method for co-transfection

In Chapter 3, co-transfection was performed by preparing a separate lipid-DNA mixture for each desired expression ratio. We also tested a co-spotting technique, in which one transfection mixture was prepared for each plasmid and spots on the array were stamped multiple times. The number of times each plasmid was stamped determined its ratio in the final transfection mixture. Co-transfection efficiency was extremely low for this technique (Fig. 6.1), perhaps due to the fact that each plasmid is incorporated into a different transfection reagent micelle; the micelles might be taken up differently by the cells based on the order in which they were spotted. For a standard transfection, plasmid size is ~22 by 50 nm, transfection reagent micelles are 200-800 nm in diameter, and 75-50,000 plasmids ultimately end up in the nucleus<sup>146,147</sup>. For the co-spotting method, protein expression ratios also did not correspond to the spotted DNA ratios. Multiple attempts were made to optimize the method including diluting the transfection mixtures before spotting, changing the arraying parameters and pin size, modifying the order in which each mixture was spotted, and by spotting only gelatin-DNA and flowing in the transfection reagent on chip.

### 6.2 Lentivirus transduction on chip

In addition to chemical transfection, we attempted viral-mediated transduction for stable protein expression. HEK cells were cultured on chip and simultaneously transfected with 3 lentiviral plasmids (transfer, packaging, and envelope) with the objective of instigating lentivirus production and subsequent self-infection. After a few days of culture on the chip, cells were removed and cultured in well plates to evaluate long-term protein expression. Some colonies of cells were observed with stable protein expression (GFP, encoded on the transfer plasmid) after 14 days (Fig. 6.2). This result was most likely due to expansion of a few cells that underwent the random genomic integration that can occur with transient transfection (1 per 10,000-1,000,000 cells). Performing the same experiment without one of the essential

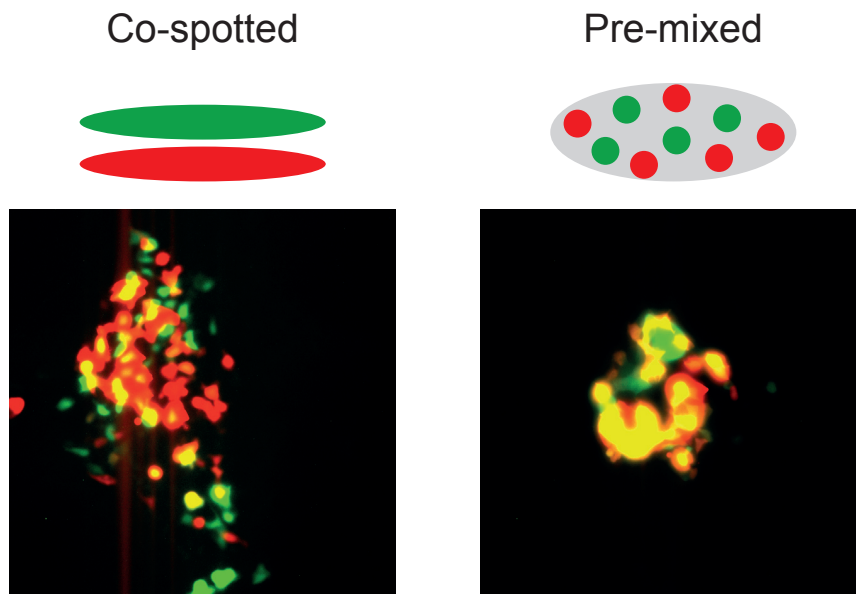


**Figure 6.1.** Co-transfection performed by co-spotting or pre-mixing transfection mixtures containing tdTomato and eGFP. The Tom:GFP DNA ratio was 1:1. The pre-mixed transfection approach results in more co-transfected (yellow) cells compared to the total number of transfected cells.

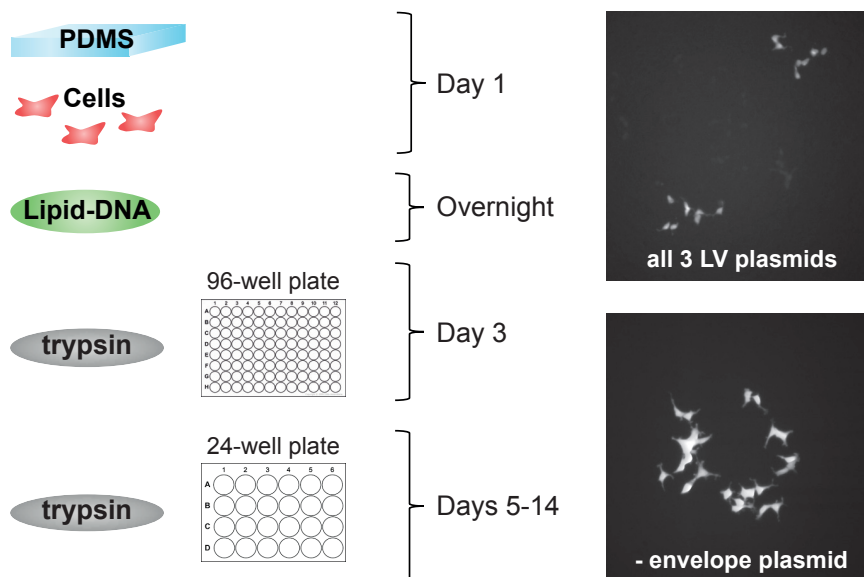


**Figure 6.2.** Generation of cell colonies stably expressing GFP 14 days after transfection on chip. Cells were transfected on the standard transfection chip (Chapter 3). Images: cells were either transfected with all 3 lentivirus plasmids (GFP-transfer, packaging, and envelope), or only 2 of the 3 essential plasmids (GFP-transfer and packaging). GFP expression was evaluated by fluorescence imaging.

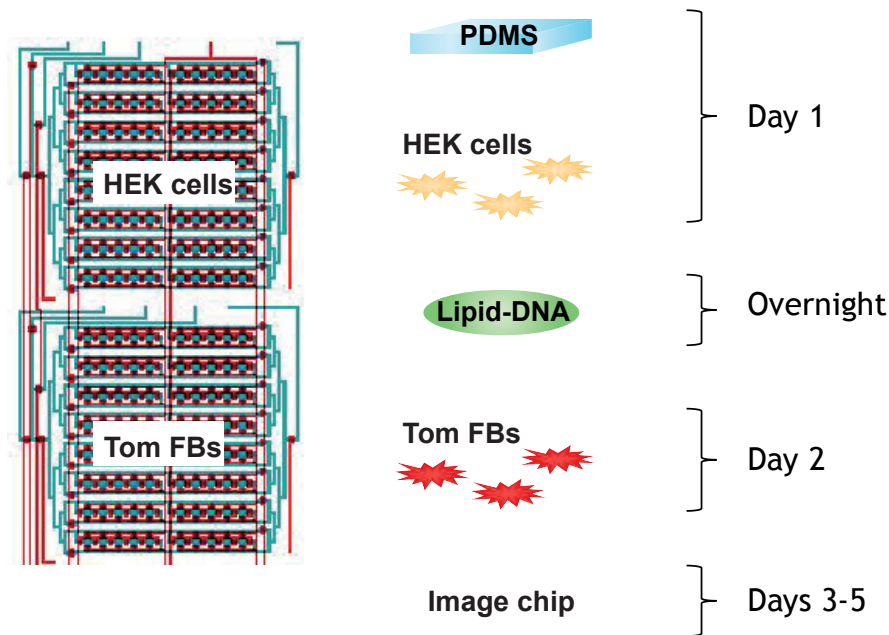


**Figure 6.3.** Chip design for a sender-receiver cell system. HEK cells are transfected with the 3 lentivirus plasmids overnight with the objective of releasing functional lentivirus into the medium. The outlet of the sender (HEK) chip segment can be connected to the inlet of the receiver (Tom FB) chip segment via flexible tubing to incubate the receiver cells with lentivirus-containing medium.

lentiviral plasmids resulted in approximately the same number of stably transfected cell colonies, indicating that the cells failed to produce functional lentivirus.

A co-culture system was also designed, in which the conditioned medium from lentivirus-producing cells was introduced to a second group of cells cultured on a separate segment of the chip. For example, in one setup we used HEK cells as virus producers and Tomato-expressing fibroblasts as receivers (Fig. 6.3). Failure of the sender-receiver experiments could be attributed to slow lentivirus diffusion into chambers (>30 min, compared to 10 min for small proteins present in serum, Fig. 6.4) or insufficient viral titer. Strategies to increase transduction efficiency, such as growing sender cells in the same chamber as receiver cells and the addition of polybrene, fibronectin, or poly-l-lysine were attempted without success.

### 6.3 Co-culture on the transfection chip

Two different cell types can be cultured in the same microfluidic chamber to facilitate the study of paracrine interactions. The sieve design of our transfection chip (Chapter 3) is well suited for studying non-adherent or rare responder cells. High local concentrations of chemokines can be created owing to the small volume contained in the microfluidic culturing chambers, and transfection of producer cells obviates the need to purchase costly purified proteins. For

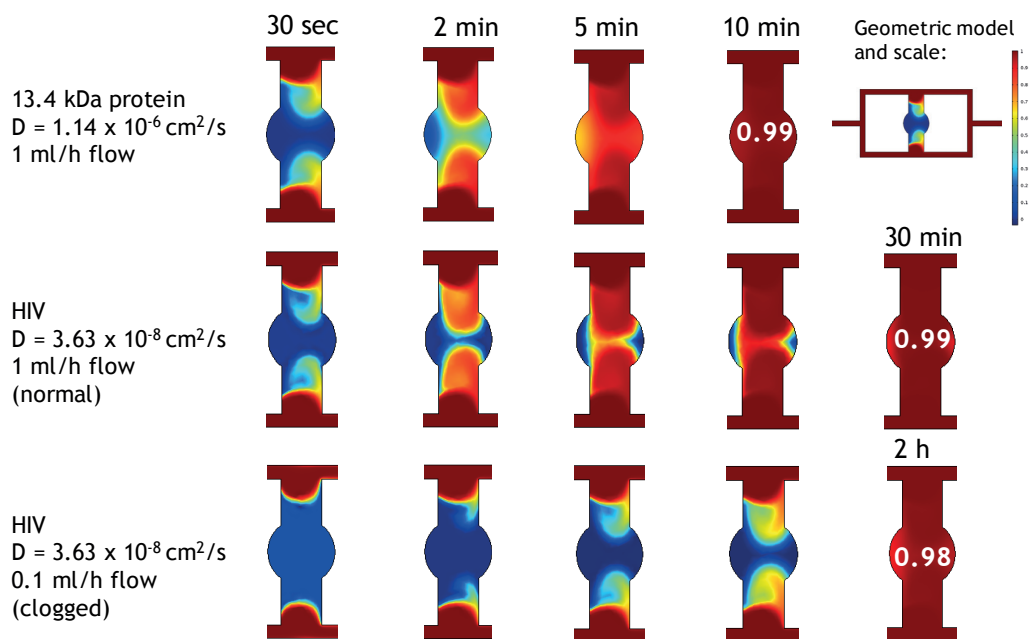


**Figure 6.4.** COMSOL modeling of lentivirus diffusion. A model was constructed to measure the time required for molecules in the feeding channel to fully diffuse into the center of the chambers during continuous flow. HIV was used to represent a lentiviral particle<sup>148</sup>.

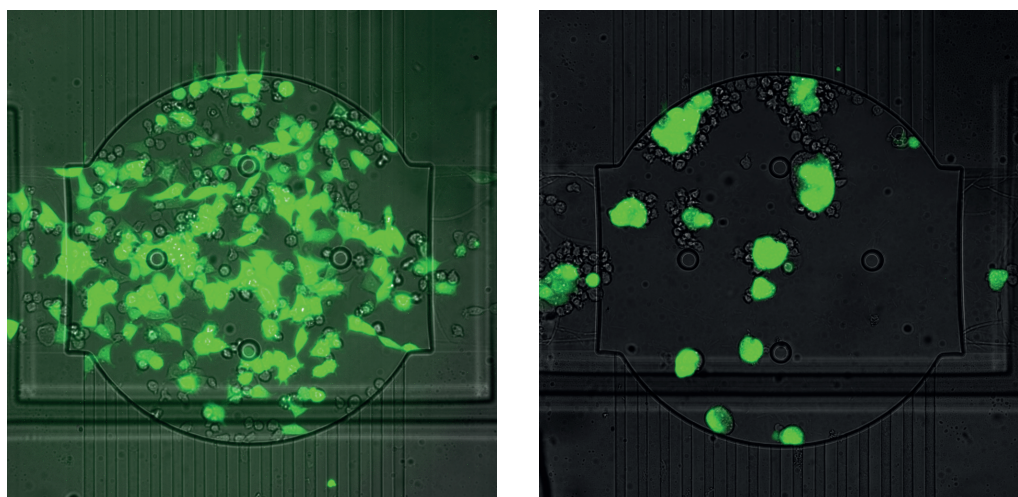


**Figure 6.5.** Co-culture of HEK (GFP-expressing) and Jurkat cells on the transfection chip. Left: a culturing chamber containing a ~1:1 ratio of HEK and Jurkat cells, imaged 5 h after loading onto the chip. Right: at low cell culturing densities, the Jurkat cells tend to cluster around the HEK cells, which may possibly serve as feeder cells (imaged 20 h after loading).

### 6.3. Co-culture on the transfection chip

example, we used our platform to co-culture HEK cells and Jurkat T lymphocytes (Fig. 6.5). Immunostaining could be used to decipher which pathways are activated when the Jurkat cells are exposed to proteins produced by transfected HEK cells. Both validated chemokines (such as IFN-alpha, CCL5, CCL3, IL-6, PDGF, and EGF) and libraries of secreted proteins could potentially be screened.

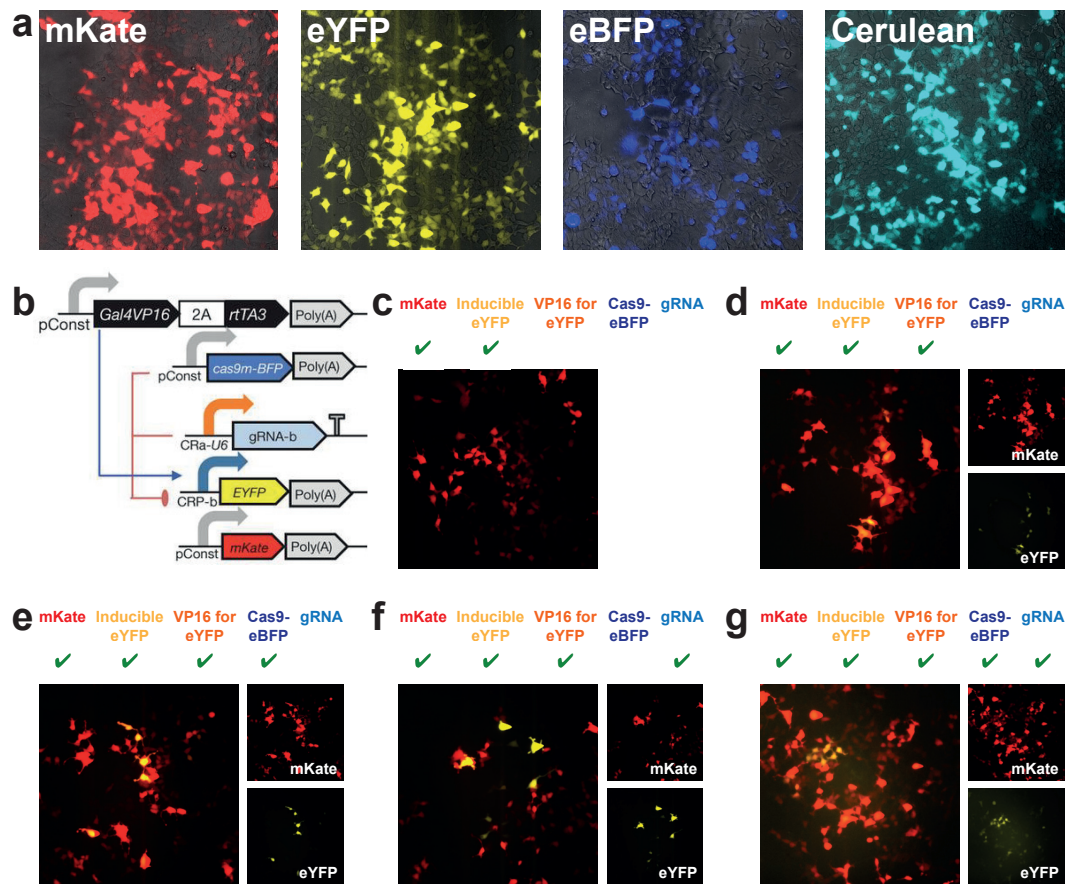


**Figure 6.6.** 96-well plate transfection of a CRISPR transcriptional repression device. (a) Transfection controls of fluorescent proteins. (b) Schematic of the repressive system. (c) eYFP is not expressed when Gal4VP16 is not expressed. (d) eYFP is expressed when Gal4VP16 is expressed. (e) eYFP is not repressed when only one component (Cas9) of the repressing mechanism is present. (f) eYFP is not repressed when only one component (gRNA) of the repressing mechanism is present. (g) eYFP expression is repressed (signified by lower fluorescence intensity) when both elements of repressive system (Cas9 and gRNA) are present. Merged images are shown on the left, and mKate and eYFP channels are shown separately on the right. mKate serves as a transfection control. We thank Samira Kiani and Ron Weiss for providing the plasmids.

### 6.4 Co-transfection of a complex synthetic system

Complex genetic circuits have been recently developed for mammalian cells, such as the modular CRISPR-Cas9 transcriptional repression system developed by Kiani et al<sup>44</sup>. Up to 5 plasmids must be co-expressed: an mKate transfection control, eYFP, Gal4VP16 for eYFP induction, and Cas9 and gRNA for eYFP repression (Fig. 6.6). The tedious process of determining ideal co-transfection ratios could be mitigated by using an automated platform such as the one presented in Chapter 3 for screening.

### 6.5 Producing protein arrays using the transfection chip

Proteins expressed in mammalian cells, opposed to those expressed *in vitro* or in prokaryotic systems, are properly folded and post-translationally modified. Protein arrays are fabricated by printing purified samples<sup>16,34,35</sup>, which is both time-consuming and costly. As an alternative, the reverse transfection chip that we presented in Chapter 3 could be processed to yield a protein array-like product. Specifically, the cells grown in the chambers, each expressing a unique epitope-tagged protein, would be lysed. Proteins released from each chamber can be specifically pulled down by using common surface patterning protocols, such as those administered for MITOMI-based devices<sup>149,150</sup>.

We created both a chip that resembled the device introduced in Chapter 3 (Fig. 6.7) and a user-friendly chip that supports pipet and vacuum loading of cell samples (Fig. 6.8). These chips could be used to test protein-protein interactions and characterize antibody-producing cell lines. A microfluidic button mechanically crushes and lyses cells, and released proteins diffuse to a separate chamber for analysis. Captured proteins can be tested for their interactions with a second protein, which is flowed perpendicular to the direction of cell sample loading. We demonstrated the operation of this device by loading it with GFP-expressing HEK cells (Fig. 6.9). To capture GFP exclusively in the button region, we arrayed BSA-biotin on a glass slide, aligning the array to a chip and flowing in neutravidin with protein capture buttons open. BSA-biotin was flowed next, with buttons closed to inactivate the area around the button. Buttons were opened for patterning with a biotinylated anti-GFP antibody and during capture of GFP released from cells. Following protein capture, buttons were closed for a final wash.



## 6.5. Producing protein arrays using the transfection chip

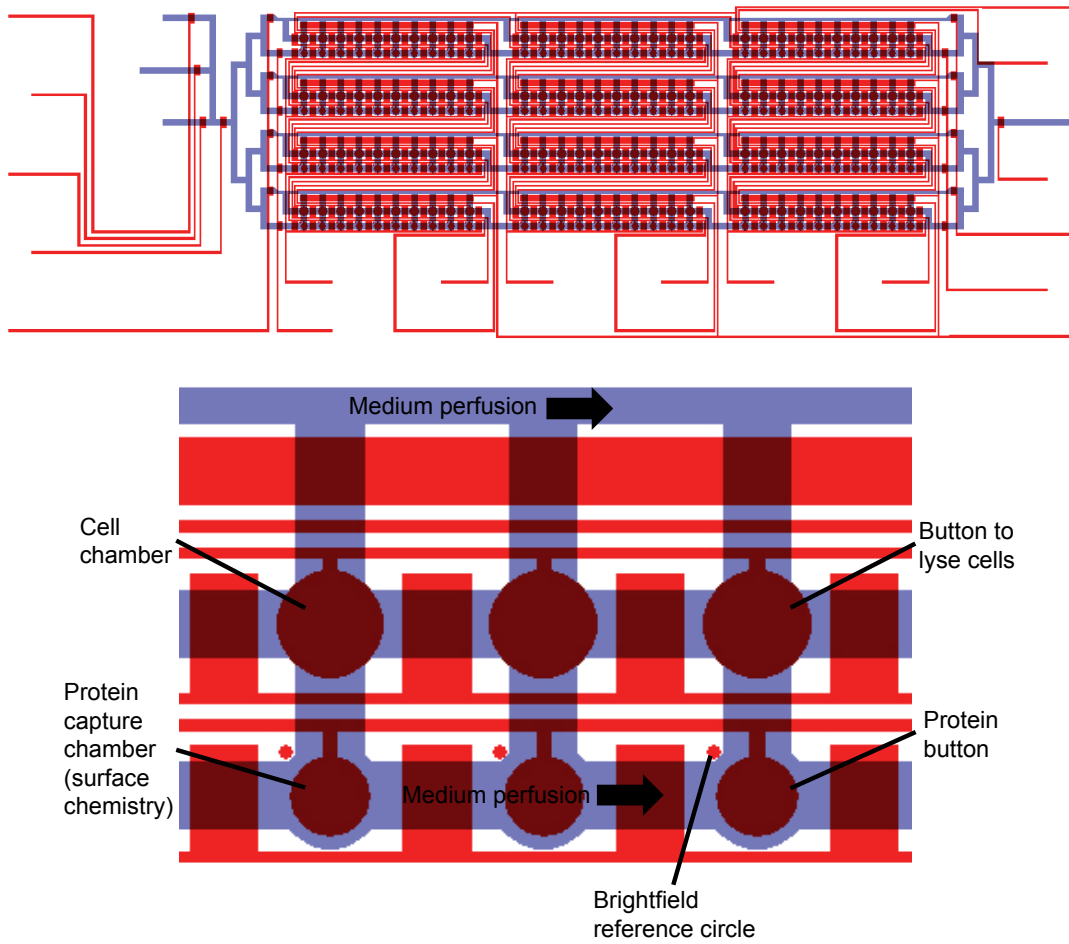


**Figure 6.7.** Microfluidic chip for protein pull-down from transfected cells. Full chip (upper) and close-up (lower). Cells can be transfected in the cell chambers, and expressed intracellular proteins are released when the button is activated to lyse the cells. Proteins diffuse into the protein chamber, where they are captured on the surface.

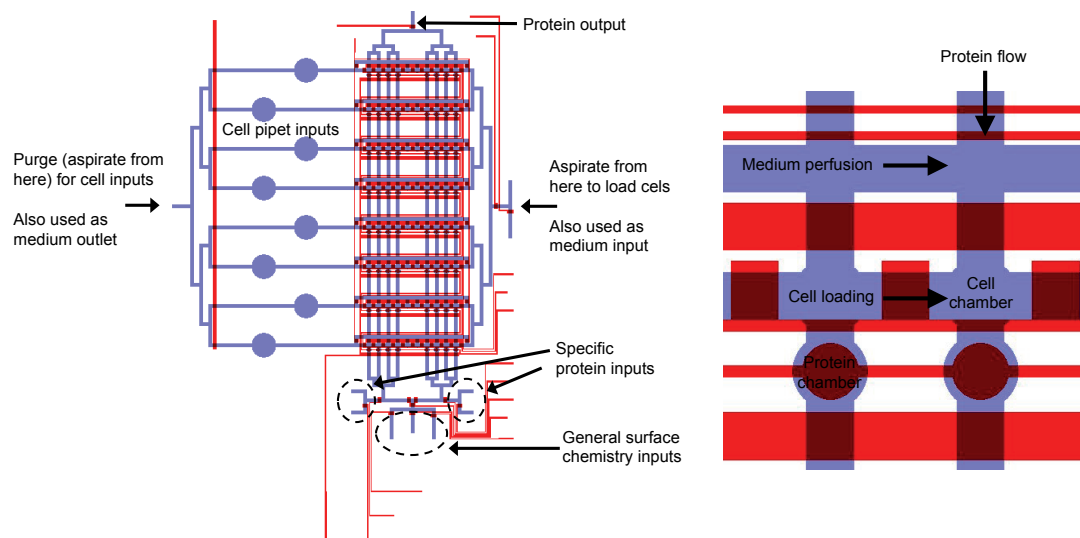
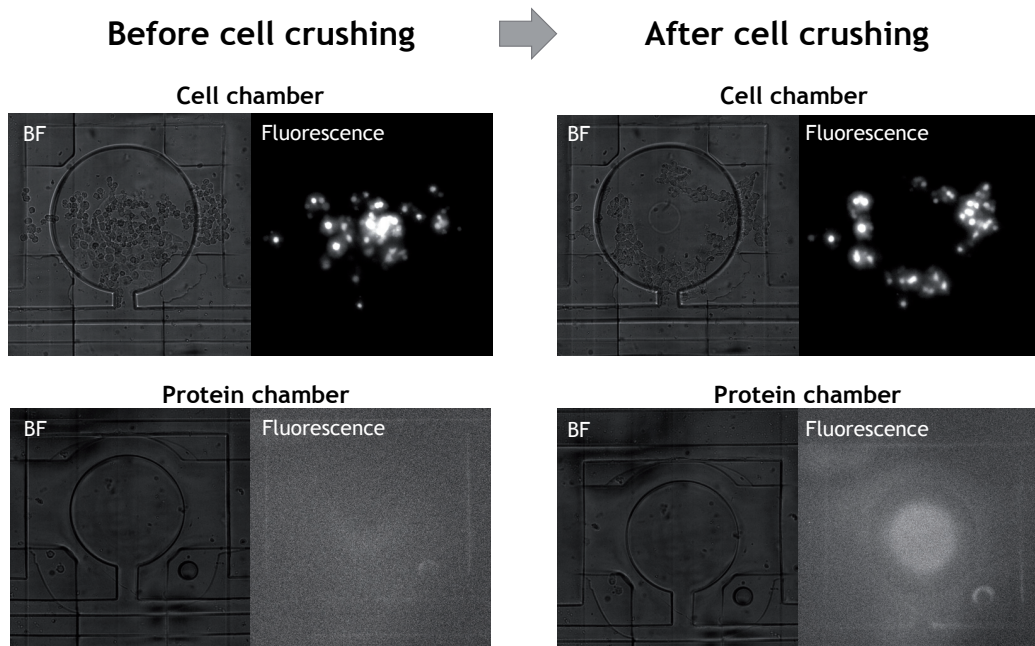


**Figure 6.8.** Microfluidic chip to study protein-protein interactions from cell samples. Full chip (left) and close-up (right). Cell samples are introduced in the chip by pipetting and vacuum loading. Protein samples can be flowed perpendicular to cell samples to generate a matrix for protein-protein interaction testing.

## 6.5. Producing protein arrays using the transfection chip

Sample images, with surface chemistry (BSA-biotin spotted)



Experimental vs. control samples

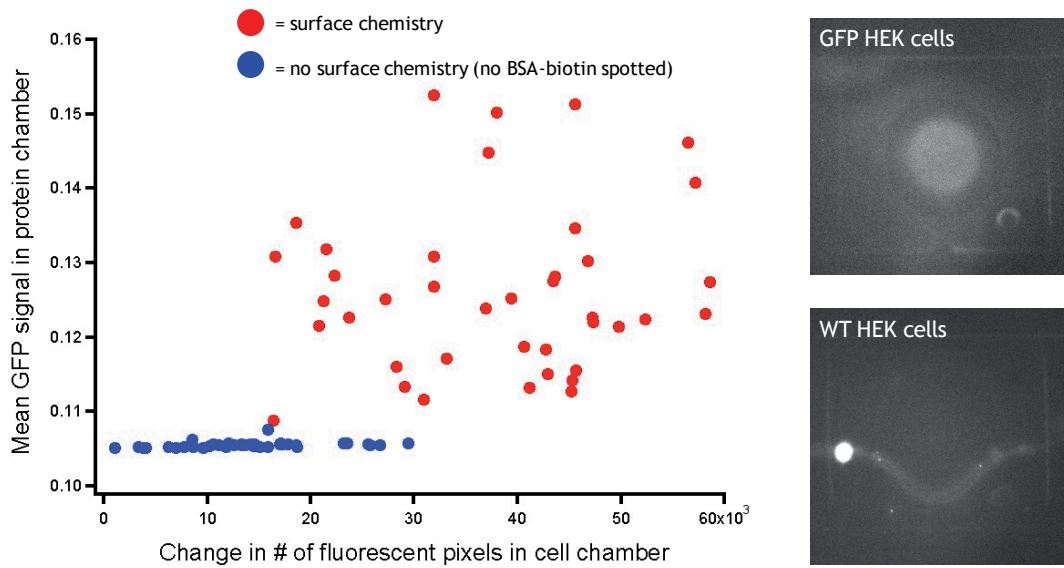


**Figure 6.9.** On-chip mechanical cell lysis and GFP capture. Cells are mechanically lysed by activating the cell-crushing button. Proteins are captured only when the protein chambers are functionalized with the correct surface chemistry.

### 6.6 MATLAB codes

MATLAB code used for analysis of co-transfection efficiencies and ratios presented in Chapter 3.

```
clear
clc
%thresh to change: for merged mask, for 1st color, for 2nd color

files2 = dir('tom***.tif');
files3 = dir('gfp***.tif');

for k = 1:(numel(files2));
for j = 1:(numel(files3));

% now load and convert the one-channel fluorescent files

bb = imread(files2(k).name);
cc = im2double(bb);

bbb = imread(files3(j).name);
ccc = im2double(bbb);

% make the composite image and the composite mask

a = imadd(bb,bbb);

%make the merge mask

aa = im2double(a);
aaa = wiener2(aa, [5 5]);
b = im2double(aaa);
thresh = 0.07;
mask = b > thresh;

%take the small dots away from the mask

[L,N] = bwlabel(mask);

stats = regionprops(L,'area','perimeter');

areas = [stats.Area];
figure,plot(areas);

%try 80 pixels as cutoff area

small = find(areas<80);
mask2 = im2double(L);
for i = 1:length(small)
mask2(L==small(i))=0;
end

%fill in the holes in the dim cells

mask3 = imfill(mask2,'holes');
%imshow(mask3)
```

```

%make the tom and gfp masks

xx = wiener2(bb, [5 5]);

xxx = im2double(xx);
thresh = 0.07;
maskto = xxx > thresh;
maskt = imfill(maskto, 'holes');

yy = wiener2(bbb, [5 5]);

yyy = im2double(yy);
thresh = 0.2;
maskgf = yyy > thresh;
maskg = imfill(maskgf, 'holes');

% for illustration purposes, put an overlay of the merge mask onto the
% original tom and gfp images. need to download imoverlay and put it in the
% same folder.

mask4 = im2bw(mask3);
%perim = bwperim(mask4);
%overlay = imoverlay(cc, perim, [1 .3 .3]);
%imshow(overlay)

%overlayn = imoverlay(ccc, perim, [1 .3 .3]);
%imshow(overlayn)

% to multiply mask by orig image, but first need to convert mask from
% double to logical.
% multiplying is what will be used for counting of the masked imagetom

mask4 = im2bw(mask3);
masktom = im2bw(maskt);
maskgfp = im2bw(maskg);

ee = mask4.*cc;
ex = im2double(ee);
eex = masktom.*ex;

eee = mask4.*ccc;
eeey = im2double(eee);
eeey = maskgfp.*eeey;

tom = im2double(eex);

gfp = im2double(eeey);

divide = eex./eeey;
qdivide = divide;

%get rid of NaNs
qdivide(isnan(qdivide))=0;

%remove numbers below and above 1/6 and 6/1 bin edges. numbers matching the
%thresh value will also be excluded

threshlo = 0.15;
%determine threshlo based on lowest possible value from mask
threshhi = 6.666667;
%determine threshlo based on highest possible value from mask
qdivide = qdivide(abs(qdivide)<threshhi);
qdivide = qdivide(abs(qdivide)>threshlo);

quantify = nnz(qdivide);
%writecounts(k,:) = quantify;

qmedian = median(qdivide);
%writemedian(k,:) = qmedian;

quantify
qmedian

end
end

%csvwrite('ratiocounts',writecounts)
%csvwrite('ratiomedian',writemedian)

```

## Chapter 6. Appendix

---

### MATLAB code used for the analysis of transfection efficiencies and protein expression levels presented in Chapter 3.

```
clear
clc

files2 = dir('tom***.tif');
for k = 1:(numel(files2));

%load and convert the one-channel fluorescent files

at = imread(files2(k).name);
at1 = im2double(at);

aaat = wiener2(at, [5 5]);

bt = im2double(aaat);
thresh = 0.06;
maskt = bt > thresh;

%take the small dots away from the mask

[L,N] = bwlabel(maskt);

stats = regionprops(L,'area','perimeter');

areas = [stats.Area];
figure,plot(areas)

%try 80 pixels as cutoff area

small = find(areas<80);
mask2t = im2double(L);
for i = 1:length(small)
mask2t(L==small(i))=0;
end

%fill in the holes in the dim cells

maskt = imfill(mask2t,'holes');

tom1 = im2bw(maskt);
tom2 = tom1.*at1;
tom = im2double(tom2);

tomcount = nonzeros(tom);

quantify = nnz(tomcount);
quantify2 = median(tomcount);

writecounts(k,:) = quantify
writebrightness(k,:) = quantify2

end

csvwrite('counts',writecounts)
csvwrite('brightness',writebrightness)
```

**MATLAB code used for the binned histogram analysis presented in Fig. 3.16, 3.18.**

```

clear
clc

%make the mask for the merged image

a = imread('merge.tif');
aa = wiener2(a, [5 5]);

b = im2double(aa);
thresh = 0.19;
mask = b > thresh;

%take the small dots away from the mask

[L,N] = bwlabel(mask);

stats = regionprops(L,'area','perimeter');

areas = [stats.Area];
figure,plot(areas)

%80 pixels = cutoff area

small = find(areas<80);
mask2 = im2double(L);
for i = 1:length(small)
mask2(L==small(i))=0;
end

%fill in the holes in the dim cells

mask3 = imfill(mask2,'holes');

imshow(mask3)
% load and convert the one-channel fluorescent files

bb = imread('tom.tif');
cc = im2double(bb);

bbb = imread('gfp.tif');
ccc = im2double(bbb);

%make the tom and gfp masks

xx = wiener2(bb, [5 5]);

xxx = im2double(xx);
thresh = 0.19;
maskto = xxx > thresh;
maskt = imfill(maskto,'holes');

yy = wiener2(bbb, [5 5]);

yyy = im2double(yy);
thresh = 0.19;
maskgf = yyy > thresh;
maskg = imfill(maskgf,'holes');

% for illustration purposes, put an overlay of the merge mask onto the
%original tom and gfp images. need to download imoverlay and put it in the
%same folder.

mask4 = im2bw(mask3);
%perim = bwperim(mask4);
%overlay = imoverlay(cc, perim, [1 .3 .3]);
%imshow(overlay)

%overlayn = imoverlay(ccc, perim, [1 .3 .3]);
%imshow(overlayn)

```

## Chapter 6. Appendix

---

```
% multiply merge mask by orig image
mask4 = im2bw(mask3);
masktom = im2bw(maskt);
maskgfp = im2bw(maskg);

ee = mask4.*cc;
ex = im2double(ee);
eex = masktom.*ex;

eee = mask4.*ccc;
eey = im2double(eee);
eeey = maskgfp.*eey;

tom = im2double(eex);

gfp = im2double(eeey);

divide = tom./gfp;
qdivide = divide;

%get rid of NaNs
qdivide(isnan(qdivide))=0;

%remove numbers below and above 1/6 and 6/1 bin edges. numbers matching the
%thresh value will also be excluded

threshlo = 0.1666666666667;
threshhi = 6;
qdivide = qdivide(abs(qdivide)<threshhi);
qdivide = qdivide(abs(qdivide)>threshlo);

qmedian = median(qdivide)
qmean = mean(qdivide)

%divide into 40 evenly spaced bins. define the edges so that from image to
image, the bins are always made in the same way.
%N is the number of items per bin
%the edges are the divisions of the bins for the ratios

edges = [0.1667 0.1818 0.2 0.2222 0.25 0.2857 0.3333 0.4 0.5 0.6667 1 1.5 2
2.5 3 3.5 4 4.5 5 5.5 6];
N = histcounts(divide,edges)

csvwrite('histogram',N)

tomcount = nonzeros(tom);
tmean = mean(tomcount)
tmedian = median(tomcount)

gfpcount = nonzeros(gfp);
gmean = mean(gfpcount)
gmedian = median(gfpcount)
```



**MATLAB code used for PWM analysis.**

```
clear
clc

%PWM image analysis
%crop a valve-sized area in the channel on a sample image
aim = imread('sulfo200.tif');
bim = im2double(aim);
imshow(bim);
him = imrect;
position = wait(him);
%double click the rectangle to proceed with the code

%image analysis, in bmp or other non-tiff format
files2 = dir('sulfo***.tif')
for k = 1:(numel(files2));
at = imread(files2(k).name);
at1 = im2double(at);
at2 = imcrop(at1, position);
quantify2 = mean2(at2);
writebrightness(k,:) = quantify2;
end
csvwrite('sulfo',writebrightness);

%to plot only the experimental result:
ylaxis = writebrightness
plot(ylaxis,'LineWidth',2,'Color',[1,0,0]);

title('Concentration over Time');
xlabel('Time (s)');
ylabel('Fluorescence Intensity');
axes = gca;
axes.FontSize = 18;
axes.TickLength = [0.02 0.02];
```

### MATLAB code used for co-plotting PWM results.

```
%to plot both experimental results together
%max sulfo = 400 nM
%max fitc = 40 uM

clear
clc

red = 400*dlmread('red.txt');
green = 40*dlmread('green.txt');

for i = 1:12000;
    time(i,1) = i/60;
end

yyaxis left
plot(time,red,'LineWidth',2,'Color',[1,0,0]);
ylim([0 400]) %manually set the lower and upper limit for y axis
xlim([0 200]) %manually set the lower and upper limit for x axis

yyaxis right
plot(time,green,'LineWidth',2,'Color',[0,0,1]);
ylim([0 40]) %manually set the lower and upper limit for y axis
xlim([0 200]) %manually set the lower and upper limit for x axis

yyaxis left
title('Concentration over Time');
xlabel('Time (min)');
ylabel('Experimental sulforhodamine concentration (nM)','Color',[1,0,0]);
ax = gca;
ax.YColor = [1,0,0];

yyaxis right
ylabel('Experimental FITC-dextran concentration (\u00b5M)','Color',[0,0,1]);
ax = gca;
ax.YColor = [0,0,1];

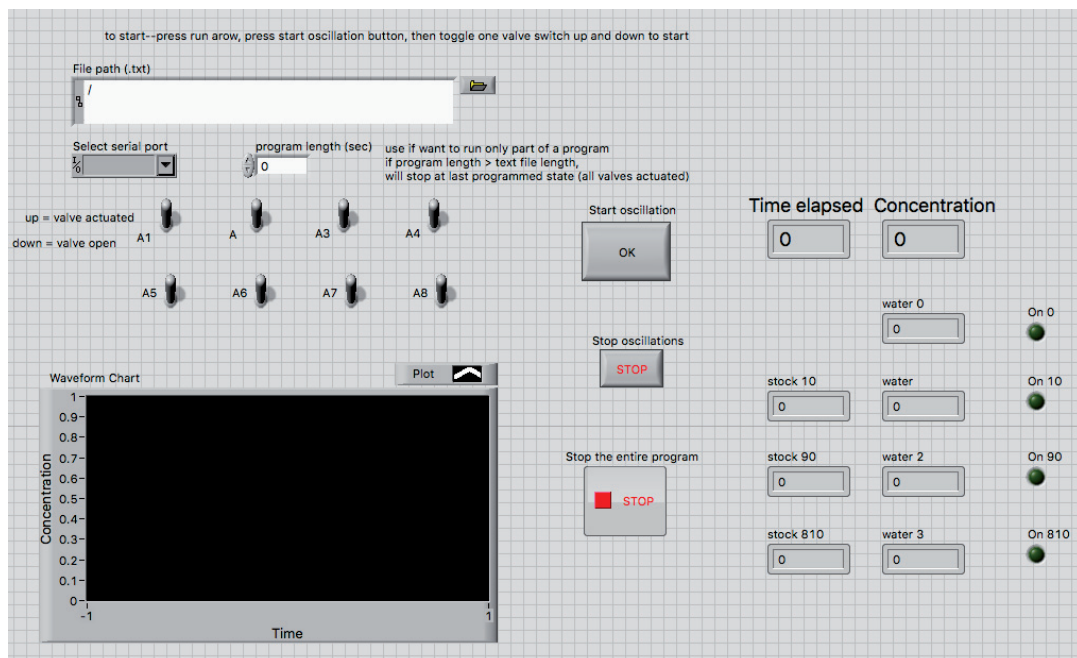
axes = gca
axes.FontSize = 18;
axes.TickLength = [0.02 0.02];

x0=10;
y0=10;
width=1000;
height=500
set(gcf,'units','points','position',[x0,y0,width,height])
```

## 6.7 LabVIEW VIs

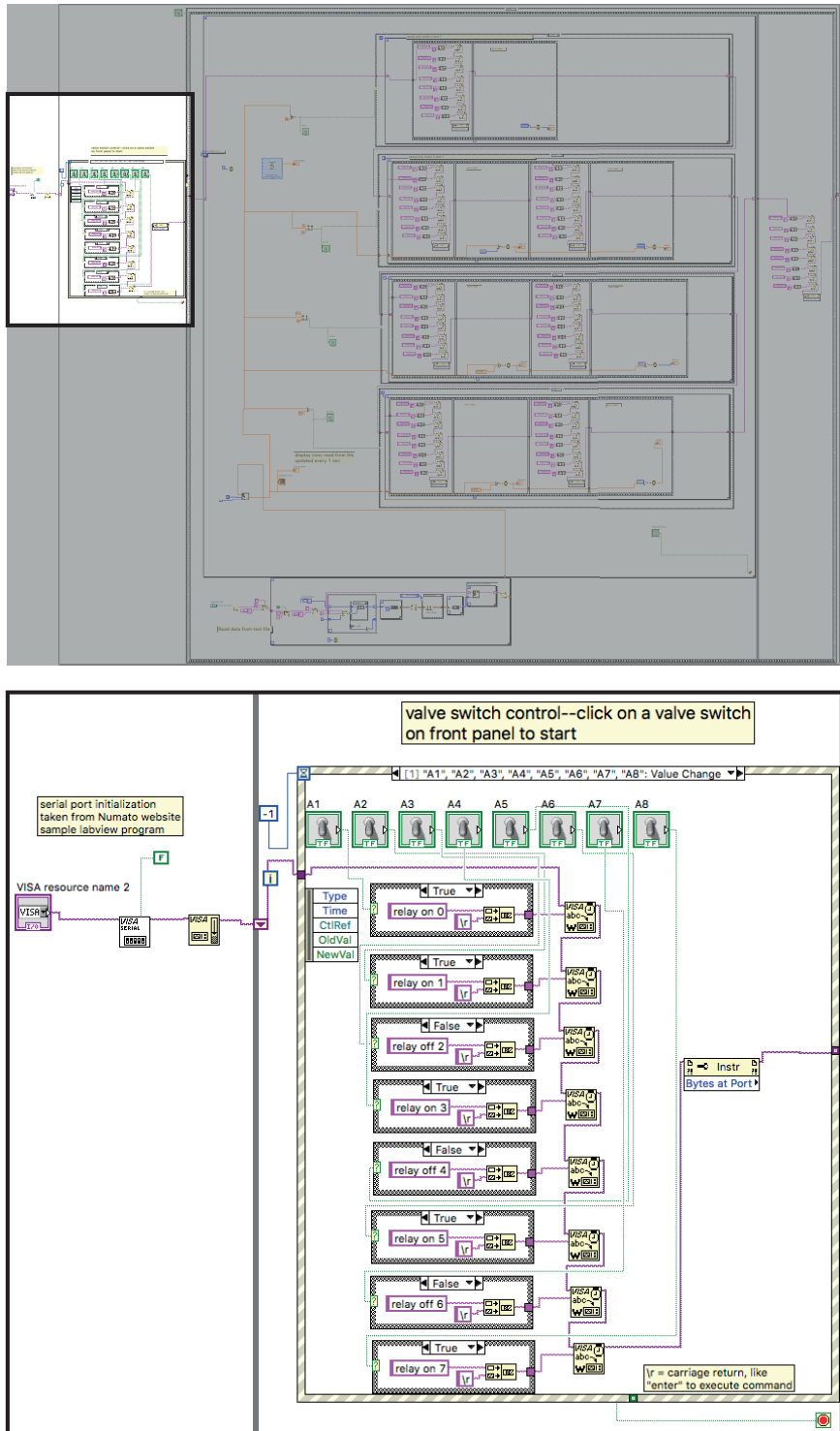
The following images show a LabVIEW VI that was used for large dynamic range PWM experiments such as the one shown in Figure 4.10. This specific VI has been adapted for a 2 s cycle time and for an input text file that has values in the range of 0-729. Depending on what concentration is desired, the VI chooses which of 3 concentrated stocks to pulse with buffer. For desired concentrations of >0-9, the program will mix buffer (0) with the stock of concentration 10. For desired concentrations of >9-81, stocks 0 and 90 will be mixed. For desired concentrations of >81-729, stocks 0 and 810 will be mixed. Time lags caused by LabVIEW calculations ranged from 1-6% of the total program time.

### LabVIEW VI used for PWM experiments, front panel.

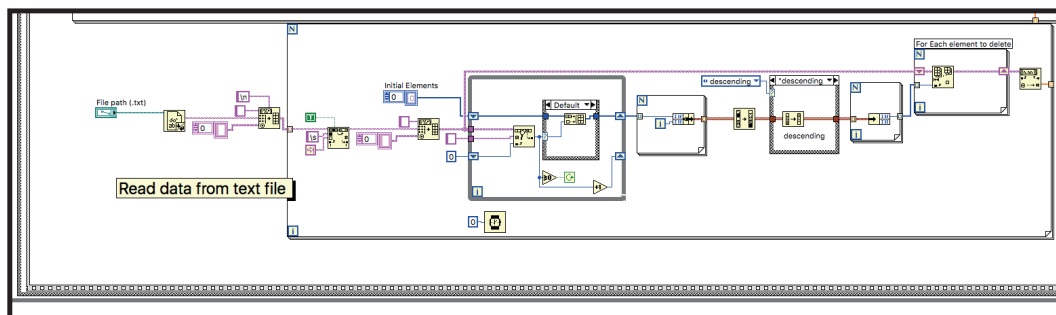


## Chapter 6. Appendix

**LabVIEW VI used for PWM experiments, manual valve-controlling region.** Shown below is the complete block diagram (upper) and an inset of the manual valve-controlling region (lower).

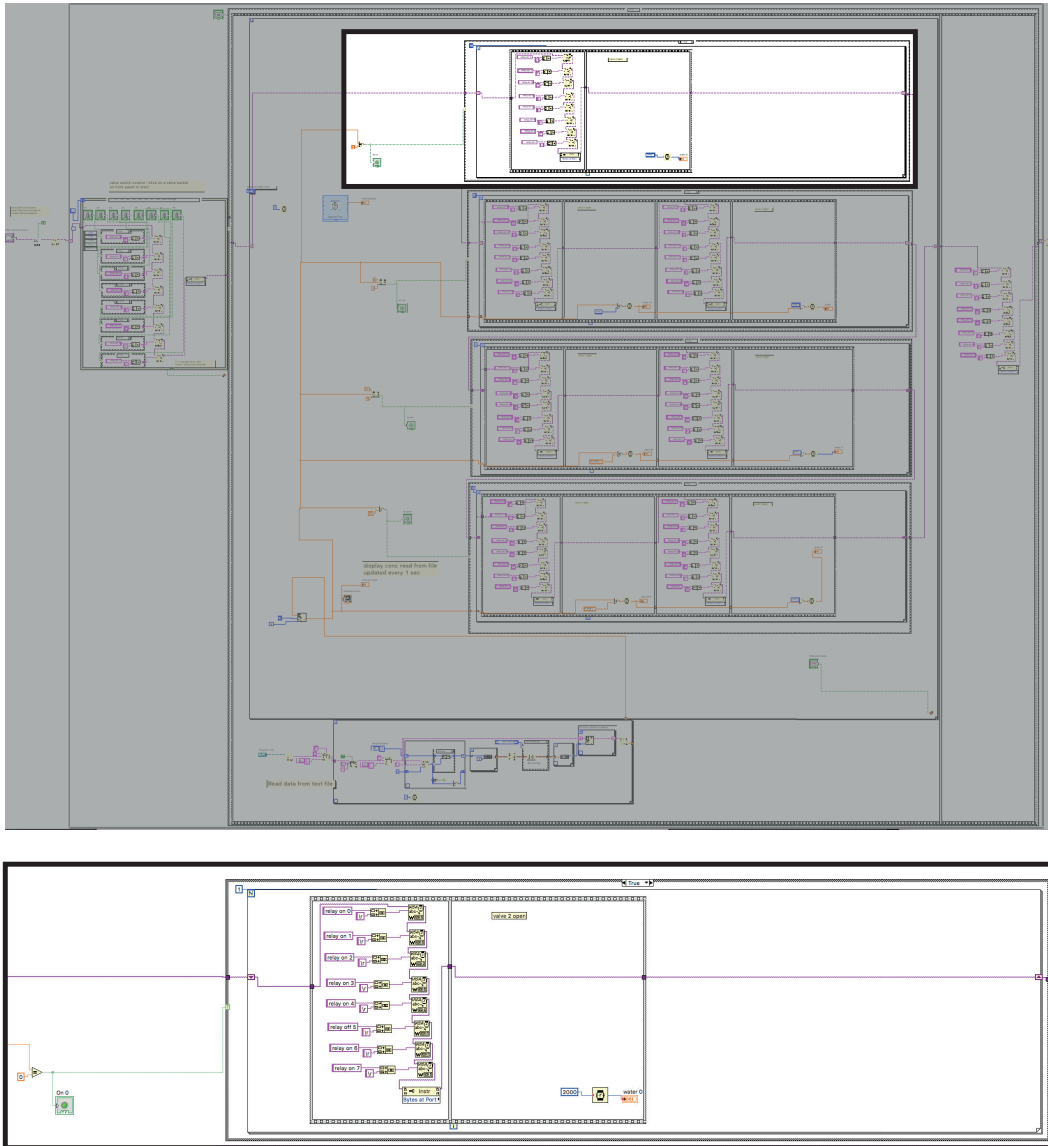


LabVIEW VI used for PWM experiments, text file input region. Shown below is the complete block diagram (upper) and an inset of the text file input region (lower).

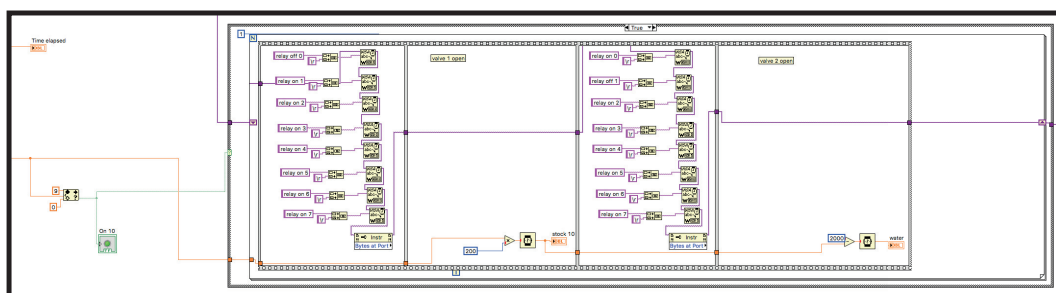
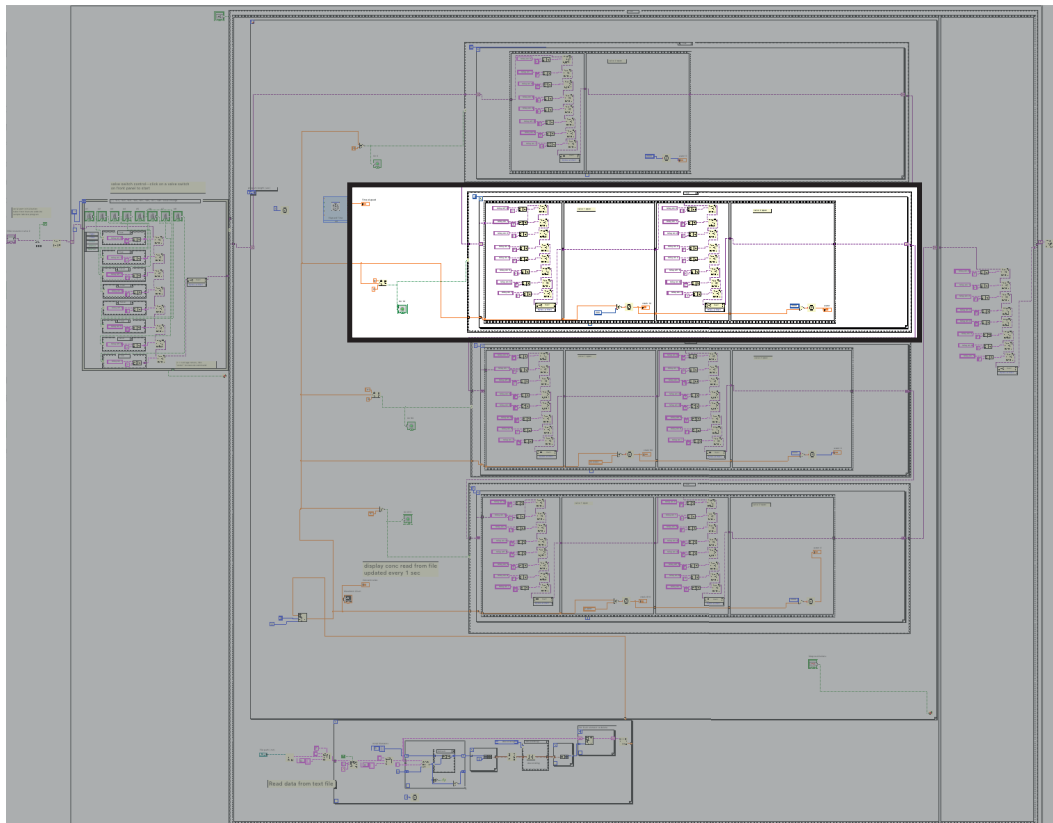


## Chapter 6. Appendix

**LabVIEW VI used for PWM experiments, buffer pulsing region.** Shown below is the complete block diagram (upper) and an inset of the valve commands selected when a concentration of 0 is required (lower).

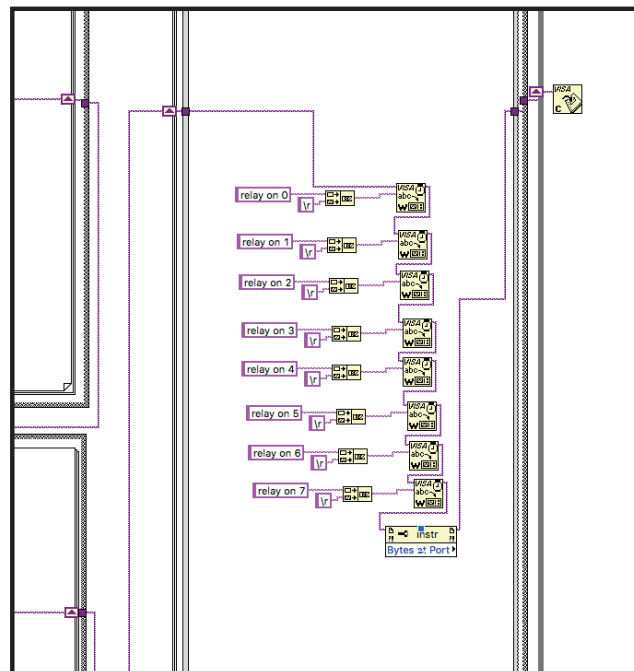
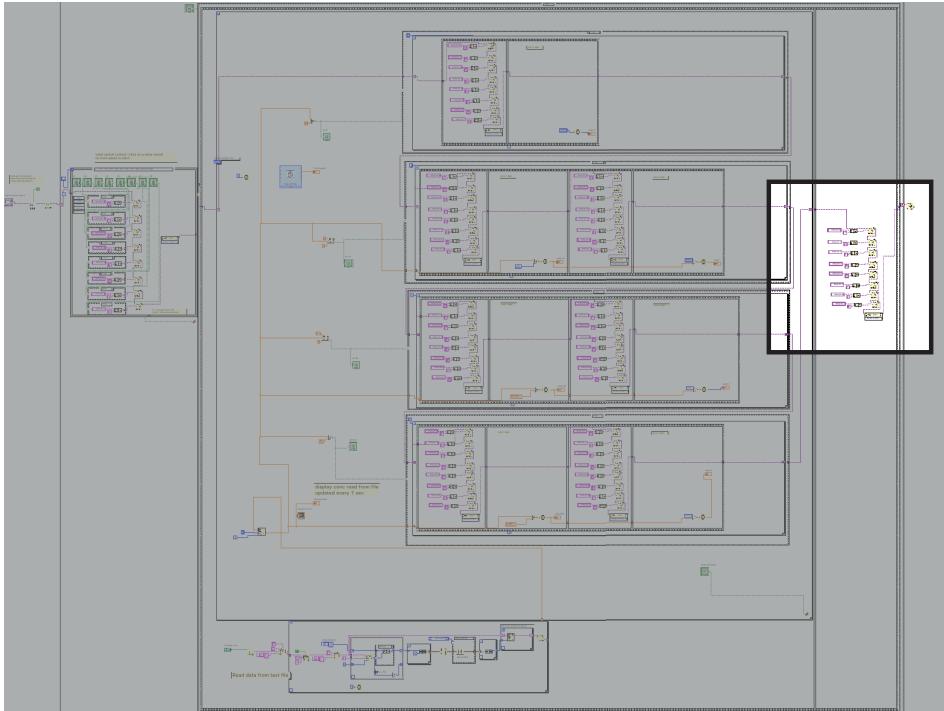


**LabVIEW VI used for PWM experiments, buffer and stock solution pulsing region.** Shown below is the complete block diagram (upper) and an inset of the valve commands selected when a concentration of  $>0-9$  is required (lower). The commands used for concentrations of  $>9-81$  and  $>81-729$  are executed similarly and represent the bottom 2 case structure boxes on the block diagram.



## Chapter 6. Appendix

**LabVIEW VI used for PWM experiments, end of program region.** Shown below is the complete block diagram (upper) and an inset of the commands to turn all valves off at the end of the program (lower).







## Bibliography

- [1] Fabian Zanella, James B Lorens, and Wolfgang Link. High content screening: seeing is believing. *Trends in biotechnology*, 28(5):237–245, 2010.
- [2] Ariel A Cohen, Naama Geva-Zatorsky, Eran Eden, Milana Frenkel-Morgenstern, Iirina Issaeva, Alex Sigal, Ron Milo, Cellina Cohen-Saidon, Yuvalal Liron, Zvi Kam, et al. Dynamic proteomics of individual cancer cells in response to a drug. *science*, 322(5907):1511–1516, 2008.
- [3] Richard M Neve, Koei Chin, Jane Fridlyand, Jennifer Yeh, Frederick L Baehner, Tea Fevr, Laura Clark, Nora Bayani, Jean-Philippe Coppe, Frances Tong, et al. A collection of breast cancer cell lines for the study of functionally distinct cancer subtypes. *Cancer cell*, 10(6):515–527, 2006.
- [4] Eric M Darling and Kyriacos A Athanasiou. Rapid phenotypic changes in passaged articular chondrocyte subpopulations. *Journal of Orthopaedic Research*, 23(2):425–432, 2005.
- [5] Matthias P Lutolf, Penney M Gilbert, and Helen M Blau. Designing materials to direct stem-cell fate. *Nature*, 462(7272):433–441, 2009.
- [6] Samy Gobaa, Sylke Hoehnel, Marta Roccio, Andrea Negro, Stefan Kobel, and Matthias P Lutolf. Artificial niche microarrays for probing single stem cell fate in high throughput. *Nature methods*, 8(11):949–955, 2011.
- [7] Martin L Yarmush and Kevin R King. Living-cell microarrays. *Annual review of biomedical engineering*, 11:235–257, 2009.
- [8] Peter O Krutzik and Garry P Nolan. Fluorescent cell barcoding in flow cytometry allows high-throughput drug screening and signaling profiling. *Nature methods*, 3(5):361–368, 2006.
- [9] Larry A Sklar, Mark B Carter, and Bruce S Edwards. Flow cytometry for drug discovery, receptor pharmacology and high-throughput screening. *Current opinion in pharmacology*, 7(5):527–534, 2007.

## Bibliography

---

- [10] Tim Chapman. Lab automation and robotics: Automation on the move. *Nature*, 421(6923):661–666, 2003.
- [11] Ivar Meyvantsson, Jay W Warrick, Steven Hayes, Allyson Skoien, and David J Beebe. Automated cell culture in high density tubeless microfluidic device arrays. *Lab on a Chip*, 8(5):717–724, 2008.
- [12] Tao Xu, Joyce Jin, Cassie Gregory, James J Hickman, and Thomas Boland. Inkjet printing of viable mammalian cells. *Biomaterials*, 26(1):93–99, 2005.
- [13] Makoto Nakamura, Akiko Kobayashi, Fumio Takagi, Akihiko Watanabe, Yuko Hiruma, Katsuhiko Ohuchi, Yasuhiko Iwasaki, Mikio Horie, Ikuo Morita, and Setsuo Takatani. Biocompatible inkjet printing technique for designed seeding of individual living cells. *Tissue engineering*, 11(11-12):1658–1666, 2005.
- [14] Azmi Yusof, Helen Keegan, Cathy D Spillane, Orla M Sheils, Cara M Martin, John J O’Leary, Roland Zengerle, and Peter Koltay. Inkjet-like printing of single-cells. *Lab on a Chip*, 11(14):2447–2454, 2011.
- [15] Michael J Heller. Dna microarray technology: devices, systems, and applications. *Annual review of biomedical engineering*, 4(1):129–153, 2002.
- [16] Gavin MacBeath. Protein microarrays and proteomics. *Nature genetics*, 32:526–532, 2002.
- [17] Traver Hart, Alice Zhao, Ankit Garg, Swetha Bolusani, and Edward M Marcotte. Human cell chips: adapting dna microarray spotting technology to cell-based imaging assays. *PLoS One*, 4(10):e7088, 2009.
- [18] Moo-Yeal Lee, R Anand Kumar, Sumitra M Sukumaran, Michael G Hogg, Douglas S Clark, and Jonathan S Dordick. Three-dimensional cellular microarray for high-throughput toxicology assays. *Proceedings of the National Academy of Sciences*, 105(1):59–63, 2008.
- [19] Tae Kyung Kim and James H Eberwine. Mammalian cell transfection: the present and the future. *Analytical and bioanalytical chemistry*, 397(8):3173–3178, 2010.
- [20] Claudia Chen and Hiroto Okayama. High-efficiency transformation of mammalian cells by plasmid dna. *Molecular and cellular biology*, 7(8):2745–2752, 1987.
- [21] Hai-Quan Mao, Krishnendu Roy, Vu L Troung-Le, Kevin A Janes, Kevin Y Lin, Yan Wang, J Thomas August, and Kam W Leong. Chitosan-dna nanoparticles as gene carriers: synthesis, characterization and transfection efficiency. *Journal of controlled release*, 70(3):399–421, 2001.
- [22] Franz Scherer, M Anton, U Schillinger, J Henke, C Bergemann, A Krüger, B Gänsbacher, and C Plank. Magnetofection: enhancing and targeting gene delivery by magnetic force in vitro and in vivo. *Gene therapy*, 9(2):102, 2002.

- [23] Motowo Tsukakoshi, S Kurata, Y Nomiya, Y Ikawa, and T Kasuya. A novel method of dna transfection by laser microbeam cell surgery. *Applied Physics B: Lasers and Optics*, 35(3):135–140, 1984.
- [24] Shiping Bao, Brian D Thrall, and Douglas L Miller. Transfection of a reporter plasmid into cultured cells by sonoporation in vitro. *Ultrasound in medicine & biology*, 23(6):953–959, 1997.
- [25] Gilbert Chu, Hiroshi Hayakawa, and Paul Berg. Electroporation for the efficient transfection of mammalian cells with dna. *Nucleic acids research*, 15(3):1311–1326, 1987.
- [26] Mario R Capecchi. High efficiency transformation by direct microinjection of dna into cultured mammalian cells. *Cell*, 22(2):479–488, 1980.
- [27] Armon Sharei, Janet Zoldan, Andrea Adamo, Woo Young Sim, Nahyun Cho, Emily Jackson, Shirley Mao, Sabine Schneider, Min-Joon Han, Abigail Lytton-Jean, et al. A vector-free microfluidic platform for intracellular delivery. *Proceedings of the National Academy of Sciences*, 110(6):2082–2087, 2013.
- [28] I Mortimer, P Tam, I MacLachlan, RW Graham, EG Saravolac, and PB Joshi. Cationic lipid-mediated transfection of cells in culture requires mitotic activity. *Gene therapy*, 6(3):403–411, 1999.
- [29] James M Wilson. Adenoviruses as gene-delivery vehicles. *New England Journal of Medicine*, 334(18):1185–1187, 1996.
- [30] Adam S Cockrell and Tal Kafri. Gene delivery by lentivirus vectors. *Molecular biotechnology*, 36(3):184–204, 2007.
- [31] Tom Dull, Romain Zufferey, Michael Kelly, RJ Mandel, Minh Nguyen, Didier Trono, and Luigi Naldini. A third-generation lentivirus vector with a conditional packaging system. *Journal of virology*, 72(11):8463–8471, 1998.
- [32] Gustavo Tiscornia, Oded Singer, Inder M Verma, et al. Production and purification of lentiviral vectors. *Nature Protocols-Electronic Edition*, 1(1):241, 2006.
- [33] Junaid Ziauddin and David M Sabatini. Microarrays of cells expressing defined cdnas. *Nature*, 411(6833):107–110, 2001.
- [34] Angelika Lueking, Martin Horn, Holger Eickhoff, Konrad Büsow, Hans Lehrach, and Gerald Walter. Protein microarrays for gene expression and antibody screening. *Analytical biochemistry*, 270(1):103–111, 1999.
- [35] Ruud MT de Wildt, Chris R Mundy, Barbara D Gorick, and Ian M Tomlinson. Antibody arrays for high-throughput screening of antibody–antigen interactions. *Nature biotechnology*, 18(9):989–994, 2000.

## Bibliography

---

- [36] Ben Lehner and Andrew G Fraser. 5,000 rna experiments on a chip. *Nature methods*, 1(2):103–104, 2004.
- [37] Satoshi Fujita, Reiko Onuki-Nagasaki, Junji Fukuda, Junko Enomoto, Suichi Yamaguchi, and Masato Miyake. Development of super-dense transfected cell microarrays generated by piezoelectric inkjet printing. *Lab on a Chip*, 13(1):77–80, 2013.
- [38] Georg Dietzl, Doris Chen, Frank Schnorrer, Kuan-Chung Su, Yulia Barinova, Michaela Fellner, Beate Gasser, Kaolin Kinsey, Silvia Oettel, Susanne Scheiblauer, et al. A genome-wide transgenic rna library for conditional gene inactivation in drosophila. *Nature*, 448(7150):151–156, 2007.
- [39] Mammalian Gene Collection (MGC) Program Team et al. Generation and initial analysis of more than 15,000 full-length human and mouse cDNA sequences. *Proceedings of the National Academy of Sciences*, 99(26):16899–16903, 2002.
- [40] Priscilla EM Purnick and Ron Weiss. The second wave of synthetic biology: from modules to systems. *Nature reviews Molecular cell biology*, 10(6):410–422, 2009.
- [41] Zoltán Kis, Hugo Sant’Ana Pereira, Takayuki Homma, Ryan M Pedrigi, and Rob Krams. Mammalian synthetic biology: emerging medical applications. *Journal of The Royal Society Interface*, 12(106):20141000, 2015.
- [42] Ahmad S Khalil and James J Collins. Synthetic biology: applications come of age. *Nature Reviews Genetics*, 11(5):367–379, 2010.
- [43] Keller Rinaudo, Leonidas Bleris, Rohan Maddamsetti, Sairam Subramanian, Ron Weiss, and Yaakov Benenson. A universal rna-based logic evaluator that operates in mammalian cells. *Nature biotechnology*, 25(7):795–801, 2007.
- [44] Samira Kiani, Jacob Beal, Mohammad R Ebrahimkhani, Jin Huh, Richard N Hall, Zhen Xie, Yinqing Li, and Ron Weiss. Crispr transcriptional repression devices and layered circuits in mammalian cells. *Nature methods*, 11(7):723–726, 2014.
- [45] Michael B Elowitz and Stanislas Leibler. A synthetic oscillatory network of transcriptional regulators. *Nature*, 403(6767):335–338, 2000.
- [46] Jose M Silva, Hana Mizuno, Amy Brady, Robert Lucito, and Gregory J Hannon. Rna interference microarrays: high-throughput loss-of-function genetics in mammalian cells. *Proceedings of the National Academy of Sciences of the United States of America*, 101(17):6548–6552, 2004.
- [47] Steve N Bailey, Siraj M Ali, Anne E Carpenter, Caitlin O Higgins, and David M Sabatini. Microarrays of lentiviruses for gene function screens in immortalized and primary cells. *Nature Methods*, 3(2):117–122, 2006.

- [48] Tomohiro Yoshikawa, Eiichiro Uchimura, Michiko Kishi, Daniel P Funeriu, Masato Miyake, and Jun Miyake. Transfection microarray of human mesenchymal stem cells and on-chip sirna gene knockdown. *Journal of controlled release*, 96(2):227–232, 2004.
- [49] Emily Hodges, Jenny Stjern Dahl Redelius, Weilin Wu, and Christer Höög. Accelerated discovery of novel protein function in cultured human cells. *Molecular & Cellular Proteomics*, 4(9):1319–1327, 2005.
- [50] Thomas Peterbauer, Johannes Heitz, Michael Olbrich, and Steffen Hering. Simple and versatile methods for the fabrication of arrays of live mammalian cells. *Lab on a Chip*, 6(7):857–863, 2006.
- [51] Endre Szili, Helmut Thissen, Jason P Hayes, and Nicolas Voelcker. A biochip platform for cell transfection assays. *Biosensors and Bioelectronics*, 19(11):1395–1400, 2004.
- [52] Sandrine Baghdoyan, Yoann Roupioz, Amandine Pitaval, David Castel, Elena Khomyakova, Alexandre Papine, Françoise Soussaline, and Xavier Gidrol. Quantitative analysis of highly parallel transfection in cell microarrays. *Nucleic acids research*, 32(9):e77–e77, 2004.
- [53] Michael Sturzl, Andreas Konrad, Gaby Sander, Effi Wies, Frank Neipel, Elisabeth Naschberger, Simone Reipschlager, Nathalie Gonin-Laurent, Raymund E Horch, and Ulrich Kneser. High throughput screening of gene functions in mammalian cells using reversely transfected cell arrays: review and protocol. *Combinatorial chemistry & high throughput screening*, 11(2):159–172, 2008.
- [54] Tilak Jain, Ryan McBride, Steven Head, and Enrique Saez. Highly parallel introduction of nucleic acids into mammalian cells grown in microwell arrays. *Lab on a Chip*, 9(24):3557–3566, 2009.
- [55] Huang Huang, Zewen Wei, Yuanyu Huang, Deyao Zhao, Lianghong Zheng, Tianjing Cai, Mengxi Wu, Wei Wang, Xianfeng Ding, Zhuan Zhou, et al. An efficient and high-throughput electroporation microchip applicable for sirna delivery. *Lab on a Chip*, 11(1):163–172, 2011.
- [56] Benjamin R Schudel, Brooke Harmon, Vinay V Abhyankar, Benjamin W Pruitt, Oscar A Negrete, and Anup K Singh. Microfluidic platforms for rna interference screening of virus–host interactions. *Lab on a Chip*, 13(5):811–817, 2013.
- [57] Junko Enomoto, Rika Takagi, Reiko Onuki-Nagasaki, Satoshi Fujita, and Junji Fukuda. Reverse transfection in microchamber arrays for cell migration assays. *Sensors and Actuators B: Chemical*, 190:896–899, 2014.
- [58] Rafael Gomez-Sjoeberg, Anne A Leyrat, Dana M Pirone, Christopher S Chen, and Stephen R Quake. Versatile, fully automated, microfluidic cell culture system. *Analytical chemistry*, 79(22):8557–8563, 2007.

## Bibliography

---

- [59] George M Whitesides. The origins and the future of microfluidics. *Nature*, 442(7101):368–373, 2006.
- [60] Todd Thorsen, Sebastian J Maerkl, and Stephen R Quake. Microfluidic large-scale integration. *Science*, 298(5593):580–584, 2002.
- [61] Jamil El-Ali, Peter K Sorger, and Klavs F Jensen. Cells on chips. *Nature*, 442(7101):403–411, 2006.
- [62] Koji Hattori, Shinji Sugiura, and Toshiyuki Kanamori. Microenvironment array chip for cell culture environment screening. *Lab on a Chip*, 11(2):212–214, 2011.
- [63] Petra S Dittrich and Andreas Manz. Lab-on-a-chip: microfluidics in drug discovery. *Nature Reviews Drug Discovery*, 5(3):210–218, 2006.
- [64] Yi-Chin Toh, Teck Chuan Lim, Dean Tai, Guangfa Xiao, Danny van Noort, and Hanry Yu. A microfluidic 3d hepatocyte chip for drug toxicity testing. *Lab on a Chip*, 9(14):2026–2035, 2009.
- [65] H Christina Fan, Jianbin Wang, Anastasia Potanina, and Stephen R Quake. Whole-genome molecular haplotyping of single cells. *Nature biotechnology*, 29(1):51–57, 2011.
- [66] Aaron R Wheeler, William R Throdset, Rebecca J Whelan, Andrew M Leach, Richard N Zare, Yish Hann Liao, Kevin Farrell, Ian D Manger, and Antoine Daridon. Microfluidic device for single-cell analysis. *Analytical chemistry*, 75(14):3581–3586, 2003.
- [67] Lily Kim, Michael D Vahey, Hsu-Yi Lee, and Joel Voldman. Microfluidic arrays for logarithmically perfused embryonic stem cell culture. *Lab on a Chip*, 6(3):394–406, 2006.
- [68] Luis Gerardo Villa-Diaz, Yu-suke Torisawa, Tomoyuki Uchida, Jun Ding, Naiara Correa Nogueira-de Souza, Kathy Sue O’Shea, Shuichi Takayama, and Gary Daniel Smith. Microfluidic culture of single human embryonic stem cell colonies. *Lab on a Chip*, 9(12):1749–1755, 2009.
- [69] Gregory A Cooksey, Christopher G Sip, and Albert Folch. A multi-purpose microfluidic perfusion system with combinatorial choice of inputs, mixtures, gradient patterns, and flow rates. *Lab on a Chip*, 9(3):417–426, 2009.
- [70] Matthew A Holden, Saurabh Kumar, Edward T Castellana, Ali Beskok, and Paul S Cremer. Generating fixed concentration arrays in a microfluidic device. *Sensors and Actuators B: Chemical*, 92(1):199–207, 2003.
- [71] Christopher Neils, Zachary Tyree, Bruce Finlayson, and Albert Folch. Combinatorial mixing of microfluidic streams. *Lab on a Chip*, 4(4):342–350, 2004.
- [72] Chia-Yen Lee, Chin-Lung Chang, Yao-Nan Wang, and Lung-Ming Fu. Microfluidic mixing: a review. *International journal of molecular sciences*, 12(5):3263–3287, 2011.

- [73] Liang-Hsuan Lu, Kee Suk Ryu, and Chang Liu. A magnetic microstirrer and array for microfluidic mixing. *Journal of microelectromechanical systems*, 11(5):462–469, 2002.
- [74] Abraham D Stroock, Stephan KW Dertinger, Armand Ajdari, Igor Mezić, Howard A Stone, and George M Whitesides. Chaotic mixer for microchannels. *Science*, 295(5555):647–651, 2002.
- [75] Hao-Yu Tseng, Chih-Hao Wang, Wang-Ying Lin, and Gwo-Bin Lee. Membrane-activated microfluidic rotary devices for pumping and mixing. *Biomedical microdevices*, 9(4):545–554, 2007.
- [76] Choong Kim, Kangsun Lee, Jong Hyun Kim, Kyeong Sik Shin, Kyu-Jung Lee, Tae Song Kim, and Ji Yoon Kang. A serial dilution microfluidic device using a ladder network generating logarithmic or linear concentrations. *Lab on a Chip*, 8(3):473–479, 2008.
- [77] Michael Barr. Pulse width modulation. *Embedded Systems Programming*, 14(10):103–104, 2001.
- [78] N Mehrotra, M Gupta, A Kovar, and B Meibohm. The role of pharmacokinetics and pharmacodynamics in phosphodiesterase-5 inhibitor therapy. *International journal of impotence research*, 19(3):253–264, 2007.
- [79] Soraya Dhillon. *Clinical pharmacokinetics*. Pharmaceutical Press, 2006.
- [80] Bernd Meibohm and Hartmut Derendorf. Pharmacokinetic/pharmacodynamic studies in drug product development. *Journal of pharmaceutical sciences*, 91(1):18–31, 2002.
- [81] Tove Tuntland, Brian Ethell, Takatoshi Kosaka, Francesca Blasco, Richard Xu Zang, Monish Jain, Ty Gould, and Keith Hoffmaster. Implementation of pharmacokinetic and pharmacodynamic strategies in early research phases of drug discovery and development at novartis institute of biomedical research. *Frontiers in pharmacology*, 5:174, 2014.
- [82] Tony Velkov, Phillip J Bergen, Jaime Lora-Tamayo, Cornelia B Landersdorfer, and Jian Li. Pk/pd models in antibacterial development. *Current opinion in microbiology*, 16(5):573–579, 2013.
- [83] Jong Hwan Sung, Carrie Kam, and Michael L Shuler. A microfluidic device for a pharmacokinetic–pharmacodynamic (pk–pd) model on a chip. *Lab on a Chip*, 10(4):446–455, 2010.
- [84] TJ Maguire, E Novik, P Chao, J Barminko, Y Nahmias, ML Yarmush, and K-C Cheng. Design and application of microfluidic systems for in vitro pharmacokinetic evaluation of drug candidates. *Current drug metabolism*, 10(10):1192–1199, 2009.
- [85] Alar Ainla, Irep Gözen, Owe Orwar, and Aldo Jesorka. A microfluidic diluter based on pulse width flow modulation. *Analytical chemistry*, 81(13):5549–5556, 2009.

## Bibliography

---

- [86] Liaoran Cao, Xinyu Zhang, Alix Grimley, Anna R Lomasney, and Michael G Roper. Microfluidic multi-analyte gradient generator. *Analytical and bioanalytical chemistry*, 398(5):1985–1991, 2010.
- [87] Xinyu Zhang, Alix Grimley, Richard Bertram, and Michael G Roper. Microfluidic system for generation of sinusoidal glucose waveforms for entrainment of islets of langerhans. *Analytical chemistry*, 82(15):6704–6711, 2010.
- [88] Nannan Ye, Jianhua Qin, Weiwei Shi, Xin Liu, and Bingcheng Lin. Cell-based high content screening using an integrated microfluidic device. *Lab on a Chip*, 7(12):1696–1704, 2007.
- [89] Raymond Cheong, Chiaochun Joanne Wang, and Andre Levchenko. High content cell screening in a microfluidic device. *Molecular & Cellular Proteomics*, 8(3):433–442, 2009.
- [90] Nicolas Déneraud, Johannes Becker, Ricard Delgado-Gonzalo, Pascal Damay, Arun S Rajkumar, Michael Unser, David Shore, Felix Naef, and Sebastian J Maerkl. A chemostat array enables the spatio-temporal analysis of the yeast proteome. *Proceedings of the National Academy of Sciences*, 110(39):15842–15847, 2013.
- [91] Feng Xu, JinHui Wu, ShuQi Wang, Naside Gozde Durmus, Umut Atakan Gurkan, and Utkan Demirci. Microengineering methods for cell-based microarrays and high-throughput drug-screening applications. *Biofabrication*, 3(3):034101, 2011.
- [92] D Lansing Taylor. Past, present, and future of high content screening and the field of cellomics. *High Content Screening: A Powerful Approach to Systems Cell Biology and Drug Discovery*, pages 3–18, 2006.
- [93] Douglas B Wheeler, Anne E Carpenter, and David M Sabatini. Cell microarrays and rna interference chip away at gene function. *Nature genetics*, 37:S25–S30, 2005.
- [94] Steve N Bailey, David M Sabatini, and Brent R Stockwell. Microarrays of small molecules embedded in biodegradable polymers for use in mammalian cell-based screens. *Proceedings of the National Academy of Sciences of the United States of America*, 101(46):16144–16149, 2004.
- [95] Satoshi Fujita, Eiji Ota, Chie Sasaki, Kota Takano, Masato Miyake, and Jun Miyake. Highly efficient reverse transfection with sirna in multiple wells of microtiter plates. *Journal of bioscience and bioengineering*, 104(4):329–333, 2007.
- [96] Rebecca J Jackman, David C Duffy, Emanuele Ostuni, Nikolaos D Willmore, and George M Whitesides. Fabricating large arrays of microwells with arbitrary dimensions and filling them using discontinuous dewetting. *Analytical chemistry*, 70(11):2280–2287, 1998.



- [97] Ying Mei, Krishanu Saha, Said R Bogatyrev, Jing Yang, Andrew L Hook, Z Ilke Kalcioğlu, Seung-Woo Cho, Maisam Mitalipova, Neena Pyzocha, Fredrick Rojas, et al. Combinatorial development of biomaterials for clonal growth of human pluripotent stem cells. *Nature materials*, 9(9):768–778, 2010.
- [98] Younan Xia and George M Whitesides. Soft lithography. *Annual review of materials science*, 28(1):153–184, 1998.
- [99] George M Whitesides. Monolayers on disordered substrates: self-assembly of alkyltrichlorosilanes on surface-modified polyethylene and poly (dimethylsiloxane). *Macromolecules*, 26(22), 1993.
- [100] Stephan Preibisch, Stephan Saalfeld, and Pavel Tomancak. Globally optimal stitching of tiled 3d microscopic image acquisitions. *Bioinformatics*, 25(11):1463–1465, 2009.
- [101] Lily Kim, Yi-Chin Toh, Joel Voldman, and Henry Yu. A practical guide to microfluidic perfusion culture of adherent mammalian cells. *Lab on a Chip*, 7(6):681–694, 2007.
- [102] Minseok S Kim, Ju Hun Yeon, and Je-Kyun Park. A microfluidic platform for 3-dimensional cell culture and cell-based assays. *Biomedical microdevices*, 9(1):25–34, 2007.
- [103] Martin Kolnik, Lev S Tsimring, and Jeff Hasty. Vacuum-assisted cell loading enables shear-free mammalian microfluidic culture. *Lab on a chip*, 12(22):4732–4737, 2012.
- [104] Luis M Fidalgo and Sebastian J Maerkl. A software-programmable microfluidic device for automated biology. *Lab on a Chip*, 11(9):1612–1619, 2011.
- [105] A Ruiz, M Zychowicz, L Buzanska, D Mehn, CA Mills, E Martinez, S Coecke, J Samitier, P Colpo, and F Rossi. Single stem cell positioning on polylysine and fibronectin microarrays. *Micro and Nanosystems*, 1(1):50–56, 2009.
- [106] John C Chang, Gregory J Brewer, and Bruce C Wheeler. A modified microstamping technique enhances polylysine transfer and neuronal cell patterning. *Biomaterials*, 24(17):2863–2870, 2003.
- [107] Conrad D James, Robert Davis, M Meyer, AATA Turner, SATS Turner, GAWG Withers, LAKL Kam, GABG Banker, HACH Craighead, MAIM Issacson, et al. Aligned microcontact printing of micrometer-scale poly-l-lysine structures for controlled growth of cultured neurons on planar microelectrode arrays. *IEEE Transactions on Biomedical Engineering*, 47(1):17–21, 2000.
- [108] Sang Beom Jun, Matthew R Hynd, Natalie Dowell-Mesfin, Karen L Smith, James N Turner, William Shain, and Sung June Kim. Low-density neuronal networks cultured using patterned poly-l-lysine on microelectrode arrays. *Journal of neuroscience methods*, 160(2):317–326, 2007.

## Bibliography

---

- [109] Michael B Eisen and Patrick O Brown. [12] dna arrays for analysis of gene expression. *Methods in enzymology*, 303:179–205, 1999.
- [110] Andras Nagy, Marina Gertsenstein, Kristina Vintersten, and Richard Behringer. Preparing glass slides and coverslips for in situ hybridization. *Cold Spring Harbor Protocols*, 2007(11):pdb-prot4817, 2007.
- [111] Martin J Hessner, Lisa Meyer, Jennifer Tackes, Sanaa Muheisen, and Xujing Wang. Immobilized probe and glass surface chemistry as variables in microarray fabrication. *BMC genomics*, 5(1):53, 2004.
- [112] Christian Conrad, Holger Erfle, Patrick Warnat, Nathalie Daigle, Thomas Lörch, Jan Ellenberg, Rainer Pepperkok, and Roland Eils. Automatic identification of subcellular phenotypes on human cell arrays. *Genome research*, 14(6):1130–1136, 2004.
- [113] Elisabeth Kuhn, Elisabeth Naschberger, Andreas Konrad, Roland S Croner, Nathalie Britzen-Laurent, Ramona Jochmann, Helmut Münstedt, and Michael Stürzl. A novel chip-based parallel transfection assay to evaluate paracrine cell interactions. *Lab on a Chip*, 12(7):1363–1372, 2012.
- [114] Jonathan Hansen, Erik Mailand, Krishna Kumar Swaminathan, Joerg Schreiber, Bartolomeo Angelici, and Yaakov Benenson. Transplantation of prokaryotic two-component signaling pathways into mammalian cells. *Proceedings of the National Academy of Sciences*, 111(44):15705–15710, 2014.
- [115] Philip L Felgner, Thomas R Gadek, Marilyn Holm, Richard Roman, Hardy W Chan, Michael Wenz, Jeffrey P Northrop, Gordon M Ringold, and Mark Danielsen. Lipofection: a highly efficient, lipid-mediated dna-transfection procedure. *Proceedings of the National Academy of Sciences*, 84(21):7413–7417, 1987.
- [116] Paul Golby, Suzanne Davies, David J Kelly, John R Guest, and Simon C Andrews. Identification and characterization of a two-component sensor-kinase and response-regulator system (dcus-dcur) controlling gene expression in response to c4-dicarboxylates in escherichia coli. *Journal of bacteriology*, 181(4):1238–1248, 1999.
- [117] Aly E Abo-Amer, Jonathan Munn, Kerry Jackson, Murat Aktas, Paul Golby, David J Kelly, and Simon C Andrews. Dna interaction and phosphotransfer of the c4-dicarboxylate-responsive dcus-dcur two-component regulatory system from escherichia coli. *Journal of bacteriology*, 186(6):1879–1889, 2004.
- [118] Nathan C Shaner, Robert E Campbell, Paul A Steinbach, Ben NG Giepmans, Amy E Palmer, and Roger Y Tsien. Improved monomeric red, orange and yellow fluorescent proteins derived from discosoma sp. red fluorescent protein. *Nature biotechnology*, 22(12):1567–1572, 2004.

- [119] Mikhail V Matz, Arkady F Fradkov, Yulii A Labas, Aleksandr P Savitsky, Andrey G Zaraisky, Mikhail L Markelov, and Sergey A Lukyanov. Fluorescent proteins from nonbioluminescent anthozoa species. *Nature biotechnology*, 17(10):969–973, 1999.
- [120] Anne E Carpenter, Thouis R Jones, Michael R Lamprecht, Colin Clarke, In Han Kang, Ola Friman, David A Guertin, Joo Han Chang, Robert A Lindquist, Jason Moffat, et al. Cellprofiler: image analysis software for identifying and quantifying cell phenotypes. *Genome biology*, 7(10):R100, 2006.
- [121] David C Duffy, J Cooper McDonald, Olivier JA Schueller, and George M Whitesides. Rapid prototyping of microfluidic systems in poly (dimethylsiloxane). *Analytical chemistry*, 70(23):4974–4984, 1998.
- [122] Farouk Azizi and Carlos H Mastrangelo. Generation of dynamic chemical signals with pulse code modulators. *Lab on a Chip*, 8(6):907–912, 2008.
- [123] Jose L Garcia-Cordero, Chiara Nembrini, Armando Stano, Jeffrey A Hubbell, and Sebastian J Maerkl. A high-throughput nanoimmunoassay chip applied to large-scale vaccine adjuvant screening. *Integrative Biology*, 5(4):650–658, 2013.
- [124] Francesco Piraino, Francesca Volpetti, Craig Watson, and Sebastian J Maerkl. A digital–analog microfluidic platform for patient-centric multiplexed biomarker diagnostics of ultralow volume samples. *ACS nano*, 10(1):1699–1710, 2016.
- [125] Christopher Probst, Alexander Grünberger, Wolfgang Wiechert, and Dietrich Kohlheyer. Polydimethylsiloxane (pdms) sub-micron traps for single-cell analysis of bacteria. *Micromachines*, 4(4):357–369, 2013.
- [126] Hanbin Mao, Paul S Cremer, and Michael D Manson. A sensitive, versatile microfluidic assay for bacterial chemotaxis. *Proceedings of the National Academy of Sciences*, 100(9):5449–5454, 2003.
- [127] Wenming Liu, Li Li, Xuming Wang, Li Ren, Xueqin Wang, Jianchun Wang, Qin Tu, Xiaowen Huang, and Jinyi Wang. An integrated microfluidic system for studying cell-microenvironmental interactions versatily and dynamically. *Lab on a Chip*, 10(13):1717–1724, 2010.
- [128] Stefan Kobel, Ana Valero, Jonas Latt, Philippe Renaud, and Matthias Lutolf. Optimization of microfluidic single cell trapping for long-term on-chip culture. *Lab on a Chip*, 10(7):857–863, 2010.
- [129] Zhicheng Long, Eileen Nugent, Avelino Javer, Pietro Cicuta, Bianca Sclavi, Marco Cosentino Lagomarsino, and Kevin D Dorfman. Microfluidic chemostat for measuring single cell dynamics in bacteria. *Lab on a Chip*, 13(5):947–954, 2013.

## Bibliography

---

- [130] Gustavo Giachetto, María Catalina Pirez, Luciana Nanni, Adriana Martínez, Alicia Montano, Gabriela Algorta, Sheldon L Kaplan, and Ana María Ferrari. Ampicillin and penicillin concentration in serum and pleural fluid of hospitalized children with community-acquired pneumonia. *The Pediatric infectious disease journal*, 23(7):625–629, 2004.
- [131] Fabio Silvio Taccone, Pierre-François Laterre, Thierry Dugernier, Herbert Spapen, Isabelle Delattre, Xavier Wittebole, Daniel De Backer, Brice Layeux, Pierre Wallemacq, Jean-Louis Vincent, et al. Insufficient  $\beta$ -lactam concentrations in the early phase of severe sepsis and septic shock. *Critical care*, 14(4):R126, 2010.
- [132] Marc A Unger, Hou-Pu Chou, Todd Thorsen, Axel Scherer, and Stephen R Quake. Monolithic microfabricated valves and pumps by multilayer soft lithography. *Science*, 288(5463):113–116, 2000.
- [133] Arun S Rajkumar, Nicolas Dénervaud, and Sebastian J Maerkl. Mapping the fine structure of a eukaryotic promoter input-output function. *Nature genetics*, 45(10):1207–1215, 2013.
- [134] Jean-Bernard Nobs and Sebastian J Maerkl. Long-term single cell analysis of *s. pombe* on a microfluidic microchemostat array. *PloS one*, 9(4):e93466, 2014.
- [135] Camilla Luni, Stefano Giulitti, Elena Serena, Luca Ferrari, Alessandro Zambon, Onelia Gagliano, Giovanni G Giobbe, Federica Michielin, Sebastian Knöbel, Andreas Bosio, et al. High-efficiency cellular reprogramming with microfluidics. *Nature methods*, 13(5):446–452, 2016.
- [136] Matthew E Levison and Julie H Levison. Pharmacokinetics and pharmacodynamics of antibacterial agents. *Infectious disease clinics of North America*, 23(4):791–815, 2009.
- [137] Elisabet I Nielsen and Lena E Friberg. Pharmacokinetic-pharmacodynamic modeling of antibacterial drugs. *Pharmacological reviews*, 65(3):1053–1090, 2013.
- [138] Sangeeta N Bhatia and Donald E Ingber. Microfluidic organs-on-chips. *Nature biotechnology*, 32(8):760–772, 2014.
- [139] Peter Ertl, Drago Sticker, Verena Charwat, Cornelia Kasper, and Günter Lepperdinger. Lab-on-a-chip technologies for stem cell analysis. *Trends in biotechnology*, 32(5):245–253, 2014.
- [140] Kristina Woodruff and Sebastian J Maerkl. A high-throughput microfluidic platform for mammalian cell transfection and culturing. *Scientific reports*, 6, 2016.
- [141] Guilhem Velve-Casquillas, Maël Le Berre, Matthieu Piel, and Phong T Tran. Microfluidic tools for cell biological research. *Nano today*, 5(1):28–47, 2010.
- [142] Matthias Mehling and Savaş Tay. Microfluidic cell culture. *Current opinion in biotechnology*, 25:95–102, 2014.

- [143] J Christopher Love, Jehnna L Ronan, Gijsbert M Grotenbreg, Annemarthe G van der Veen, and Hidde L Ploegh. A microengraving method for rapid selection of single cells producing antigen-specific antibodies. *Nature biotechnology*, 24(6):703–707, 2006.
- [144] Z Tatárová, JP Abbuehl, S Maerkl, and J Huelsken. Microfluidic co-culture platform to quantify chemotaxis of primary stem cells. *Lab on a Chip*, 16(10):1934–1945, 2016.
- [145] Yuichi Wakamoto, Neeraj Dhar, Remy Chait, Katrin Schneider, François Signorino-Gelo, Stanislas Leibler, and John D McKinney. Dynamic persistence of antibiotic-stressed mycobacteria. *Science*, 339(6115):91–95, 2013.
- [146] Marija Brgles, Maja Šantak, Beata Halassy, Dubravko Forcic, and Jelka Tomašić. Influence of charge ratio of liposome/dna complexes on their size after extrusion and transfection efficiency. *International journal of nanomedicine*, 7(1):393–401, 2012.
- [147] Richard N Cohen, Marieke AEM van der Aa, Nichole Macaraeg, Ai Ping Lee, and Francis C Szoka. Quantification of plasmid dna copies in the nucleus after lipoplex and polyplex transfection. *Journal of Controlled Release*, 135(2):166–174, 2009.
- [148] Bonnie E Lai, Marcus H Henderson, Jennifer J Peters, David K Walmer, and David F Katz. Transport theory for hiv diffusion through in vivo distributions of topical microbicide gels. *Biophysical journal*, 97(9):2379–2387, 2009.
- [149] Sebastian J Maerkl and Stephen R Quake. A systems approach to measuring the binding energy landscapes of transcription factors. *Science*, 315(5809):233–237, 2007.
- [150] Sylvie Rockel, Marcel Geertz, and Sebastian J Maerkl. Mitomi: A microfluidic platform for in vitro characterization of transcription factor–dna interaction. *Gene Regulatory Networks: Methods and Protocols*, pages 97–114, 2012.



# Kristina Woodruff

BIOENGINEER · MICROFLUIDIC AND HIGH-THROUGHPUT CELL TECHNOLOGY EXPERT

Rue du Crêt 7, 1006 Lausanne, Switzerland

(+41) (0)78.665.41.63 | kristinawdrff@gmail.com | <https://www.linkedin.com/in/kristina-woodruff>

## Education

---

### Ph.D. in Biotechnology and Bioengineering

Aug. 2012 - July 2017 (expected)

EPFL (ÉCOLE POLYTECHNIQUE FÉDÉRALE DE LAUSANNE), SWITZERLAND

### M.S. in Biochemistry

2011-2012

UCLA (UNIVERSITY OF CALIFORNIA, LOS ANGELES), USA

- GPA: 3.9/4.0

### B.S. in Biochemistry

2007-2011

UCLA (UNIVERSITY OF CALIFORNIA, LOS ANGELES), USA

- GPA: 3.9/4.0

### GRE Scores

2011

- Verbal reasoning: 730 (98 percentile)
- Quantitative reasoning: 790 (91 percentile)
- Analytical writing: 5.0 (87 percentile)
- Biochemistry, cell & molecular biology: 750 (99 percentile)

## Experience

---

### Department of Bioengineering, EPFL, Switzerland

Aug. 2012-present

DOCTORAL RESEARCH (ADVISOR: PROF. SEBASTIAN MAERKL)

- Generated a high-throughput protein production chip for protein engineering and synthetic biology
- Developed microarraying techniques for live mammalian cell printing
- Engineered microfluidic chips for mammalian cell culture, transfection, and cell-based assays
- Created modular microfluidic platforms for pharmacokinetic/pharmacodynamic and dosage-dependent studies

### Department of Biochemistry, UCLA, USA

2011-2012

MASTERS RESEARCH PROJECT (ADVISOR: PROF. JOSEPH LOO)

- Developed ion mobility techniques to elucidate the structure and assembly mechanisms of large protein complexes
- Used mass spectrometry to quantify drug encapsulation inside therapeutic protein complexes

### Department of Biological Chemistry, UCLA, USA

2009-2011

UNDERGRADUATE RESEARCH PROJECT (ADVISOR: PROF. MICHAEL CAREY)

- Developed *in-vitro* models and assays to investigate the biochemical mechanism of transcriptional silencing in post-translationally modified chromatin
- Analyzed protein-protein and protein-DNA interactions

### Department of Neuroscience, UCLA Medical Center, USA

2008

UNDERGRADUATE RESEARCH PROJECT (ADVISOR: ERIC BEHNKE)

- Assembled and tested electrodes, performed microdialysis on patients, audited data

### Research & Development, Aridis Pharmaceuticals, USA

2008

INTERN (ADVISOR: DR. DAVID LECHUGA)

- Used cell culture, molecular biology, chemistry, and immunology techniques to develop vaccines, antibacterial drugs, and monoclonal antibody therapies

## Awards & Honors

---

<b>Journal cover image</b> Nature Methods	Oct. 2014
<b>Award</b> Dolores Cannon Southam Award for Excellence in Research	2012
<b>Scholarship</b> UCLA Undergraduate Research Scholars Scholarship	2010
<b>Stipend</b> UCLA Honors Undergraduate Summer Research	2010
<b>Award</b> UCLA Dean's Prize for Undergraduate Research	2010
<b>Award</b> UCLA Dean's List	2007-2012
<b>Finalist</b> National Merit Competition	2007
<b>Valedictorian</b> Monta Vista High School	2007

## Publications

---

Woodruff, K. and Maerkl, S. J. A microfluidic module for real-time generation of complex multi-molecule temporal concentration profiles. Manuscript submitted (March 2017) and in revision (*Analytical Chemistry*).

Woodruff K, and Maerkl SJ. A High-Throughput Microfluidic Platform for Mammalian Cell Transfection and Culturing. *Scientific Reports* 6, 23937 (2016).

Woodruff K, Fidalgo LM, Gobaa S, Lutolf MP, and Maerkl SJ. Live mammalian cell arrays. *Nature Methods* 10, 550–552 (2013).

Master's thesis: Applying ESI-GEMMA towards the study of large protein complexes (2012).

## Skills

---

### Laboratory Skills

- Microfluidic chip design, fabrication (photolithography & soft lithography), and operation
- Microarraying, high-throughput assays, high-content screening
- *In vitro* diagnostic devices, surface chemistry
- Immunohistochemistry, fluorescence microscopy, image processing and analysis
- Biochemical & molecular biology techniques (Molecular cloning, PCR, ELISA, Western blotting, mass spectrometry, etc.)
- Protein expression & purification
- Bacteria & mammalian cell culture, stem cell culture

### Software Skills

- Device engineering and programming: CAD software, LabVIEW
- Image processing: ImageJ, CellProfiler, MATLAB
- Modeling: MATLAB, COMSOL Multiphysics
- Presentation and design: MS Office (Word, Excel, Powerpoint), Adobe Illustrator, Igor Pro, LaTeX

### Project Management and Teaching

- Prepared and led lecture and laboratory courses for undergraduate students
- Trained and mentored Masters students working on research projects
- Directed a team of students in the 2013 International Genetically Engineered Machine (iGEM) competition

### Communication Skills

- Poster presentations, oral presentations, and scientific writing
- Coordinated collaborative projects between laboratories

### Languages

- English (native speaker)
- French (fluent)
- Spanish (basic)

## Organizations

---

### Bioscience Network Lausanne

2015-2017

- Fundraising, organization of an annual Life Science Career Day, events that bridge the gap between academia and industry, and career preparation events

### Pole Emotion Dance School

2016-present

- Dance and fitness instructor



